# EXPERIMENTAL AND THEORETICAL ANALYSIS OF THE PERFORMANCE OF DIESEL BLENDED FUELED ENGINE WITH ALUMINUM OXIDE NANOPARTICLE AS ADDITIVES

**2025**
**PhD THESIS**
**MECHANICAL ENGINEERING**

**Ameer Hasan Hamzah AL MAMOORI**

**Thesis Advisors**
**Assist. Prof. Dr. Abdulrazzak Ahmed Saleh AKROOT**
**Assoc. Prof. Dr. Hasanain Adnan ABDUL WAHHAB**

# EXPERIMENTAL AND THEORETICAL ANALYSIS OF THE PERFORMANCE OF DIESEL BLENDED FUELED ENGINE WITH ALUMINUM OXIDE NANOPARTICLE AS ADDITIVES

**Ameer Hasan Hamzah AL-MAMOORI**

**Thesis Advisors**
**Assist. Prof. Abdulrazzak Ahmed Saleh AKROOT**
**Assoc. Prof. Dr. Hasanain Adnan ABDUL WAHHAB**

**T.C.**
**Karabuk University**
**Institute of Graduate Programs**
**Department of Mechanical Engineering**
**Prepared as**
**PhD Thesis**

**KARABUK**
**April 2025**

I certify that in my opinion the thesis submitted by Ameer Hasan Hamzah AL-MAMOORI titled "EXPERİMENTAL AND THEORETİCAL ANALYSİS OF THE PERFORMANCE OF DİESEL BLENDED FUELED ENGİNE WİTH ALUMİNUM OXİDE NANOPARTİCLE AS ADDİTİVES" is fully adequate in scope and in quality as a thesis for the degree of PhD.

Assist. Prof. Dr. Abdulrazzak Ahmed Saleh AKROOT .....
Thesis Advisor, Department of Mechanical Engineering
Assoc. Prof. Dr. Hasanain A. ABDUL WAHHAB .....
Second Thesis Advisor, Department of Mechanical Engineering

This thesis is accepted by the examining committee with a unanimous vote in the Department of Mechanical Engineering as a PhD thesis. April 9, 2025

| Examining Committee Members (Institutions) | Signature |
|---|---|
| Chairman : Assoc. Prof. Dr. Samet USLU (KBU) | ..... |
| Member : Prof. Dr. Mehmet ÖZKAYMAK (KBU) | ..... |
| Member : Prof. Dr. Miqdam Tariq CHICHAN (UOT) | ..... |
| Member : Prof. Dr. Louay Abd AlAzez MAHDI (UOT) | ..... |
| Member : Assoc. Prof. Dr. Hasanain ABDUL WAHHAB (UOT) | ..... |
| Member : Assist. Prof. Dr. Abdulrazzak AKROOT (KBU) | ..... |

The degree of PhD by the thesis submitted is approved by the Administrative Board of the Institute of Graduate Programs, Karabuk University.

Assoc. Prof. Dr. Zeynep ÖZCAN .....
Director of the Institute of Graduate Programs

*"I declare that all the information within this thesis has been gathered and presented in accordance with academic regulations and ethical principles and I have according to the requirements of these regulations and principles cited all those which do not originate in this work as well."*

Ameer Hasan Hamzah AL-MAMOORI

## ABSTRACT

**Ph.D. Thesis**

**EXPERMNTER AND THEORETICAL ANALYSIS OF THE PERFORMANCE OF DIESEL BLENDED FUELED ENGINE WITH ALUMINUM OXIDE NANOPARTICLE AS ADDITIVES**

**Ameer Hasan Hamzah AL-MAMOORI**

**Karabuk University**
**Institute of Graduate Programs**
**Department of Mechanical Engineering**

**Thesis Advisors:**
**Assist. Prof. Dr. Abdulrazzak Ahmed Saleh AKROOT**
**Assoc. Prof. Dr. Hasanain Adnan ABDUL WAHHAB**
**April 2025, 156 pages**

This work was conducted experimentally and theoretically in the Department of Power Mechanics Technology, Al-Furat Al-Awsat Technical University/Al-Musayyab Technical Institute, 65 km from Baghdad, using a four-stroke, four-cylinder diesel engine. There are three fuel inputs: In the first stage, pure diesel fuel was used. The biofuel extracted from Water Hyacinth was blended with pure diesel in the second stage. Third-stage nanomaterial ($Al_2O_3$) and three mixture ratios of 50, 100, and 150 ppm were blended. The following indicators were studied under the influence of conventional fuel: Thermal efficiency of braking, specific fuel consumption, exhaust temperature, carbon monoxide, carbon dioxide, unburned hydrocarbons, and nitrogen oxides. While the highest value of braking thermal

efficiency was recorded at half and full loads for the fuel type (D80B20N150) compared to pure diesel fuel (D100) as it reached 39%, 45%, 47%, and 48%, with increases of 6%, 7%, and 9%, respectively, compared to the conventional fuel. In comparison, the lowest braking thermal efficiency was recorded in the fuel type (D80B20) at a full load level, reaching 34%, which is an increase of 9% compared to conventional fuel. The fuel type also recorded a decrease in the consumption of fuel mixed with nanoparticles and biodiesel (BSFC) at the half and full loads, and the percentages were 52%, 55%, and 58%, respectively, compared to pure fuel (D100). The best decrease was when adding nanoparticles with biodiesel (D80B20N150) ppm. At the same time, fuel consumption (D80B20) decreased by 3% compared to pure diesel fuel. Also, carbon monoxide (CO) emissions decreased by adding biodiesel from (D80B20) to biodiesel compared to pure diesel fuel D100 at half and full loads at an engine speed of 1800 rpm. CO emissions decreased by 4%, where the best blend was (D80B20N15 0) compared to pure diesel fuel. $CO_2$ emissions rose at half load at 1150 rpm when biodiesel was added to pure fuel, while compared to pure diesel fuel, they fell at full load and engine speed of 1800 rpm. The optimal blend was D80B20N150 relative to pure diesel fuel D100, with a reduction of 8%. The combustion of diesel fuel with biodiesel and different blends was simulated for all fuel blends. Here, the mass fraction was 11.7%, and it seems that with increasing engine speed, fraction mass was observed at (D80B20N150) higher than diesel fuel with biodiesel (D80B20). The work includes numerical analysis by using the ANSYS Fluent software. The anticipated outcomes were strongly concorded with the empirical findings. Nitrogen oxide (NOx) emissions increased by increasing the proportion of biodiesel (D80B20) with biodiesel compared to pure diesel fuel D100 at half and full loads. The percentage of the increase was 10% compared to pure diesel fuel. When adding nanoparticles ($AL_2O_3$) to diesel fuel blends with biodiesel, a decrease in NOx emissions was observed in all blends, but the best case was at D80B20N150. With the increase of the nanoparticles at D80B20N150, the mass fraction decreased regularly less than pure diesel and biodiesel by 1.3%. It appears that with increasing speed, a decrease in mass fraction was observed for D80B20N150 compared with diesel blends biodiesel D80B20, and this decrease is considered a good factor. The unburned hydrocarbon (HC) emissions are also at half load for all tested mixtures. It was observed that the emissions of most tested fuels decreased D80B20N150 by 1.5%

compared with pure diesel fuel by incorporating nanoparticles of aluminum oxide. The calorific value of biodiesel blends increases, viscosity diminishes, and full combustion occurs, resulting in reduced hydrocarbon emissions.

**Key Word** : CFD modeling, Eichhornia crassipes biodiesel, Alternative fuel, Diesel engine.

**Science Code** : 91440

# ÖZET

**Doktora Tezi**

## IRAK'TA BİR GÜNEŞ HİBRİT GAZ TÜRBİNİ ENERJİ SANTRALİ İÇİN ENERJİ YÖNETİMİ VE 4E ANALİZİ

**Ameer Hasan Hamzah AL-MAMOORI**

**Karabük Üniversitesi**
**Lisansüstü Eğitim Enstitüsü**
**Makine Mühendisliği Anabilim Dalı**

**Tez Danışmanları:**
**Dr. Öğr. Üyesi Abdulrazzak Ahmed Saleh AKROOT**
**Doç. Dr. Hasanain Adnan ABDUL WAHHAB**
**Nisan 2025, 156 sayfa**

Bu çalışma deneysel ve teorik olarak Bağdat'a 65 km uzaklıktaki El-Furat El-Awsat Teknik Üniversitesi/El-Müseyyeb Teknik Enstitüsü, Güç Mekaniği Teknolojisi Bölümü'nde dört zamanlı, dört silindirli bir dizel motor kullanılarak yürütülmüştür. Üç yakıt girişi vardır: İlk aşamada saf dizel yakıtı kullanılmıştır. İkinci aşamada Su Sümbülünden elde edilen biyoyakıt saf dizel ile harmanlanmıştır. Üçüncü aşamada nanomalzeme ($Al_2O_3$) ve 50, 100 ve 150 ppm'lik üç karışım oranı harmanlanmıştır. Aşağıdaki göstergeler geleneksel yakıtın etkisi altında incelenmiştir: Frenlemenin termal verimliliği, özgül yakıt tüketimi, egzoz sıcaklığı, karbon monoksit, karbon dioksit, yanmamış hidrokarbonlar ve azot oksitler. En yüksek fren termal verimi değeri, saf dizel yakıtı (D100) ile karşılaştırıldığında, yarım ve tam yüklerde yakıt türü (D80B20N150) için sırasıyla %6, %7 ve %9 artışla %39, %45, %47 ve %48'e ulaşarak kaydedilirken, konvansiyonel yakıta göre en düşük fren termal verimi, tam

yük seviyesinde %34'e ulaşarak, konvansiyonel yakıta göre %9 artışla kaydedildi. Yakıt türü ayrıca, nanopartiküller ve biyodizel (BSFC) ile karıştırılmış yakıt tüketiminde yarım ve tam yüklerde bir düşüş kaydetti ve yüzdeler, saf yakıta (D100) kıyasla sırasıyla %52, %55 ve %58 olarak gerçekleşti. En iyi düşüş, biyodizel (D80B20N150) ppm ile nanopartiküllerin eklenmesiyle gerçekleşti. Aynı zamanda yakıt tüketimi (D80B20) saf dizel yakıta göre %3 oranında düşmüştür. Ayrıca, (D80B20)'den biyodizelin biyodizel ile birlikte eklenmesiyle, 1800 devir/dakika motor devrinde, yarım ve tam yüklerde saf dizel yakıtı D100'e kıyasla karbon monoksit (CO) emisyonları azalmıştır. CO emisyonları %4 oranında azalmış olup, en iyi karışım saf dizel yakıta göre (D80B20N15 0) olmuştur. CO2 emisyonları, biyodizelin saf yakıtla birlikte eklenmesiyle yarım yükte ve 1150 devir/dakika devrinde artarken, 1800 devir/dakika ve tam yükte saf dizel yakıta göre azalmıştır ve en iyi karışım D80B20N150 olup, yüzdesi %8 olmuştur. Dizel yakıtın biyodizel ve farklı karışımlarla yanması tüm yakıt karışımları için simüle edilmiştir. Burada kütle kesri %11,7 idi ve artan motor devriyle birlikte, kesir kütlesinde (D80B20N150)'de biyodizelli dizel yakıtından (D80B20) daha yüksek bir artış gözlemlendiği görülmektedir. Çalışma, ANSYS Fluent yazılımını kullanarak sayısal analizi içermektedir. Beklenen sonuçlar deneysel sonuçlarla iyi bir uyum içindeydi. Azot oksit (NOx) emisyonları, biyodizelli biyodizel (D80B20) oranının artmasıyla, saf dizel yakıtı D100'e kıyasla yarı ve tam yüklerde artmıştır. Saf dizel yakıtına kıyasla artış yüzdesi %10'dur. Biyodizelli dizel yakıt karışımlarına nanopartiküller ($AL_2O_3$) eklendiğinde, tüm karışımlarda NOx emisyonlarında bir azalma gözlemlenmiştir, ancak en iyi durum D80B20N150'de olmuştur. D80B20N150'deki nanopartiküllerin artmasıyla, kütle kesri de saf dizel ve biyodizelden düzenli olarak daha az %1,3 oranında azalmıştır. Görünüşe göre artan hızla birlikte, dizel karışımlı biyodizel D80B20 ile karşılaştırıldığında D80B20N150 için kütle oranında bir azalma gözlemlendi ve bu azalma iyi bir faktör olarak kabul edildi. Ayrıca, tüm test edilen karışımlar için yük ile yanmamış hidrokarbon (HC) emisyonları yarım yüktedir. Alüminyum oksit nanopartikülleri dahil edilerek test edilen yakıtların çoğunun emisyonlarının saf dizel yakıtına kıyasla D80B20N150'yi %1,5 oranında azalttığı gözlemlendi. Biyodizel karışımlarında, kalorifik değer iyileşir, viskozite azalır ve yakıt tamamen yanar, bu da hidrokarbon emisyonlarını azaltır

**Anahtar Kelimeler** **:** CFD modelleme, Eichhornia crassipes biyodizel, Alternatif yakıt, Dizel motor.

**Bilim Kodu** **:** 91440

## ACKNOWLEDGMENT

In the name of Allah, the Most Gracious, the Most Merciful. All praise and gratitude belong to Allah, the Lord of the Worlds. Peace and blessings be upon His Messenger, Muhammad, his family, and all his companions.

First and foremost, I sincerely thank Allah Almighty for granting me the courage, guidance, and determination to embark on this academic journey and successfully complete my doctoral studies. His mercy and countless blessings have consistently guided me, and I remain eternally grateful for His infinite generosity.

My heartfelt appreciation goes to my supervisor, Assistant Professor Dr. Abdulrazak Ahmed Salih AKROOT, for his invaluable advice, continuous encouragement, and unwavering support throughout my doctoral program. I am also deeply grateful to Associate Professor Dr. Hasanain Adnan Abdul WAHHAB for his profound knowledge, patience, and steadfast commitment, which have significantly shaped my research and advanced my scientific growth.

Special thanks to the staff and administration of Karabuk University for their professional assistance and administrative support, which have considerably facilitated the progress of my doctoral work.

I wish to extend my sincere gratitude to my colleagues and research collaborators for their cooperation, camaraderie, and valuable intellectual exchanges. Their diverse insights and collective efforts were instrumental in the success of this research endeavor.

Additionally, I am thankful to Al-Furat Al-Awsat Technical University for allowing me to pursue my studies. My deepest gratitude goes to Prof. Dr. Muzaffar AL-ZUHAIRI, the president of the university; Prof. Dr. Ahmed GHANEM, the scientific assistant; and Prof. Dr. Jabbar AL-KHAFAJI, the dean of the institute, for their support and guidance.

Finally, I express my profound appreciation to my beloved family for their constant encouragement, boundless love, and patience throughout this journey. Their unwavering support and selflessness have been my greatest source of inspiration and strength. My sincere thanks to everyone who offered help and encouragement along the way. I proudly dedicate this accomplishment to my beloved country, Iraq, and my cherished city, Babylon, which is resilient through its people, and to Turkey, which warmly welcomed me during my studies.

## CONTENTS

**Page**

**Page**

**Page**

**Page**

## LIST OF FIGURES

**Page**

**Page**

**Page**

**Page**

## LIST OF TABLES

**Page**

## SYMBOLS AND ABBREVIATIONS INDEX

### SYMBOLS

B : Bore (mm)

Do : Orifice diameter (cm)

g : Gravity acceleration (9.81)m/$s^2$

ho : Height of the manometer (Cm $H_2$ O)

$\dot{m}a$ : Air consumption rate (Kg/sec)

$\dot{m}f$ : Fuel consumption rate (Kg/sec)

P : pressure (bar)

N : Engine speed (rpm)

V : Volumetric flow rate ($m^3$/ses)

r : Radius of electrical dynamiter (cm)

S : Stroke (mm)

T : Temperature (C)

$T_b$ : Brake Torque (N.m)

t : Tim (sec)

ρ : Density (Kg/$m^3$)

$\rho_f$ : Density of air (Kg/m3)

$\rho_{air}$ : Density of nanoparticle (Kg/m3)

$\eta_{Bth}$ : Barack thermal efficiency (%)

$\eta_v$ : Volumetric efficiency (%)

Φ : Equivalence ratio ()

$V_{dis}$ : Displacement volume ($m^3$)

**ABBREVITIONS**

| | |
|---|---|
| a | : Air |
| atm | : Atmosphere |
| EC | : Echornya Crasybs |
| ECB | : Echornya Crasybs Biodiesel |
| f | : Fuel |
| k | : Number of cylinder |
| sto | : Stoichiometric |
| v | : Volume |

# PART 1

# INTRODUCTION

## 1.1. STUDY BACKGROUND

In recent years, researchers have increasingly explored alternative fuels to replace oil and its derivatives, driven by growing awareness of energy and environmental concerns [1]. Biofuels, defined formally, are hydrocarbons derived from living organisms. Practically speaking, biofuels refer to any hydrocarbon fuels produced relatively quickly (within days, weeks, or months) from organic material, whether currently living or previously alive. This differentiates biofuels from fossil fuels—such as coal, oil, and gas—which have formed over millions of years, as well as from non-hydrocarbon fuels like nuclear fission [2,3]

Humans have utilized solid biofuels since the discovery of fire, with ancient populations relying on wood, the earliest biofuel for heating and cooking. The development of electricity introduced new applications for biofuels, expanding their utility beyond traditional uses [4]. Indeed, biofuels were used for electricity generation before fossil fuels became prevalent. However, fossil fuel emergence and widespread adoption have significantly affected biofuel production and consumption patterns. The advantages of fossil fuels have led to their predominant usage, particularly in developed nations. Nonetheless, since their introduction, liquid biofuels have played a notable role in the automotive industry [5].

### 1.1.1. Combating Climate Change

The world urgently needs to identify and adopt new, low-carbon fuel and energy sources to combat climate change effectively. Since transportation significantly contributes to global carbon emissions, replacing fossil fuels with renewable

alternatives like biofuels is a particularly effective approach to reducing greenhouse gases[6]. When alternative solutions, such as transitioning to electric vehicles, are impractical due to high costs or insufficient charging infrastructure, biofuels offer a practical means of lowering emissions associated with vehicle traffic [7].

### 1.1.2. Responding to Higher Energy Consumption

Energy demand is expected to skyrocket due to a combination of factors, including a projected increase in the global population to 8 or 10.5 billion by 2050 and robust economic development in developing nations [8,9]. More efficient use of natural resources and increased usage of renewable energy sources like biofuels are necessary to fulfill this growing demand [10].

### 1.1.3. The Availability of Energy

As energy demand develops, ensuring supply security will be difficult due to global resource dispersion. According to the International Energy Agency, worldwide crude oil output in existing fields fell after 2009 [11–13]. It is projected to fall to 25% of its current capacity by 2035, significantly reducing global reliance on fossil fuels. Consequently, high fossil fuel prices pose challenges, compelling automobile manufacturers to seek alternative energy sources, as illustrated in Figure 1.1. Research efforts have notably advanced the development and utilization of biofuels for energy production. Biomass, in particular, stands out as one of the most widely distributed renewable resources globally.

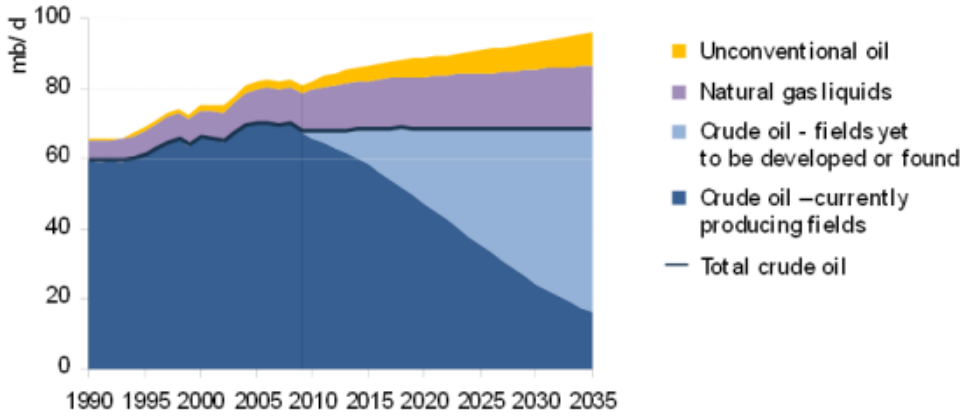


Figure 1.1. Forecast of global oil production from 1990 to 2035 (mb/d: million barrels per day) [2,3].

### 1.1.4. Taking Advantage of Limited and Scarce Resources

One effective approach to meeting global energy demands involves utilizing waste and residues as feedstock for biofuel production. Minimizing waste and maximizing the efficient use of our precious natural resources are essential strategies for ensuring sustainability and long-term survival [14–16]

## 1.2. BENEFITS OF USING BIOFUEL

Biofuels were in high demand during World War II, as they were frequently used to replace imported fuels [17]. This period marked a significant surge in biofuel usage. Notably, several innovations emerged during this time, including developing gasoline alternatives such as alcohol derived from potatoes. Many important scientific advancements were made during the war; however, in peacetime, interest in biofuels declined due to the availability of cheap oil, which was influenced by geopolitical and geoeconomic factors. As ethanol supplies from the Middle East and Gulf nations decreased, interest in biofuels waned. In response, the Organization of Petroleum Exporting Countries (OPEC) significantly reduced oil exports, especially to non-OPEC countries [18].

The resulting fuel shortages drew the attention of scientists and policymakers to the broader energy crisis and the urgent need to explore alternative fuels. This shift in

focus is illustrated in Figure 1.2, which presents the International Energy Agency's forecast for global energy consumption, particularly in the transportation sector, by 2050, including the projected role of biofuels [19]. Public interest in biofuels emerged in the twentieth century, driven largely by rising oil prices and a growing emphasis on rural development. These factors were instrumental in reviving global interest in biofuels as a viable energy alternative.

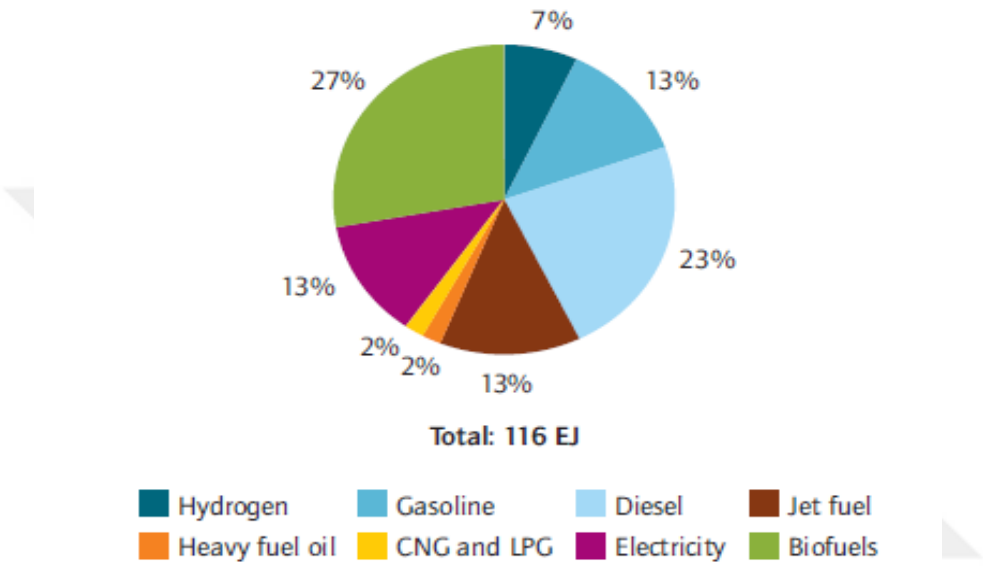


Figure 1.2. The transportation sector's global energy consumption in 2050 [19].

### 1.2.1. Impact on the Environment

Biofuels represent a challenging category because, despite being renewable, they share many chemical characteristics with traditional hydrocarbons and can contribute to similar emission issues [20]. However, if their production and distribution are managed sustainably, biofuels have the potential to be significantly more environmentally friendly. Examining the different subcategories of biofuels is essential, as their environmental impact goes beyond just emissions and includes factors such as land use, water consumption, and resource management.

### 1.2.2. Surface Contamination and Spills

Although biofuels are not completely risk-free, they are considerably safer than fossil fuels. In large quantities, biofuel spills in a confined area can threaten nearby organisms and contaminate surrounding soil or water. However, the environmental impact is generally much less severe than fossil fuels. One key advantage of biofuels is their biodegradability, owing to their organic origin [21].

Naturally occurring soil and water microorganisms, such as bacteria, can metabolize biofuels as an energy source, breaking them down into harmless byproducts. This suggests that, although concentrated biofuel spills have the potential to kill tiny organisms and plants, they will not remain in the ecosystem for long enough to damage it or make a place uninhabitable.

### 1.2.3. Atmospheric Contamination and Sulfur

Sulfur, a major contributor to acid rain, may be completely removed via biofuel production. However, the high nitrogen concentration of biofuels may lead to the creation of compounds that pollute the air and produce acid rain. Biofuels can potentially reduce acid rain since their total impact on acid rain production is generally negative. Biofuels offer an advantage over fossil fuels since they may be properly prepared to ensure as little pollution as possible [22].

### 1.2.4. Global Warming and Greenhouse Gas (GHG) Emissions

Biofuels have the potential to drastically reduce greenhouse gas emissions if generated in the "right" way. Erroneous manufacturing may increase emissions [23]. The most effective way to reduce greenhouse gas emissions is to utilize biofuels. They may also be considered as a method of creating energy security by substituting fossil fuels, which are limited in quantity. Biofuels are becoming more popular [24,25].

Biogas, a type of biofuel, is produced and utilized globally, with Asia, Europe, and the Americas leading in both production and consumption. Photosynthetic plants are the

most commonly used feedstock for biofuel production, as ethanol can theoretically be derived from any carbon-based source. In fact, biogas can be generated from nearly any plant-derived material, making it a highly versatile and sustainable energy option [26].

### 1.2.5. Independence Energy

The advantages of biofuels are clear and come with minimal immediate drawbacks. A country with sufficient land to cultivate biofuel feedstock can produce its own energy, reducing or even eliminating dependence on fossil fuels, which are concentrated in specific regions of the world. In light of fluctuating fuel prices and supply uncertainties, achieving energy independence through biofuels is a highly favorable prospect. The primary distinction between fossil fuels and biofuels lies in their renewability: fossil fuels are finite and will eventually be depleted, whereas biofuels can be replenished.

Historically, it was believed that if hydrocarbons could be produced quickly and by alternative means, global energy needs could be more easily met. Since fossil fuels require millions of years to form and humans cannot wait such durations, they are not considered renewable energy sources. In contrast, biofuels are derived from biomass that can be cultivated year-round through sustainable agricultural practices. This demonstrates the renewable nature of biomass and biofuels, which can be regenerated relatively quickly. However, while biofuels are renewable, they are not inherently environmentally friendly, as their combustion still results in greenhouse gas emissions [27,28].

## 1.3. BIODIESEL AS A SOURCE OF RENEWABLE ENERGY

The consumption of petroleum products continues to rise daily, paralleling the number of road vehicles. This growing reliance on hydrocarbon fuels contributes significantly to environmental pollution [29]. Therefore, addressing the dual challenges of fuel supply and environmental degradation has become increasingly urgent. Non-

renewable fuels release higher hydrocarbons, sulfur, nitrogen oxides, and carbon monoxide levels than renewable biofuels [30].

The challenges of fuel supply and environmental pollution must be addressed. Non-renewable fuels emit more hydrocarbons, sulfur, nitrogen oxides, and carbon monoxide than renewable biofuels. Various alternative fuels are being researched as prospective substitutes for petroleum products, and a feasibility and demonstration study has been completed. Renewable fuels are gaining popularity because they minimize environmental pollution (by finishing the carbon cycle) and the need for oil imports [31]. Alternative fuels, such as biodiesel, are gaining popularity as a viable alternative to diesel oil for internal combustion engines to fulfill the world's ever-increasing energy demands. Biodiesel is made from fats that can be used repeatedly, like vegetable and animal fats [32]. It is a biodegradable, safe mixture of long-chain fatty acids without sulfur or aromatics. It may also be derived from animal fats, discarded vegetable oils, or regenerated vegetable oils.

By 2026, 40.5 billion liters of biodiesel will be produced globally, a 12% increase from 2016. Policy will continue to impact production patterns more than market forces. The European Union is expected to continue to generate the bulk of biodiesel. By 2026, output is predicted to be 13 billion liters, down from 13.3 billion in 2016 and 14.3 billion in 2020, when the RED goal is scheduled to be met [33].

Vegetable oil remains the primary feedstock for biodiesel production. However, both the United States and the European Union are projected to see an increase in alternative feedstocks, such as waste tallow and used cooking oil. In the United States, biodiesel production is expected to remain stable at approximately 7.4 billion liters[34–36]

Argentine biodiesel is expected to help offset the shortfall in meeting the U.S. advanced biofuel mandate, particularly during the early years of the forecast period. Driven by increasing domestic and international demand, Argentina’s biodiesel production is projected to grow from 3.1 billion liters in 2016 to 3.7 billion liters by 2019. However, by 2026, as the need for imports diminishes, production is anticipated to decline to approximately 2.9 billion liters.

Other key contributors to global biodiesel production include Brazil, Indonesia, and Thailand. In its effort to meet its 8% domestic blending mandate and maintain its position as the world's third-largest biodiesel producer, Brazil is expected to account for 36% of the global increase in biodiesel output. Following a decline due to policy changes in 2015, Indonesian biodiesel production rebounded in 2016, primarily due to growing domestic demand. While exports are projected to increase slightly over the forecast period, they are no longer expected to be the main driver of Indonesia's biodiesel industry. By 2026, Indonesia is projected to produce 4.4 billion liters of biodiesel. A key factor influencing this growth is the sustainability of the export levy on crude palm oil (CPO), which finances subsidies for biodiesel producers.

Meanwhile, the Philippines and Malaysia are expected to increase their biodiesel production. The Philippines mainly produces for domestic consumption, whereas Malaysia exports approximately 40% of its output. As a result, global biodiesel prices are expected to rise by 11% in nominal terms. However, realistically, prices may decline slightly toward the end of the forecast period as demand in the U.S. and EU tapers. The projected biodiesel production volumes and price trends are illustrated in Figure 3 [37].

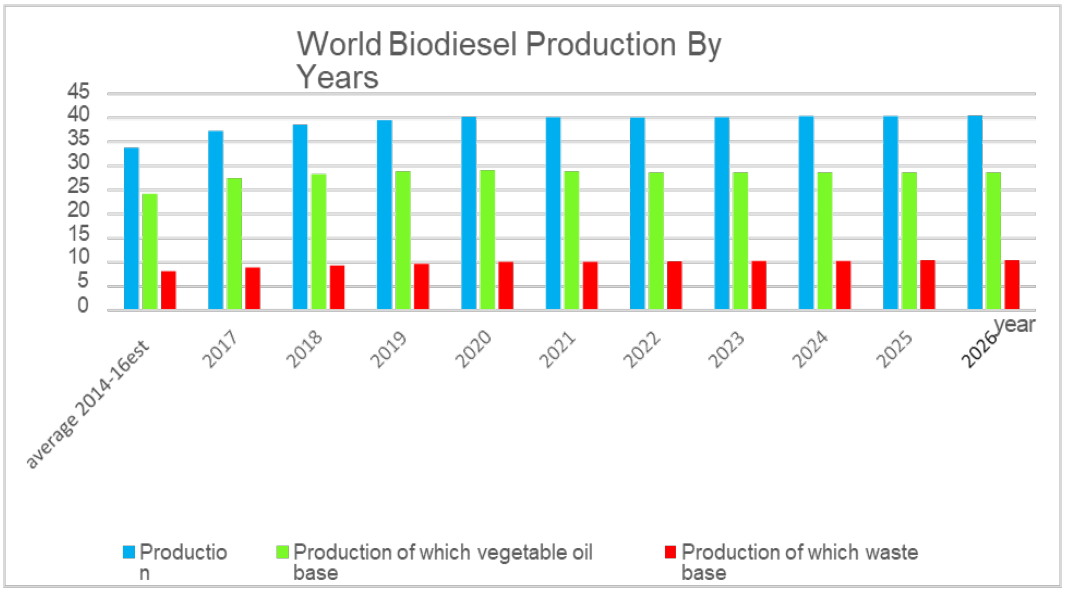


Figure 1.3. Production quantity and the biofuel are depicted.

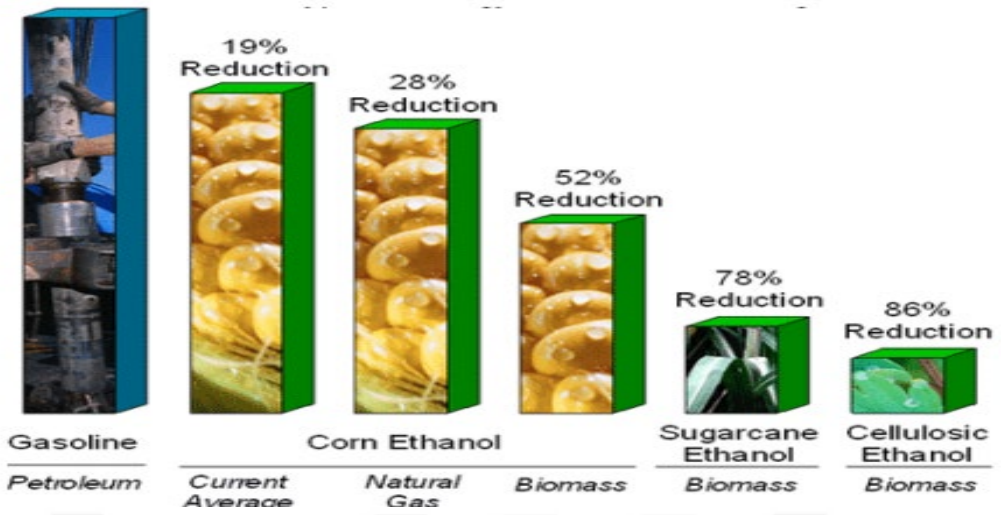


Figure 1.4. GHG emissions by transportation fuel[38].

Global biofuel production for transportation was projected to reach 144 billion liters in 2020, equivalent to approximately 2,480 thousand barrels per day. This marked an 11.6% decline from the record-high production in 2019 and represented the first annual decrease in two decades. Despite a slight upward revision from the International Energy Agency's (IEA) May 2020 update, this figure remains significantly below the 3% growth initially forecasted before the COVID-19 pandemic. The most substantial declines in production were observed in ethanol output from the United States and Brazil. Nevertheless, researchers consistently agree on the effectiveness of all ethanol types in reducing carbon dioxide emissions. Notably, cellulosic ethanol reduces $CO_2$ emissions by as much as 86% compared to ethanol derived from corn or sugarcane.

To help limit global warming to below 2.4°C by 2050, a $CO_2$ reduction target was established by the G8 leaders at the Heiligendamm Summit in 2007, as illustrated in Figure 1.4. In countries with mandates requiring the blending of biofuels with fossil fuels, Brazil experienced a 17% decrease in the volume of unblended ethanol purchased in the first half of 2020. Similarly, such countries' biofuel blending rates dropped by 17%. Meanwhile, the ASEAN region is expected to see increased growth in biofuel production, spurred by government investments to maintain competitiveness with fossil fuels like gasoline and diesel.

At the same time, the sharp drop in crude oil prices in 2020 led to a corresponding decline in biofuel prices. Although this did not entirely halt biofuel usage, it did raise economic concerns for some biofuel production facilities. In response to the need for cost-effective and sustainable alternatives, significant efforts have been made to extract ethanol from abundant plant sources such as water hyacinth, which thrives in riverine regions across the globe [39]. For instance, scientists in India have developed biological conversion techniques using enzymes and diluted sulfuric acid under high pressure and temperature to produce bioethanol from plant material. These innovations have inspired further research into modern biofuel production technologies that enable blending with diesel [40].

Looking ahead, it is anticipated that the first generation of fuels dominated by fossil sources will gradually be replaced by second-generation biofuels, including biodiesel, vegetable oils, and ethanol, by the year 2050, as depicted in Figure 1.4 [41].

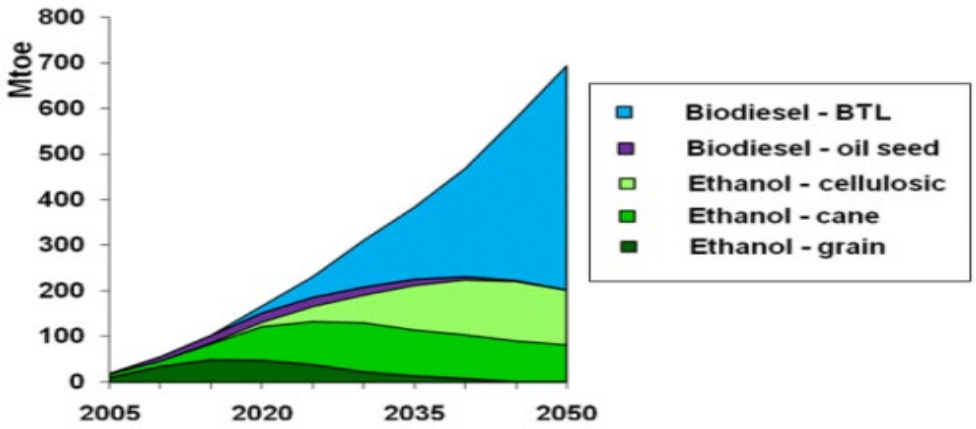


Figure 1.5. Projected transition from first- to second-generation biofuels, 2005–2050 [42](Mtoe: million tons equivalent to oil).

## 1.4. PROPERTIES OF DIESEL FUEL

### 1.4.1. Cetane Number

Diesel fuel is characterized by its cetane number, which indicates its ignition quality. Diesel undergoes self-ignition when the necessary conditions—such as proper injection, pressure, and heat, are present in the combustion chamber and within the cylinder. Several design factors influence engine performance, including temperature, which is affected by the compression ratio and fuel injection rate. Additionally, the fuel's chemical composition and its volatility play important roles. A higher cetane number generally leads to shorter ignition delays, resulting in more efficient combustion and smoother engine operation.

### 1.4.2. Viscosity

Viscosity is one of the most critical properties influencing diesel fuel performance. It decreases with rising temperature and increases as temperature drops. Viscosity directly affects fuel flow and is typically measured before use. The ability of the fuel to flow smoothly into the injection system is essential, as diesel also serves a lubricating function within engine components. Viscosity impacts the spray pattern of the fuel as it exits the injector and enters the combustion chamber. When the fuel is less viscous, it may lead to reduced lubrication and less efficient combustion, resulting in lower fuel economy and mileage [43].

### 1.4.3. Calorific Value

Key thermal properties of fuel include its calorific value (thermal value), which represents the energy the fuel can deliver to the engine, and the engine's efficiency in converting this energy into useful mechanical work. The specific fuel consumption is often used to infer the thermal value and efficiency of the fuel.

### 1.4.4. Gravity

Using a hydrometer, the specific gravity of fuel, defined as the ratio of the fuel's density to that of water at 15°C, can be determined. Specific gravity plays an important role in the combustion process, influencing how fuel is atomized and injected into the combustion chamber. Its value ranges from 0.80 to 0.94. The specific gravity of a fuel is a factor in determining its thermal value, as its density will increase as it burns. The calorific value is because the density increases the carbon in diesel fuel, as the density of paraffins and naphthalene increases. The fuel's density is the ratio of the fuel's volume at a temperature of 15°C to density units of $kg/m^3$. This information can provide an idea of the economy regarding fuel consumption, erosion, exhaust smoke, and energy.

### 1.4.5. Flashpoint

The flashpoint is the temperature at which a fuel evaporates adequately to ignite upon exposure to a heat source. It also sets a special flashpoint for each fuel to avoid fires. The fuel is needed for transportation and storage. Diesel fuel has a very low temperature due to its danger when transported or stored [43].

## 1.5. ENHANCING DIESEL FUEL BY ADDITIVES

The primary goal of many studies is to increase efficiency and reduce emissions from diesel engines. One of these methods is introducing nanoparticles as additives to diesel, which increases efficiency and reduces emissions. Incorporating nanoparticles into diesel results in a marked enhancement of combustion quality, augmenting engine performance [44]. Researchers have investigated the impact of diverse oxygenated compounds on biofuels to enhance the combustion and emission properties of internal combustion engines.

Incorporating metal oxide nanoparticles into the fuel mixture has augmented engine performance and combustion attributes by enhancing thermal efficiency and heat release rate. The most important advantages of metal oxides are that additional

nanoparticles can provide oxygen atoms to the fuel mixture and increase the surface size; they effectively act as a highly reactive medium during combustion [45]. In addition, the nanoparticles raise thermal conductivity, flash point temperature, and kinematic viscosity.

## 1.6. NANOMATERIAL

To begin with, the term “nano” originates from the Greek word meaning “dwarf,” and in scientific terms, it refers to one-billionth (1/1,000,000,000) of a unit. The nanometer, abbreviated as nm, is a unit of measurement equal to one billionth of a meter. To put it into perspective, one nanometer is approximately the length of a row of 13 hydrogen atoms placed side by side, as illustrated in Figure 1.6.

Nanomaterials are distinct from conventional materials because they possess unique physical, chemical, and mechanical properties, making them highly efficient and effective across various scientific applications [46]. Due to these enhanced properties, nanotechnology has become integral to different scientific disciplines, including physics, chemistry, life sciences, and applied sciences such as engineering, medicine, agriculture, environmental science, and even military technology [32].

Diesel engines, known for their high efficiency, are widely used today; however, one of their primary drawbacks is the pollution resulting from fuel combustion [46]. Nanomaterials such as aluminum oxide ($AL_2O_3$) and titanium dioxide ($TiO_2$) have been introduced as fuel additives to address this issue. These nanoparticles enhance combustion by increasing the surface area of the fuel, promoting better mixing with air, and raising the thermal energy of combustion due to their oxygen-rich composition [47].

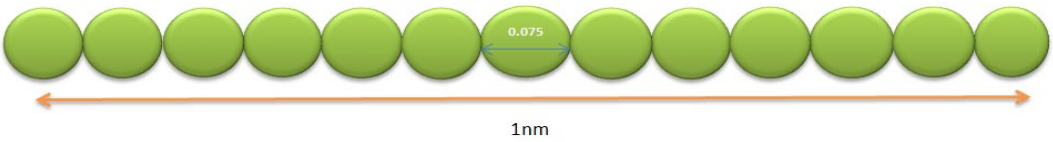


Figure 1.6. Visualizing the nanometer: hydrogen atoms in perspective

### 1.6.1. The Definition of Aluminum Oxide

Aluminum oxide, commonly known as alumina, is a chemical compound composed of aluminum and oxygen, with the formula $AL_2O_3$. Depending on its structure or intended application, it may also be referred to as alkoxide or alundum. One of the most stable crystalline forms of alumina is alpha-$AL_2O_3$, a polymorph of aluminum oxide [48].

Alumina nanofibers have attracted significant research interest due to their wide range of potential applications [49]. These include heat pipes, fuel cells, solar water heating systems, chillers, refrigerators, diesel combustion, drilling operations, lubrication processes, and thermal energy storage systems. Their versatility and superior thermal and chemical properties make them particularly valuable in advanced energy and engineering applications.

### 1.6.2. Properties

Aluminum oxide ($AL_2O_3$) has various physical and chemical properties, making it highly valuable in industrial and scientific applications. Its unique characteristics distinguish it from other ceramic materials and contribute to its widespread use in electronics, thermal management, and materials engineering. The following are some of the most notable properties of aluminum oxide [50]:

- Aluminum oxide is an electrical insulator.
- Compared to other ceramic materials, it has relatively high thermal conductivity, approximately 30 $W \cdot m^{-1} \cdot K^{-1}$.
- Aluminum oxide is insoluble in water.

- Corundum, also known as alpha-aluminum oxide, is the most common crystalline form of aluminum oxide.

### 1.6.3. Applications

Due to its high melting point, aluminum oxide is widely used and classified as a refractory material. As of 2015, global production of aluminum oxide reached approximately 115 million tons annually, with over 90% utilized in the aluminum industry. Specialty aluminum oxides are primarily employed in refractory applications, ceramics, polishing, and abrasives. Additionally, large quantities of aluminum hydroxide, derived from alumina, are used to manufacture zeolites, titanium dioxide pigment coatings, and fire and smoke retardants.

Aluminum oxide also plays a key role in various energy and thermal applications, including heat pipes, fuel cells, solar water heating systems, chillers, domestic refrigerators, diesel combustion, drilling, lubrication, and thermal energy storage [51–53].

### 1.6.4. Advantages of Nanofluids

Nanoparticles offer numerous advantages when used in heat transfer and fluid systems, particularly due to their unique physical and chemical characteristics. These benefits are especially relevant in thermal management applications, where improved efficiency and stability are essential. Key advantages include [54]:

- Their high specific surface area provides greater surface contact between particles and fluids, enhancing heat transfer efficiency.
- Their properties, including thermal conductivity, can be tailored or significantly improved.
- They reduce particle entanglement compared to conventional slurries, resulting in better flow behavior.
- They exhibit excellent dispersion stability, ensuring consistent performance over time.

## 1.7. PROBLEM STATEMENT

Utilizing water hyacinth (Eichhornia crassipes) for biofuel production presents significant economic benefits, including saving millions of dollars in removal and management costs. This invasive aquatic plant obstructs water flow and disrupts ecosystems. Before extraction, quantitative data on the distribution of water hyacinth was collected. According to the Water Treatment Directorate, the spread of water hyacinth in southern Iraq is expected to reach 900 square kilometers by 2023. This prompted a feasibility study on using biodiesel extracted from the water hyacinth plant as an alternative to conventional diesel. The study also explores the integration of aluminum oxide ($AL_2O_3$) nanoparticles to enhance fuel performance [52,53].

Key areas of investigation include:

- Experimental and theoretical analysis of the performance characteristics of compression ignition engines using biodiesel derived from water hyacinth and its blends. This includes evaluating the impact of hyacinth-based fuels on engine efficiency and combustion behavior.
- Examining the role of nanoparticles in improving biodiesel performance, particularly in reducing emissions from internal combustion engines equipped with injection pumps.
- Investigating nano-additives to enhance the chemical and physical properties of biodiesel fuel blends.
- Studying the effects of varying nanoparticle concentrations in biodiesel on key engine performance metrics, including Brake Specific Fuel Consumption (BSFC), Brake Mean Effective Pressure (BMEP), Brake Power (BP), and thermal efficiency ($\eta_t$).
- Utilizing the ANSYS Fluent 20 software to simulate and visualize temperature distribution within the combustion chamber, pressure profiles, the behavior of nanomaterials, and their interaction with the fuel.

## 1.8. OBJECTIVES

The current study aims to investigate the impact of biodiesel blends derived from water hyacinth on exhaust emissions and the performance characteristics of diesel engines. The primary objectives of this research are as follows:

- To evaluate the influence of biodiesel blends made from water hyacinth on diesel engine performance and exhaust emissions, with the addition of aluminum oxide ($AL_2O_3$) nanoparticles.
- To enhance understanding through thermodynamic analysis of diesel engines operating under full load and varying engine speeds. This includes applying the first and second laws of thermodynamics for comprehensive numerical analysis.
- To experimentally examine the effects of blending pure diesel and biodiesel with $AL_2O_3$ nanoparticles on emission components and validate the numerical findings through comparison with experimental data.
- To assess the effects of blending $AL_2O_3$ nanoparticles with diesel and biodiesel on engine performance, emission levels, and potential long-term environmental impacts.

## 1.9. OBJECTIVES AND SCOPE OF THE STUDY

This study aims to evaluate and enhance the performance and emission characteristics of compression ignition (CI) engines using biodiesel derived from water hyacinth (Eichhornia crassipes) and its blends, with the incorporation of aluminum oxide ($AL_2O_3$) nanoparticles.

The specific objectives and scope are as follows:

- To conduct experimental and theoretical analyses of CI engine performance using biodiesel extracted from water hyacinth and its mixtures with diesel fuel. The study assesses the impact of these blends on combustion characteristics and engine efficiency.

- To examine nano-additives' effects on the chemical and physical properties of biodiesel-diesel blends, including improvements in thermal conductivity, viscosity, and ignition behavior.
- To investigate the role of $AL_2O_3$ nanoparticles in enhancing biodiesel properties, particularly their effectiveness in reducing harmful emissions from internal combustion engines operating with injection pumps.
- To apply ANSYS Fluent 20 software for simulating temperature distribution, pressure fields, and the interaction between nanomaterials and fuel within the combustion chamber, offering a detailed visualization of the combustion process.
- To study the influence of varying nanoparticle concentrations on key engine performance indicators such as Brake Specific Fuel Consumption (BSFC), Brake Mean Effective Pressure (BMEP), Brake Power (BP), and thermal efficiency ($\eta_t$).
- To validate numerical simulation results with experimental findings, providing a comprehensive understanding of the impact of nanoparticle-enhanced biofuels on engine performance and environmental sustainability.

## 1.10. THESIS OUTLINE

This thesis is organized into the following six chapters:

- The first chapter presents general information about the topic. The background to the study is provided, and it begins with a discussion of environmentally friendly fuels, efficiency, and fuel economy. Nano additives are used to improve diesel fuel's physical and chemical properties and increase the combustion surface area. Problem statements, the study's objectives, and the investigation scope are also included.
- Chapter two provides an overview of the literature studies that have been carried out, as well as experimental and theoretical background on the impact of biofuels on the properties and performance of C.I. internal combustion engines with injection.

- Chapter three provides an overview of the research methodology used and experimental and numerical analysis on the impact of biofuel blends of $Al_2O_3$ nanoparticles on the properties and performance of C.I. engines and emissions.
- Chapter four describes the experimental approach and measurement tools used in experiments, uncertainty analysis, and data collection through practical programs and preparing the testing device in the combustion site.
- Chapter five presents the results and discussion for both experimental and numerical approaches and the validation of a numerical model for the main engine performance and emissions parameters.
- Chapter six records the main conclusions of the results and recommendations for future development on combustion operation in diesel engines.

# PART 2

# LITERATURE REVIEW

## 2.1. INTRODUCTION

This study has focused on the application of nanoparticle enhancers in diesel engines. These additives improve diesel fuel's combustion properties, leading to more efficient engine operation. This section aims to compile research on diesel engine performance related to nanoparticle additives [55]. Diesel fuel remains a widely used energy source in industrial operations, transportation, and electricity generation.

However, diesel fuel and coal combustion release harmful atmospheric pollutants, including sulfur dioxide and various nitrogen-based compounds. These emissions contribute significantly to air pollution and harm environmental and human health [56]. Exhaust gases often contain nitric acid, carbon dioxide, and nitrogen dioxide derivatives. If emissions from the estimated 600 million diesel-powered units globally are not properly controlled, even small urban areas can become severely polluted, experiencing reduced visibility and poor air quality [57].

Such pollutants can negatively affect respiratory health, particularly in individuals with pre-existing conditions such as asthma and bronchitis. Moreover, they pose serious threats to agricultural productivity and contribute to the degradation of the ozone layer [58,59]. Thanks to the concerted efforts of the scientific community, several strategies have been developed to mitigate these issues.

Figure 2.1 illustrates the evolution of exhaust gas treatment systems, highlighting the progression from early approaches focused solely on improving diesel combustion efficiency to more recent advancements aimed at reducing emissions and enhancing overall engine performance [60].

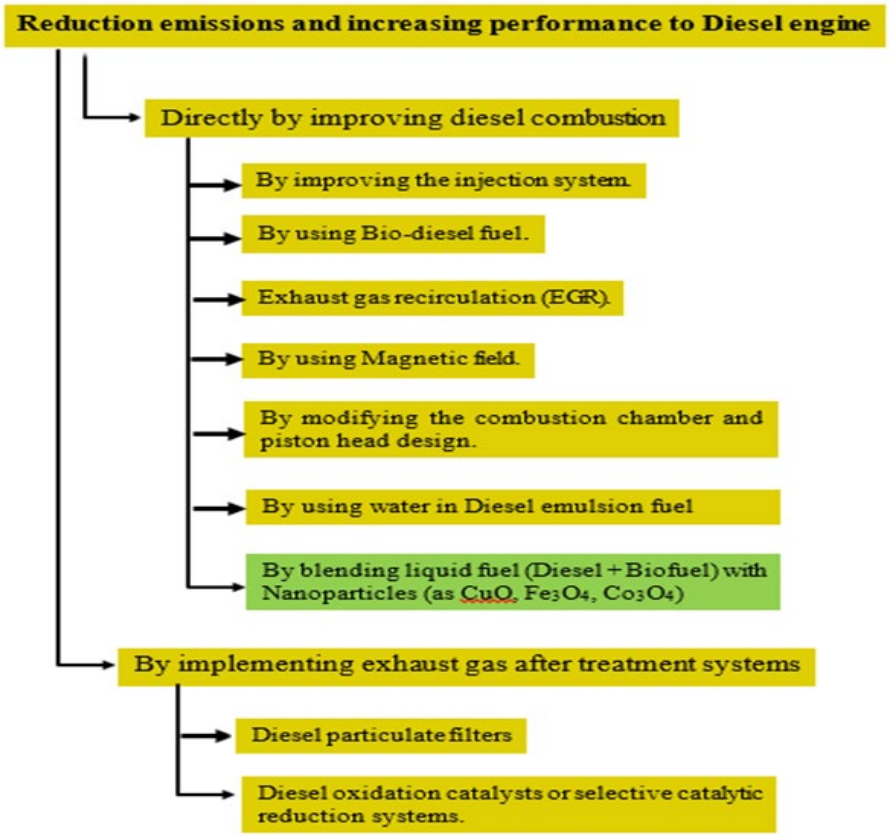


Figure 2.1. Overview of methods for improving diesel engines[60].

Incorporating nanomaterials into fuel has shown promising results in reducing specific fuel consumption, a key performance indicator that reflects the engine's efficiency in converting fuel into usable energy. The precise amount of fuel consumed can vary depending on the concentration of additives and engine load conditions. For instance, a notable reduction of 12.12% in fuel consumption (micro fuel) was observed, attributed to the nanoparticles' presence. These particles increase the fuel's calorific value slightly, thereby improving combustion efficiency and lowering specific fuel consumption. The enhanced surface area provided by the nanomaterials promotes better fuel-air mixing and ignition within the combustion chamber [61].

Figure 2.2 illustrates the application of the Takashi method, which involves natural aspiration and water cooling via direct injection, in evaluating a four-stroke, single-cylinder gasoline engine. The tested diesel engine operates using a blend of biodiesel derived from recycled oil and iron oxide nanoparticles ($Fe_2O_3$), maintaining a constant speed of 1800 rpm under varying load conditions. For experimental purposes,

biodiesel blends were prepared with additive concentrations of 10 ppm, 30 ppm, 50 ppm, 70 ppm, and 100 ppm for combustion and heating applications [60].

Figure 2.2. Single-cylinder four-stroke diesel engine [62].

Biodiesel requires government subsidies and nano-additives as a viable direct replacement for petroleum-based fuels. Biodiesel enhanced with nanoparticles is a promising alternative fuel due to its strong environmental potential and ability to power internal combustion engines effectively.

Some nanoparticles work especially well as gasoline additives. For instance, they may enhance combustion speed characteristics and decrease ignition delay time, two important aspects of engine responsiveness and fuel economy. Furthermore, flame propagation and stability may be affected by modifying combustion dynamics using nanoparticles, particularly those containing elements like lithium.

Fuel compatibility and phase separability are important considerations when blending nanomaterials with biodiesel. This thesis investigates improvements in biodiesel technology, emphasizing nanomaterials to improve fuel efficiency and environmental sustainability.

## 2.2. FINDINGS REGARDING NANOPARTICLE ADDITIVES

Researchers are increasingly interested in using additives to enhance the performance of internal combustion engines. Significant attempts have been made to improve engine efficiency and reduce exhaust emissions in future vehicle technology. Most gasoline additives are available in liquid or solid form, mainly enhancing engine performance while reducing dangerous gas emissions into the environment. Recent research has focused on novel materials, such as graphite-based additives, to improve engine performance [61].

An experiment tested the efficacy of nanoparticle-enhanced fuels using a diesel engine operating on water-diesel emulsion fuel and two kinds of alumina ($Al_2O_3$) nanoparticles. This research used a three-stage assessment approach, first assessing a water-pure diesel emulsion, then a water-diesel combination incorporating two types of alumina nanoparticles, and lastly a diesel-water emulsion with integrated alumina nanoparticles. The results showed enhanced engine performance and lower harmful emissions [63].

Concerns about the depletion of fossil fuels have increased interest in clean and sustainable energy options. Biodiesel has emerged as a prominent, environmentally friendly alternative to standard diesel, with benefits such as improved lubricity, a higher cetane number, and reduced carbon emissions. Devarajan et al. [64] examined the impact of adding 0.01 wt.% alumina nanoparticles to biodiesel derived from waste cooking oil in a single-cylinder diesel engine. The results revealed substantial improvements in thermal efficiency, brake power, and fuel consumption. Moreover, biodiesel and nanoparticles' blends significantly reduced carbon monoxide emissions, unburned hydrocarbons, and particulate matter. However, a slight increase in nitrogen oxide (NOx) emissions was observed compared to pure biodiesel.

Current research supports the potential of nanoparticle-enhanced biodiesel to improve engine performance and reduce emissions. Nonetheless, further investigation is essential to evaluate nanoparticle-infused biodiesel's long-term effects, environmental impact, and practical feasibility in commercial diesel engines [65,66].

Soudagar et al. [67] evaluated the influence of introducing aluminum oxide ($Al_2O_3$) nanoparticles into diesel engines powered by honge oil methyl esters, a form of biodiesel. While biodiesel has the potential to reduce greenhouse gas emissions and reliance on fossil fuels, it is also associated with several drawbacks, including decreased engine efficiency, increased emissions in engines not designed for light oil combustion, and poor ignition due to higher viscosity and lower heating value.

Nanoparticles have shown potential for improving engine efficiency and emissions. They increase brake-specific fuel consumption (BSFC), and lower exhaust gas temperature (EGT). Their ability to minimize emissions of carbon monoxide (CO), hydrocarbons (HC), nitrogen oxides (NOx), and smoke opacity makes them a promising choice for optimizing biodiesel combustion. However, many studies fail to account for the various impacts of nanoparticles on biodiesel types and engine setups. Fuel mix, combustion chamber shape, and injection time substantially impact combustion efficiency and emission characteristics [68]

Several research studies have looked at the use of nanoparticles to improve engine performance while reducing environmental effects [69,70]. The combustion chamber design and fuel injection time have been demonstrated to impact engine efficiency and emissions significantly. According to a current study, integrating nanomaterials, changing combustion chamber design, and improving injection timing may considerably boost performance and lower emissions. Despite the positive findings, further research is needed to determine nanoparticle-enhanced biodiesel's long-term impacts and viability in real-world diesel engines.

The addition of graphene oxide–titanium dioxide ($GO–TiO_2$) nanocomposites into diesel fuel has also been explored to enhance combustion efficiency and reduce emissions. These nanocomposites increased brake thermal efficiency and decreased BSFC [71]. Turbine engine tests revealed that these nanocomposites reduced NOx and CO emissions [72] but increased particulate matter (PM) emissions while decreasing smoke opacity. This suggests that, although nanocomposites can improve, additional tuning is required to reduce unfavorable trade-offs [73].

Hosseinzadeh-Bandbafha et al. [74]tested the impact of carbon nanoparticles combined with diesel/biodiesel emulsions on a single-cylinder, direct-injection, air-cooled diesel engine. The research looked at BSFC, brake thermal efficiency (BTE), CO, NOx, and PM emissions. The results revealed increased engine efficiency, decreased fuel consumption, and lower CO and PM emissions. However, there was a slight increase in NOx emissions. Their life cycle analysis concluded that carbon nanoparticles mitigated the environmental impacts of biodiesel use in several categories, including degradation and climate change.

Similarly, Sunil et al. [75] investigated the use of titanium dioxide ($TiO_2$) nanoparticles in biodiesel blends for CI engines. The optimal concentration of $TiO_2$ nanoparticles was approximately 50 ppm, resulting in improved fuel economy and reduced CO, HC, and smoke emissions. However, ensuring that NOx emissions do not rise is essential for maintaining environmental sustainability.

Rangabashiam et al. [76] studied the effects of aluminum oxide nanoparticles blended with diesel fuel on engine efficiency, combustion by-products, and exhaust emissions. The findings showed increased performance, including higher BSFC and brake thermal efficiency. The ignition latency was reduced, and peak cylinder pressure was raised. Nonetheless, a considerable increase in NOx emissions was detected.

Gad et al. [77] compared three distinct nanoparticles—alumina, cerium oxide, and cupric oxide—blended with Jatropha biodiesel. Their findings showed higher thermal efficiency, indicated power, and specific fuel usage. Additionally, reductions were observed in smoke opacity, CO, and HC emissions, while NOx emissions increased.

Jin et al. [78] investigated adding several nanoparticles to diesel fuel, including silicon oxide, carbon nanotubes, and aluminum oxide. They investigated combustion characteristics and emissions in a water-cooled, single-cylinder, direct-injection diesel engine with a compression ratio of 18.5:1. The findings indicated that nanoparticle-enhanced diesel fuel increased heat release rates, combustion efficiency, and ignition

delay. Furthermore, CO, HC, and smoke emissions were decreased, whereas NOx emissions slightly increased.

Perumal et al. [79] studied how copper oxide (CuO) nanoparticles combined with Pongamia methyl ester biodiesel affected diesel engine performance, combustion parameters, and emissions. The research used a single-cylinder, four-stroke, direct-injection diesel engine with a compression ratio of 17.5:1. The findings showed that adding CuO nanoparticles greatly improved engine performance, as demonstrated by increased brake thermal efficiency (BTE) and decreased brake-specific fuel consumption (BSFC). Furthermore, emissions of NOx, CO, smoke, and other exhaust pollutants were significantly reduced.

Similarly, El-Seesy et al. [80] investigated the influence of adding multi-walled carbon nanotubes (MWCNTs) into a biodiesel-diesel oil mix. The trials used a water-cooled, single-cylinder, direct-injection diesel engine with dimensions of 138 mm × 158 mm and a compression ratio of 17.5:1. The results showed that the use of MWCNTs enhanced engine performance, notably in terms of higher BTE. Additionally, specific fuel consumption (SFC) and smoke opacity decreased. However, utilizing MWCNTs resulted in greater exhaust gas temperatures and NOx emissions.

Chandrasekaran et al. [81] studied the fuel parameters of biodiesel and their influence on combustion characteristics and pollutant emissions. The research discovered that adding nanoparticles—specifically alumina ($Al_2O_3$), titanium dioxide ($TiO_2$), and cerium oxide ($CeO_2$)—significantly improved fuel characteristics, increased combustion efficiency, and decreased emissions. These results demonstrate nanotechnology's potential to improve the quality of transportation fuels and environmental sustainability. While the findings are promising, the authors emphasized the need for additional research to determine the long-term effects of higher nanoparticle concentrations in nano-diesel blends, particularly regarding engine durability and sustained emission performance.

El-Seesy et al. [82] tested diesel engines' performance, combustion, and emissions utilizing a combination of Jojoba Treat ester and diesel fuel, augmented with

aluminum oxide ($Al_2O_3$) nanoparticles. The research found that a 40:60 (v/v) blend ratio was ideal and that adding 20 ppm of nanoparticles considerably enhanced engine efficiency. Furthermore, nanoparticles improved combustion attributes by shortening ignition time and increasing combustion duration.

## 2.3. EFFECTS OF TINY CHEMICALS ON EMISSIONS AND ENGINE EFFICIENCY

Nano-additives have lately received a lot of interest due to their capacity to increase engine efficiency while lowering hazardous emissions. Several studies have examined these additives' effects on engine performance and pollutant emissions. Yaser et al. [82] adding aluminum oxide ($Al_2O_3$) nanoparticles to diesel engine fuel improved performance and reduced emissions. In the investigation, a four-stroke engine was directly fed with gasoline at a constant pressure of 400 bar, with 100 and 150 ultrasonic mixers used to ensure adequate fuel mixing. The mixed fuel produced less nitrogen oxides (NOx) and particulate matter (PM) than traditional diesel fuel.

Researchers also tested engines driven by a blend of vegetable oil-derived diesel and diesel methyl ester, especially biodiesel made from pumpkin seeds. This study examines the effects of incorporating copper oxide (CuO) nanoparticles at various concentrations (50 ppm and 100 ppm) on engine efficiency, emissions, and combustion characteristics. Previous research has shown that CuO nano-additives increase combustion efficiency and greatly decrease hazardous exhaust emissions during biofuel use[83,84].

Khan [85] conducted experiments using a blended fuel to reduce pollutant emissions under standard operating conditions of a direct-injection internal combustion engine. The engine was tested at various load levels while maintaining a constant speed. Building on previous research, the current study confirms that blends of pure diesel and biodiesel with aluminum oxide nanoparticles (ALNPs) are more effective in reducing emissions than carbon-based fuels treated with ammonium trioxide at concentrations of 40, 80, and 120 parts per million (ppm). The economic analysis further supports these findings, indicating a significant reduction in nitrogen oxide

(NOx) emissions. The fuel composition was also identified as the primary factor contributing to the most notable decrease in carbon dioxide ($CO_2$) emission.

Dharsini et al. [86] examined the effects of incorporating nano-catalytic materials into a blend of soybean-based biodiesel and conventional diesel fuel using a single-cylinder, four-stroke internal combustion engine. The study found that using $SiO_2$ nanoparticles improved brake thermal efficiency (BTE) and lowered brake-specific fuel consumption (BSFC). Furthermore, significant decreases in $CO_2$, CO, and NOx emissions were detected compared to baseline diesel fuel. The $SiO_2$ nano-additives improved combustion efficiency, resulting in these gains.

Bunyan and Abed [87] studied the potential of vegetable oils as a sustainable energy source for biodiesel manufacturing. Biodiesel may be made from several raw resources, including animal fats, non-edible vegetable oils, waste cooking oils, and other low bioenergy feedstocks. This study examined the impact of adding $CeO_2$ nanoparticles at 50 and 75 ppm concentrations to cottonseed oil-based biodiesel. To assess the influence of the nano-additives, a water-cooled, three-cylinder diesel engine was subjected to four different trial loads. The study found that increasing the concentration of $CeO_2$ nanoparticles led to higher soot emissions. This growth coincided with an increase in nitrogen oxide (NOx) emissions.

Gumus et al. [88] studied the performance of internal combustion engines using computational and experimental approaches. They focused on the impacts of $Al_2O_3$ nanoparticles combined with pure diesel fuel. A single-cylinder, four-stroke diesel engine was tested under a variety of load circumstances. Diesel fuel was mixed with $Al_2O_3$ nanoparticles at three different concentrations: 25 ppm, 50 ppm, and 100 ppm. The analysis found a slight difference of 20.2% between the two numerical methodologies. Additionally, the presence of nanoparticles led to a 2.5% reduction in smoke opacity and a substantial drop in nitrogen oxide (NOx) emissions.

Matus et al. [89]used $CeO_2/ZrO_2$ nanoparticles to improve engine efficiency and lower exhaust pollutants. The researchers combined three different nanoparticle concentrations (25 ppm, 50 ppm, and 100 ppm) with cottonseed and agarwood oil

biodiesel. The results showed that these nanoparticles increased engine performance without needing any changes to the internal combustion engine while also helping to reduce nitrogen oxides (NOx) and other pollutants. For the experimental analysis, a four-stroke diesel engine was utilized. The fuel mixes included ammonium trioxide and CZ nanoparticles at the same concentrations. The nanoparticles were distributed in the gasoline using an ultrasonic processor and a mechanical homogenizer (electric hand mixer) to guarantee adequate blending. The findings showed a 20% decrease in $CO_2$ emissions and a 12% reduction in NOx emissions. Fuel consumption dropped by 14%, and thermal efficiency improved noticeably.

Ali et al. [90] studied how different alcohol additions in blended fuels affected the cyclic variation of diesel engines. The research used a single-cylinder, four-stroke diesel engine to do trials with various mixtures of diesel fuel and alcohol, such as methanol, ethanol, and butanol. Alcohols in gasoline mixes enhanced brake thermal efficiency while lowering carbon monoxide (CO) and hydrocarbon (HC) emissions. However, the data also showed a rise in nitrogen oxide (NOx) emissions and a reduction in the amplitude of pressure changes during burning.

Ors et al. [91] examined how adding titanium dioxide ($TiO_2$) nanoparticles to diesel, biodiesel, and n-butanol mixes affected a diesel engine's performance, combustion, and emission profiles. According to the results, $TiO_2$ nanoparticles considerably enhanced engine performance and decreased emissions. This was demonstrated by improved specific fuel consumption (SFC), reduced exhaust gas temperature (EGT), enhanced brake thermal efficiency (BTE), and reduced emissions of nitrogen oxides (NOx), hydrocarbons (HC), and carbon monoxide (CO). Additionally, using nanoparticles decreased the ignition delay and boosted the heat release rate.

Kumar et al. [92] studied the performance and emission characteristics of a biodiesel-fueled engine utilizing a single-cylinder, four-stroke, air-cooled diesel engine with a compression ratio of 17.5:1. The studied fuels comprised B20, a combination consisting of 80% diesel and 20% biodiesel, as well as B20 combined with aluminum oxide ($Al_2O_3$) nanoparticles at concentrations of 50 ppm, 100 ppm, and 150 ppm. Brake-specific fuel consumption (BSFC), exhaust gas temperature, and brake thermal

efficiency (BTE) measures were among the performance studies that showed that B20 gasoline supplemented with aluminum oxide nanoparticles produced better results than B20 alone.

Nithya et al. [93] investigated the effects of titanium dioxide ($TiO_2$) nanoparticles on the performance and emissions of a single-cylinder diesel engine fueled with various blends of canola biodiesel. The results demonstrated that adding nanoparticles reduced carbon monoxide (CO) and particulate matter (PM) emissions, with the most significant decrease observed in the 20% biodiesel blend containing 0.1% $TiO_2$ nanoparticles. However, the study also noted increased nitrogen oxide (NOx) emissions.

Ramesh et al. [94] conducted a study using a single-cylinder, four-stroke, direct-injection diesel engine, achieving a maximum power output of 3.7 kW at 1500 revolutions per minute. The incorporation of alumina ($Al_2O_3$) nanoparticles into biodiesel/diesel blends derived from poultry dung significantly improved engine performance and combustion characteristics. As a result, notable reductions were observed in the emissions of carbon monoxide (CO), hydrocarbons (HC), and particulate matter (PM). However, nitrogen oxide (NOx) emissions remained largely unchanged. An energy and exergy analysis of the nanoparticle-enhanced engine indicated that the observed energy and exergy efficiency improvements were primarily attributable to alumina nanoparticles. The study above also examined the impact of various nano-additives—including alumina, copper oxide (CuO), and titanium oxide ($TiO_2$)—on engine performance and emissions. The results revealed that nano-additives enhance fuel combustion efficiency while reducing CO, HC, and particulate pollutants. However, the effectiveness of these improvements was found to depend significantly on the morphology (topography) of the nanoparticles used and the specific composition of the fuel blends.

## 2.4. THE IMPACT OF THE CATALYST ON THE EFFICIENCY AND EMISSIONS OF DIESEL-BIODIESEL COMBINATIONS

As environmental awareness continues to grow, the use of biodiesel as an alternative to conventional diesel fuel is also increasing. However, biodiesel-diesel blends often fall short of pure diesel in terms of performance and emission characteristics. Chemical catalysts can potentially improve both the efficiency and emission profiles of these fuel mixtures. The following sections of this study explore the influence of catalysts on the performance and emissions of diesel-biodiesel blends.

Wu et al.[95] used ultrasonic mixing methods to add carbon-coated aluminum (Al-C) nanoparticles to diesel-biodiesel blends to examine fuel additives' impact on engine performance and emissions. Three kinds of fuel were evaluated in the experiments, which were conducted using a diesel engine. 4% ethanol and 20%, 30%, and 50% quantities of aluminum oxide ($AlO_3$) nanoparticles were included in one of the mixes. The load was changed throughout the testing, but the engine speed remained constant. The findings unequivocally showed that the use of $AlO_3$ nanoparticles decreased fuel consumption, particularly in brakes.

Hosseini et al. [96] used biodiesel blends enriched with alumina ($AlO_3$) nanoparticles as a catalytic additive to study a compression ignition engine's performance and emission characteristics. The research discovered that at an alumina concentration of 50 ppm, the optimum brake thermal efficiency (BTE) was improved. Specific fuel consumption (SFC) and carbon monoxide (CO) emissions decreased with the addition of alumina nanoparticles, although nitrogen oxide (NOx) emissions slightly increased. Additionally, the improved performance of the gasoline combined with nanoparticles was better than that of the base fuel alone, especially in lower emissions of suspended particulate matter (PM) and smoke.

Ong et al. [97] examined the manufacturing procedure and characterization of biodiesel made from a blend of two inedible oils—Pentandra and Calophyllum epiphyllous—using a two-step transesterification process. Methanol and potassium hydroxide were used as catalysts in the process. Ninety minutes of reaction time, 60°C,

and a 9:1 methanol-to-oil molar ratio were found to be the ideal parameters for the generation of biodiesel. The maximum biodiesel output of 95.8% showed a comparatively high conversion efficiency.

Bitire et al. [98] used both homogeneous and heterogeneous catalysts to study the catalytic conversion of parsley seed oil (PSO) to biodiesel. The goal of the research was to increase the output of biodiesel by using calcium oxide (CaO), a heterogeneous catalyst. A reaction temperature of 65°C, a reaction duration of 4 hours, and a catalyst concentration of 4% with 0.75 weight percent were found to be the ideal parameters for the generation of biodiesel.

Bitire et al. [99] used potassium hydroxide (KOH) as a catalyst to study biodiesel synthesis from parsley seed oil. Optimizing the manufacturing process and assessing the quality of the finished biodiesel product were the two primary stages of the study. A catalyst concentration of 0.6% (w/w), a methanol-to-oil molar ratio of 6:1, and a reaction period of 60 minutes were the ideal parameters for biodiesel synthesis. A yield of 93.6% biodiesel was produced under these circumstances.

Parida et al. [100] investigated a direct-injection compression ignition engine fueled with a diesel blend of titanium dioxide ($TiO_2$) nanoparticles and Karanja biodiesel for performance and emissions characteristics. According to the results, $TiO_2$ nanoparticles improved brake thermal efficiency and reduced exhaust gas temperatures. However, adding nanoparticles also increased carbon monoxide (CO) emissions, which may indicate a breakdown in the combustion process and a decrease in combustion completeness. However, due to the nanoparticles, there was a significant decrease in nitrogen oxide (NOx) emissions, which was explained by the reduced oxygen availability in the combustion chamber. Particulate matter (PM) emissions were further reduced because the $TiO_2$ nanoparticles acted as a catalyst, promoting the oxidation of soot particles and further reducing emissions.

Keera et al. [101] studied biodiesel production from castor oil, focusing on optimizing the production process. The experiment evaluated several key factors influencing biodiesel yield, including reaction time, temperature, methanol-to-oil molar ratio, and

catalyst concentration. In addition to yield, the researchers analyzed the physical and chemical properties of the produced biodiesel, including density, kinematic viscosity, flash point, pour point, and calorific value. The results indicated that the biodiesel met ASTM standards and exhibited properties comparable to conventional diesel fuel. Based on these findings, castor oil is a promising feedstock for biodiesel production.

Ala'a et al. [102] studied the pyrolysis and hydro-treatment of waste pits to produce green diesel and jet fuel fractions. The results showed that green diesel yield increased with higher reaction temperatures, although product selectivity decreased. An optimal reaction temperature of 325°C was identified, yielding a 15% increase in product weight and a 50% improvement in fuel quality for specific applications when catalyst loading and reaction pressure were properly adjusted. The fuel properties of the resulting products were found to comply with ASTM D975 and ASTM D1655 standards, indicating their suitability as alternatives to conventional gasoline and jet fuel. Furthermore, the study included an economic assessment, concluding that the process could be financially viable if crude oil prices exceeded $70 per barrel.

## 2.5. OPTIMIZATION OF ENGINE PARAMETERS AND BIODIESEL PRODUCTION

To lessen the negative environmental effects of fossil fuels, optimizing both engine operating parameters and biodiesel manufacturing procedures is crucial. The ideal circumstances that maximize engine performance while reducing emissions have been the subject of several research studies. This area of study focuses on how several parameters, including compression ratio, injection time, and fuel characteristics, affect engine efficiency and pollution production. Increasing the output and quality of biodiesel fuels also entails improving biodiesel manufacturing methods like transesterification and esterification.

Fattah et al. [103] investigated the influence of antioxidants on the oxidative stability of biodiesel derived from both vegetable and animal oil feedstocks. The results showed that ascorbic acid and tocopherol were the most effective in enhancing oxidative stability. Among synthetic antioxidants, butylated hydroxytoluene (BHT) performed

better than tert-butylhydroquinone (TBHQ), although its effectiveness varied depending on the type of feedstock used. Furthermore, the study noted that antioxidants can reduce the formation of toxic compounds generated during the biodiesel oxidation process. The researchers concluded that improving biodiesel's oxidative stability through antioxidants can significantly enhance the fuel's shelf life and overall quality.

Parmar et al. [104] studied a single-cylinder, four-stroke diesel engine that was used for numerical experiments using Minitab statistical software. The research investigated the effects of key operational parameters—including mixing ratio, compression ratio, injection pressure, and engine load—on engine performance and fuel consumption. Specifically, the study was evaluated using a 50:50 blend of palm oil biodiesel and conventional diesel under naturally aspirated conditions. It was observed that these operational variables significantly affected engine performance and specific fuel consumption. As the number and levels of influencing factors increased, so did the number of potential model combinations for optimization.

Agrawal et al. [105] aimed to improve a compression ignition engine's performance and emission characteristics by using biodiesel–alcohol blends. The optimal fuel mixture demonstrated enhanced engine efficiency and significantly reduced exhaust emissions compared to conventional diesel fuel. Specifically, emissions were reduced by up to 41% for carbon monoxide (CO), 40% for hydrocarbons (HC), and 35% for nitrogen oxides (NOx), primarily due to the presence of alcohol in the blend, which contributed to cleaner combustion. The study emphasized that the efficiency and cost-effectiveness of fuel blends can be greatly improved by applying advanced optimization techniques such as the Taguchi method, multiple regression analysis, or artificial neural networks.

Figure 2.3 presents the layout of the experimental setup conducted by Raja et al. [106]on a biodiesel-fueled direct injection engine. The study involved comprehensive energy and exergy analysis and multi-objective optimization. It was found that the use of biodiesel significantly influenced engine performance parameters. However, two major challenges associated with biodiesel use were identified: its lower calorific value

and higher viscosity than conventional diesel. To address these issues, the study focused on optimizing key engine parameters, including compression ratio, injection timing, and fuel injection pressure. The Taguchi method was employed to determine the optimal settings for operating a direct injection engine using biodiesel fuel. Interestingly, adding carbon nanotubes had a more pronounced effect on engine performance and emission characteristics than diesel alone.

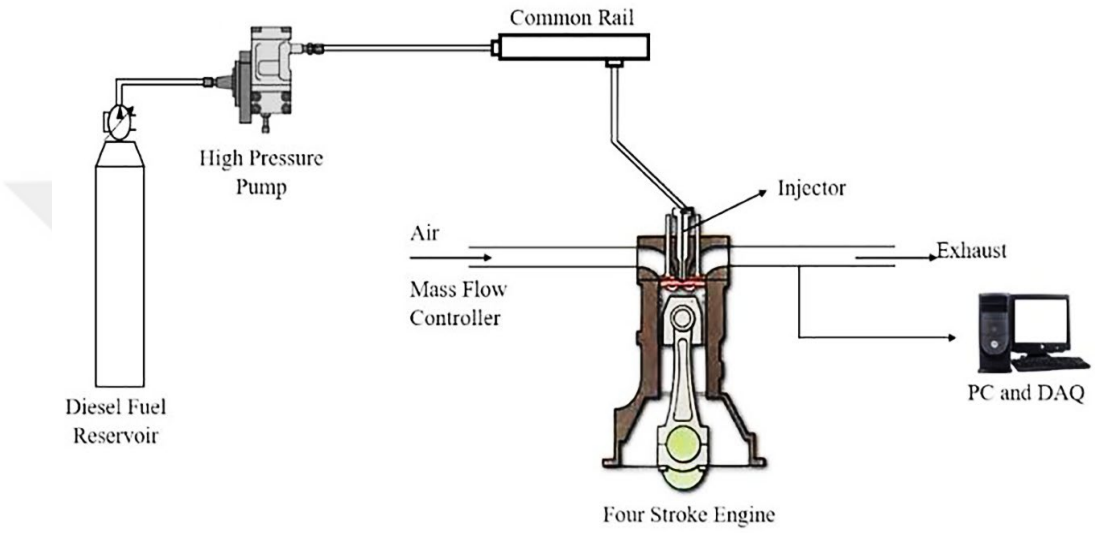


Figure 2.3. Layout of the experimental setup[106].

## 2.6. THE IMPACT OF NON-CONVENTIONAL DIESEL FUELS ON ENGINE EFFICIENCY AND POLLUTANT EMISSIONS

Growing awareness of environmental degradation and the finite supply of fossil fuels has increased interest in alternative diesel fuels. Options such as biodiesel, sustainable diesel, and bio-petrol have been widely studied for their impact on engine efficiency and emissions. This review examines the effects of using non-conventional diesel fuels on engine performance and pollutant output.

Asokan et al. [107] evaluated the performance and emission characteristics of a diesel engine fueled with kapok methyl ester (KME) blended with conventional diesel. The results demonstrated that KME improved brake thermal efficiency (BTE) across various load conditions, with the most significant gains observed at higher loads.

Additionally, KME contributed to a reduction in smoke opacity and nitrogen oxide (NOx) emissions. However, at elevated loads, hydrocarbon (HC) and carbon monoxide (CO) emissions from KME–diesel blends were higher than those from pure diesel. Despite this drawback, the authors concluded that KME represents a promising alternative fuel for diesel engines.

Datta and Mandal [108] conducted a study in 2017 to evaluate the performance, combustion, and emission characteristics of a compression-ignition engine fueled with various alcohol–biodiesel blends. The investigation involved mixing diesel fuel with three types of biodiesel, palm, jatropha, and mustard, and three types of alcohols, methanol, ethanol, and butanol, at blend ratios ranging from 10% to 30%. The results indicated a general decrease in brake thermal efficiency and an increase in specific fuel consumption across all blends compared to pure diesel. Although NOx emissions increased, the rise was offset by significant reductions in carbon monoxide (CO), hydrocarbons (HC), and sulfur oxides (SOx), resulting in an overall decline in harmful emissions. Among the tested blends, the mixture containing 20% biodiesel (from palm or jatropha) and 10% butanol had the least adverse effect on brake thermal efficiency.

Aliyu et al. [109] investigated the performance and emission characteristics of a diesel engine fueled with Croton megalocarpus methyl ester (CME) blended with conventional diesel fuel. The study evaluated blends containing 20%, 40%, 60%, and 80% CME. Compared to pure diesel, the CME–diesel blends resulted in reduced engine power output and brake thermal efficiency. However, they also led to notable decreases in emissions of carbon monoxide (CO), unburned hydrocarbons (HC), and particulate matter (PM). Interestingly, increasing the CME content further reduced CO, HC, and PM emissions, but the improvements became less pronounced at higher blend ratios. Additionally, the study reported a net increase in nitrogen oxide (NOx) emissions across all blends.

Jado and Pan [110] conducted a study to evaluate a diesel engine's performance and emission characteristics fueled with Jatropha biodiesel and its blends under varying engine loads. The experimental results indicated that increasing the proportion of biodiesel in the fuel blends led to reductions in brake power, air-fuel ratio (AFR), brake

thermal efficiency (BTE), volumetric efficiency (VE), and brake-specific fuel consumption (BSFC). The study observed an increase in the total emissions of carbon dioxide ($CO_2$) and nitrogen oxides (NOx) with higher biodiesel content. However, specific $CO_2$ emissions (per power output unit) were reduced.

Masera [111] conducted a study using a three-cylinder, in-line, four-stroke direct-injection diesel engine to investigate the effects of biodiesel derived from various sources as an alternative to fossil diesel fuel. The study aimed to address the challenges related to engine performance and emissions by evaluating the combustion and emission characteristics of biodiesel blends. For the experiments, biodiesel was produced from diverse feedstocks, including sheep fat, chicken fat, and waste cooking oil. These components were blended in varying proportions. The findings revealed that when mixed with plant-based biodiesel or waste cooking oil, biodiesel derived from animal fats resulted in fuel blends with different combustion behaviour than pure diesel. Specifically, blends with lower levels of unsaturation exhibited shorter combustion durations and an earlier high-temperature combustion phase.

Gao et al. [112] focused on applying hydrogen fuel in internal combustion engines due to its carbon-free nature and potential to achieve high thermal efficiency with minimal emissions. Hydrogen is considered one of the most promising alternative fuels, as it can be introduced into internal combustion engines while offering superior thermal performance and a cleaner exhaust profile. However, the use of hydrogen presents several technical challenges. Poor fuel-air mixing in hydrogen-injected engines can lead to abnormal combustion phenomena, such as backfiring.

Udayakumar and Kasiraman [113] conducted a study to evaluate the use of a fuel blend of turpentine oil and cottonseed oil ester as an alternative fuel in internal combustion engines. The research aimed to investigate both engine performance characteristics and the effects of varying injection pressures on exhaust gas emissions. Suitable diesel engine models were selected for testing, specifically a four-stroke, water-cooled diesel engine operating at a constant speed of 1500 rpm. The experiments involved testing various blend ratios of turpentine oil, ranging from 20% to 50%, each formulated with high-quality fuel components to ensure performance consistency. The results revealed

that an injection pressure of 210 bar yielded the most favorable outcomes among the pressures tested.

Özgür [114] focused on optimizing biodiesel production from used cooking oil and evaluating the performance of a diesel engine operating on the resulting biodiesel. According to the findings, the optimal biodiesel yield was achieved using a catalyst concentration of 1.1%, a methanol-to-oil molar ratio of 6.2:1, and a reaction time of 50 minutes. Engine tests showed that biodiesel produced under these conditions delivered power and torque comparable to conventional diesel fuel. However, it exhibited slightly higher brake-specific fuel consumption (BSFC) and increased smoke emissions from the exhaust.

Feng et al. [115] evaluated the effectiveness of aftertreatment systems in reducing emissions from marine diesel engines. The research focused on using various alternative fuels—including methanol, liquefied natural gas (LNG), and biofuels such as biodiesel and bioethanol—and their influence on overall emission profiles. The study found that treatment technologies such as Selective Catalytic Reduction (SCR) and Exhaust Gas Recirculation (EGR) were effective in lowering nitrogen oxide (NOx) emissions. However, these systems had limited effectiveness in reducing other harmful pollutants, such as particulate matter and unburned hydrocarbons.

Xiao et al.[116] studied the flame combustion characteristics and pollutant emissions of a diesel engine fueled with a blend of isobutanol and biodiesel. The experiments used a single-cylinder diesel engine with a common rail injection system. The results showed that the isobutanol–biodiesel blends exhibited improved brake thermal efficiency (BTE) and reduced specific fuel consumption (SFC) compared to pure biodiesel or conventional diesel fuel. However, the increased oxygen content in the blend led to higher combustion temperatures and pressures, resulting in a notable rise in nitrogen oxide (NOx) emissions.

Biodiesel, renewable diesel, and biogas were the subjects of a number of studies that looked at how they affected engine performance and emissions from diesel engines. In addition, its researchers aimed to find out how such fuels influence gasoline

consumption and emissions. Several pollutants, including fine particles, hydrocarbons, nitrogen oxides, and carbon monoxide, can be decreased, according to the study, by switching to alternative diesel fuels. On the other hand, of course certain alternative fuels lead to increased nitrogen oxide emissions too. The studies also indicate that to achieve an optimal alternative-fuel performance, some modifications might be vital for engines.

Numerous studies have also explored the effects of alternative fuels, such as biodiesel, renewable diesel, and biogas, on engine performance and emissions. These studies aimed to determine how such fuels influence fuel consumption and pollutant emissions. Overall, findings suggest that alternative diesel fuels can reduce several pollutants, including particulate matter, hydrocarbons, nitrogen oxides, and carbon monoxide. However, some alternative fuels have also been associated with increased NOx emissions, indicating the need for careful fuel formulation and engine calibration.

The reviewed literature includes extensive research efforts to enhance engine performance and reduce emissions. Promising approaches include nanoparticle additives, such as copper and carbon nanotubes, which have demonstrated potential to improve combustion efficiency and lower emissions. Nonetheless, further investigation is needed to understand the long-term effects of these additives on engine durability and environmental safety.

Moreover, combining diesel and biodiesel with appropriate catalytic agents has significantly reduced harmful emissions. However, identifying the optimal type and concentration of catalyst for different engine types and fuel blends remains a key area for future research. Similarly, optimizing biodiesel production processes and fine-tuning engine operating parameters have yielded encouraging results, but further refinement is necessary to ensure compatibility across various engine platforms and fuel compositions.

Finally, alternative fuels such as biogas, ethanol, hydrogen, and hydropower-derived fuels present considerable potential for reducing dependence on fossil fuels and lowering pollutant emissions. While these alternatives show promise for improving

engine efficiency and environmental outcomes, comprehensive research is still required to support their widespread implementation in commercial diesel engines.

## 2.7. SUMMARY

Based on the findings from the aforementioned literature review, the following conclusions can be drawn:

- The addition of nano-additives to fuel significantly enhances the amount of energy released during combustion and contributes to notable improvements in engine performance. Typically, treating fuel with nanoparticles leads to a reduction in both pollutant emissions and fuel consumption. Compared to modifications involving diesel fuel alone, including various nanoparticles, induce more substantial changes to the fuel's microstructure.
- Diesel engines utilizing nanoparticle-enhanced fuel have shown a reduction in fuel consumption ranging from 9% to 13%, outperforming other modification methods, which achieved up to 8% reductions. As illustrated in Figure 2.4(a), nano-additives reduced fuel usage by 56%, while conventional diesel fuel achieved a 44% reduction. Furthermore, the integration of nanomaterials into diesel fuel improved its overall quality, resulting in a decrease in harmful emissions. This outcome is depicted in Figure 2.4(b), which demonstrates the emission-reducing benefits of nanoparticle-enhanced fuels.

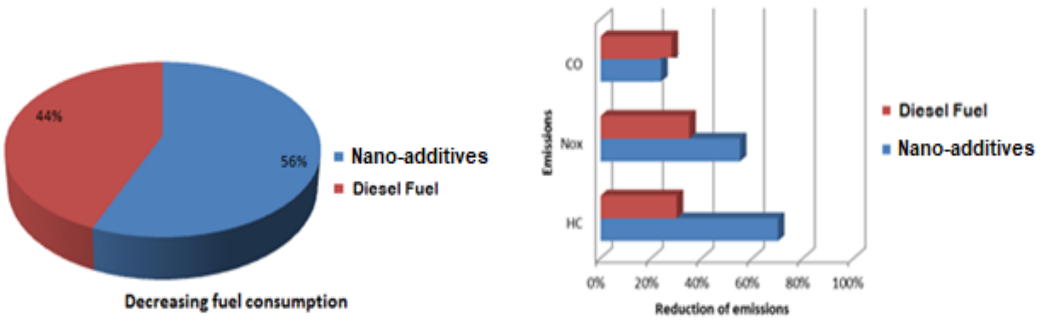


Figure 2.4. The use of various types of nano-additives and their effects on (a) fuel consumption and (b) exhaust emissions.

# PART 3

# RESEARCH METHODOLOGY AND NUMERICAL ANALYSIS

## 3.1. INTRODUCTION

Internal combustion engine behaviour, performance, and structural integrity may be thoroughly studied utilizing IC Engine simulation using ANSYS Fluent and ANSYS Mechanical (Static Structural) software. These two software modules, a component of the ANSYS package, IC engine fluent, cater to many areas of engine simulation by integrating structural evaluation and fluid dynamics analysis to provide a comprehensive knowledge of engine operation and interactions with the environment. The complicated fluid movement, heat transport, combustion, and structural stresses in internal combustion engines make them complex systems.

## 3.2. METHODOLOGY

In Figure 3.1, the details of the research methodology were explained step by step. In the first step, the objectives of the research work were determined (four step) and theoretical calculations were made to find the thermal efficiency, fuel consumption rate, the force acting on the piston inside the cylinder and emissions, as well as finding the lowest emission of unburned hydrocarbons and the lowest unburned nitrogen oxides. In the second step, the addition of biodiesel (extracted from water hyacinths) to pure diesel fuel was chosen, as well as the addition of nanomaterials from ($AL_2O_3$) in different proportions, to improve engine performance and reduce gaseous emissions resulting from the combustion process. The third step, where the experiments were conducted using the Ansys Fluent program and all information was entered into the program, including engine data, chemical and physical properties of the nanomaterials, biodiesel, and pure diesel. The four steps are comparing the practical and theoretical results and verifying the validity of the results.

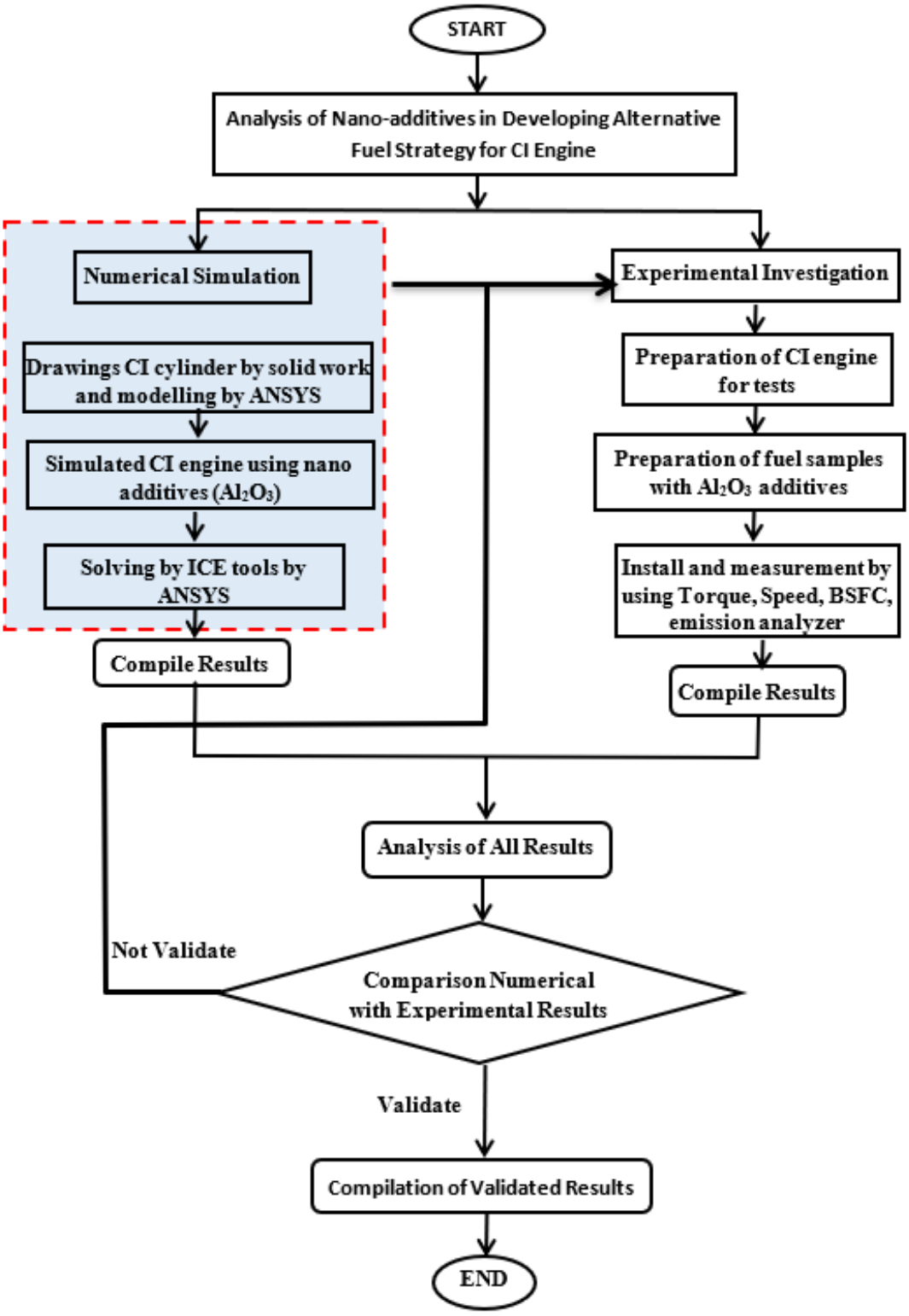


Figure 3.1. Research methodology flow chart

## 3.3 NUMERICAL ANALYSIS

Internal combustion engine behaviour, performance, and structural integrity may be thoroughly studied utilizing IC Engine simulation using ANSYS Fluent and ANSYS Mechanical (Static Structural) software. These two software modules, a component of the ANSYS package, IC engine fluent, cater to many areas of engine simulation by integrating structural evaluation and fluid dynamics analysis to provide a comprehensive knowledge of engine operation and interactions with the environment. The complicated fluid movement, heat transport, combustion, and structural stresses found in internal combustion engines make them complex systems.

### 3.3.1. IC Engine Fluent

Considered IC Engine Fluent, a specialized computational method in the ANSYS software, can simulate the fluid dynamics and combustion processes of internal combustion engines. It provides scientists and engineers with a comprehensive platform to assess and enhance the efficiency, emissions, and performance of many internal combustion engine types used in automotive, aerospace, and industrial applications. Internal combustion engines are complex devices that produce mechanical work by burning fuel in a small space. The fluid dynamics inside these engines significantly determine their temperature, pressure, and velocity. Figure 3.2

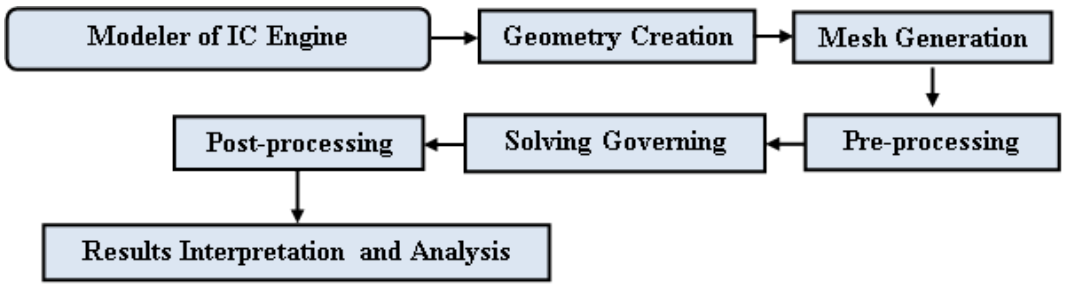


Figure 3.2. Numerical analysis flowchart.

### 3.3.1.1. Geometry Creation

With IC Engine Fluent, users may create complex 3D geometries for cylinders, pistons, valves, and combustion chambers, among other engine components. The correctness of the geometry modelling ensures the accuracy of the simulation results. However, as illustrated in Figure 3.3, the combustion chamber's dimensions were developed, considering previous research on crankshaft length, piston diameter, and other variables.

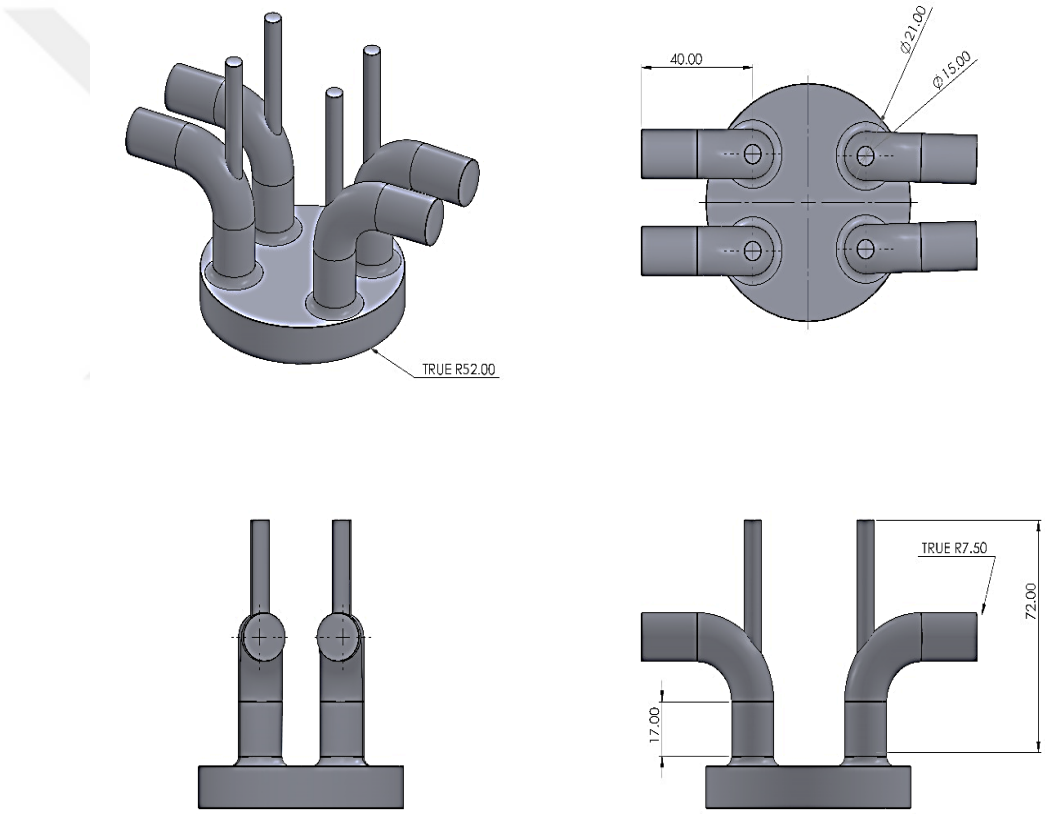


Figure 3.3. Internal combustion design.

Upon input, the internal combustion chamber model is converted into a geometry suitable for simulation to derive results, as depicted in Figure 3.16, after the entry of requisite data, as shown in Figure 3.4.

| | |
|---|---|
| Slice | InputManager2 |
| Decomposition Position | IVC |
| Decomposition Angle | 570 ° |
| Sector Decomposition Type | Complete Geometry |
| Cylinder Liner Faces | 1 Face |
| Sector Angle | 60 ° |
| Validate Compression Ratio | Yes |
| Compression Ratio | 21 |
| Crevice H/T Ratio | 3 |
| Spark Points (Optional) | Not selected |
| **IC Valves Data 1 (RMB)** | |
| Valve Bodies | 4 Bodies |
| Valve Seat Faces | 4 Faces |
| **IC Injection 1 (RMB)** | |
| Spray Location Option | Height and Radius |
| Spray Location,Height | 0.02 mm |
| Spray Location,Radius | 0.02 mm |
| Spray Direction Option | Spray Angle |
| Spray Angle | 70 ° |
| **IC Advanced Options (RMB)** | |

Figure 3.4. Input manager

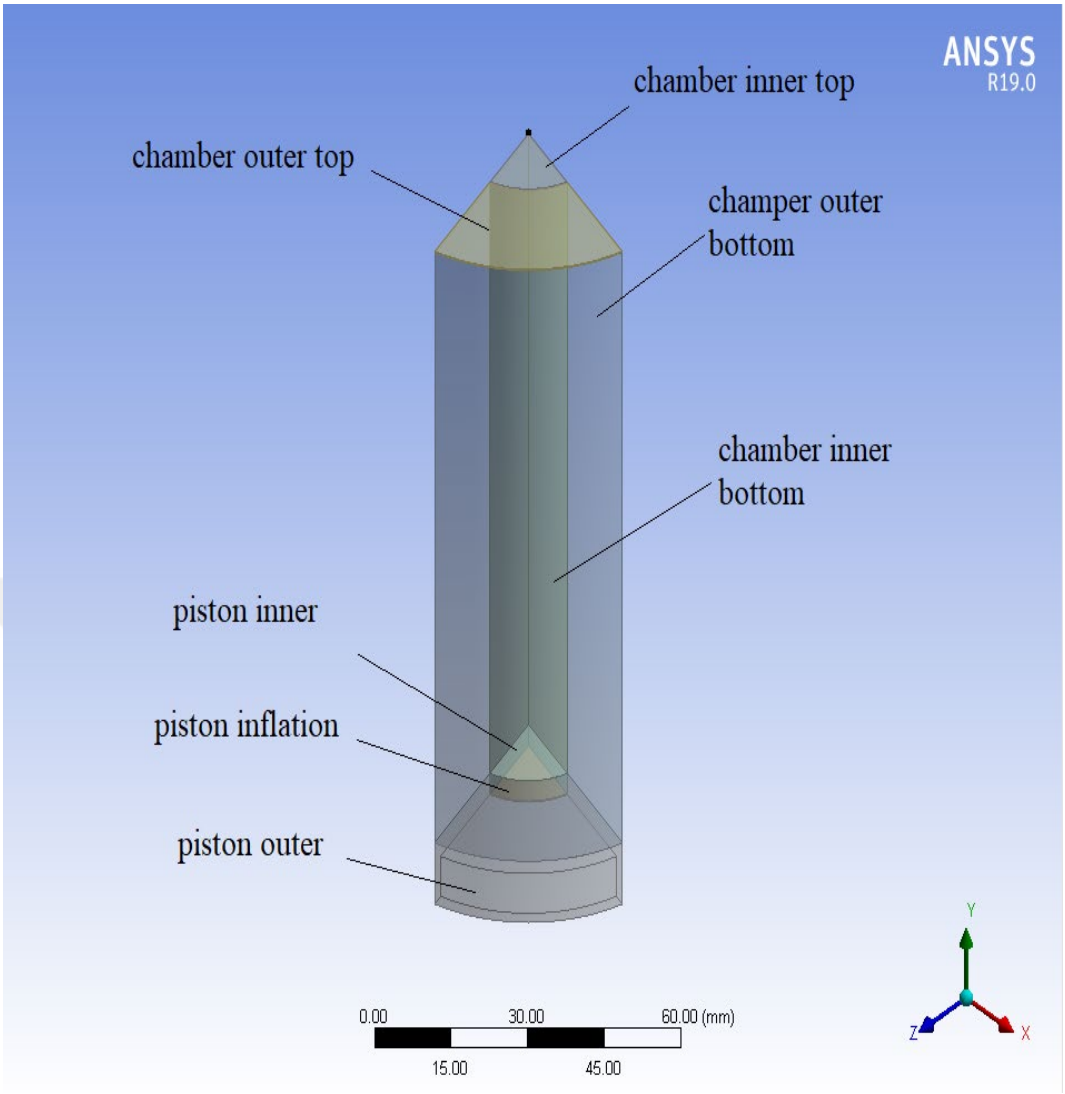


Figure 3.5. IC engine domain.

Where parameters including crankshaft length 115 mm and minimum lift 0.2 mm are entered directly, the inlet valve (IVC) is closed at 570 degrees, while the exhaust valve (EVO) is opened at 833 degrees.

### 3.3.1.2. Mesh Generation

Structured hexahedral grids were chosen for this study due to their effectiveness in handling complex geometries. ANSYS facilitates solid geometry mesh generation, three-dimensional modelling, and IC engine simulations. The study utilized 2,062,218 cells, as shown in Figure 3.6 and Table 3.1.

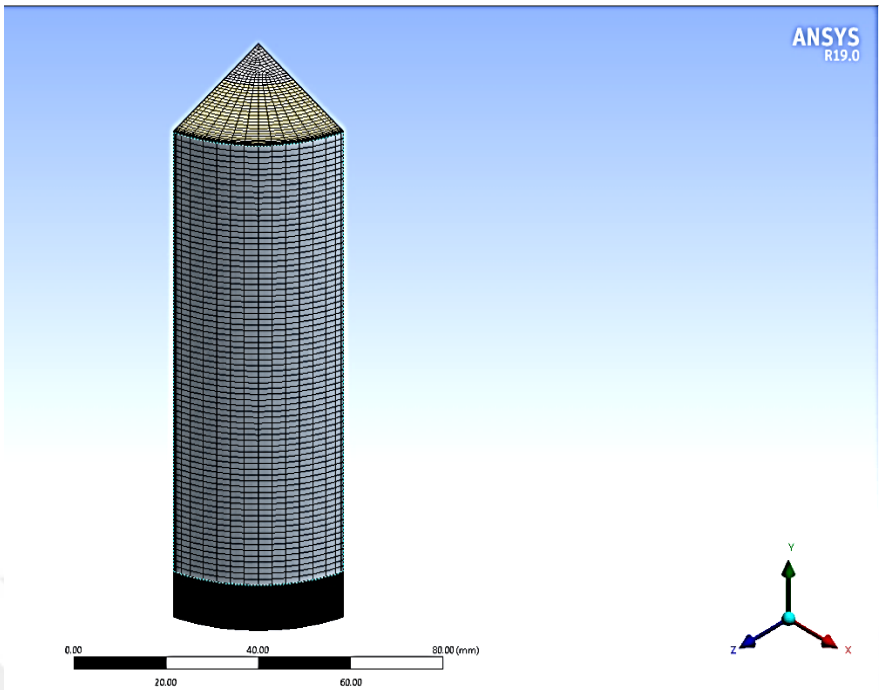


Figure 3.6 IC cylinder mesh generated.

The mesh must be independent to ensure accurate and reliable results, as shown in Figures 3.6 and 3.7(Generative mesh). The process involved analyzing the differences in the output as the number of elements changed and stopped once the results were stable. In this study, an element size of 0.001 m was used.

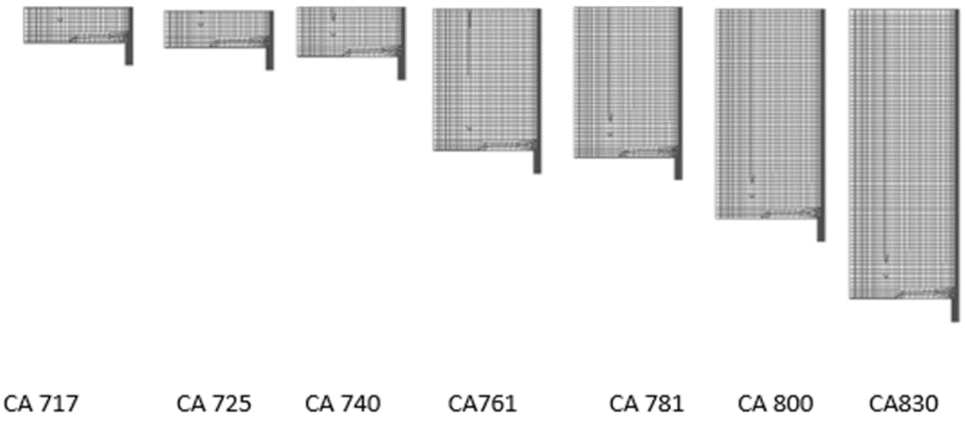


Figure 3.7. CI engine domain and Mesh generated.

Table 3.1. Mesh independence.

| Case | Element | Node | Max. temperature (K) |
|---|---|---|---|
| **1** | 1405636 | 1711567 | 961 |
| **2** | 1612356 | 1967825 | 949 |
| **3** | 1805436 | 2056732 | 946 |
| **4** | 2062218 | 2256711 | 945 |

### 3.3.1.3. Physics Setup

ANSYS Fluent is often used for fluid flow simulations, which is relevant for IC engine simulations. Set up the physics by specifying the appropriate boundary conditions, material properties, and modelling assumptions. For an IC engine simulation, we must define the fluid properties, combustion model, turbulence model, heat transfer, and other relevant parameters, as shown in Figure 3.8.

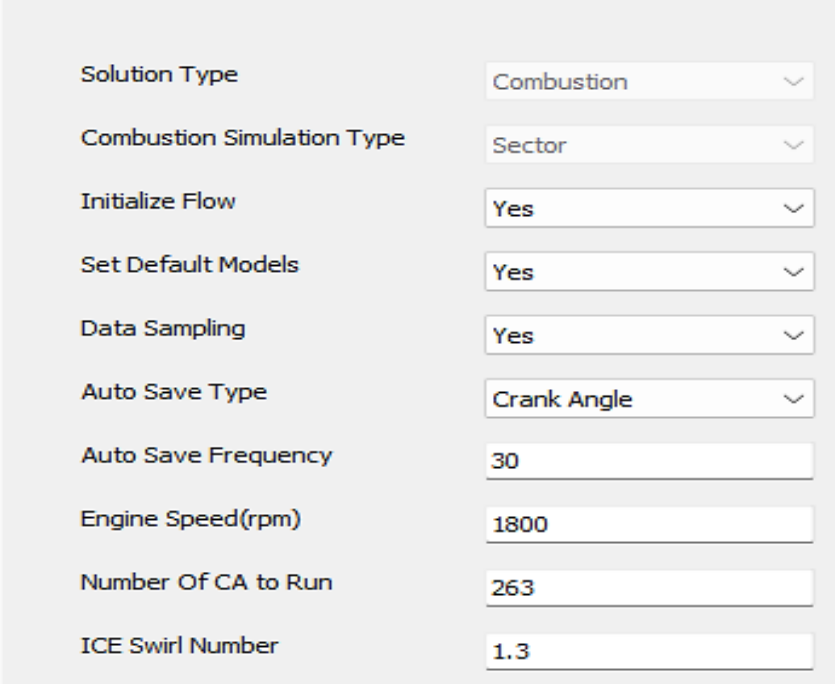


Figure 3.8. Physics setup.

### 3.3.1.4. Boundary Conditions

Setting boundary conditions is essential to creating an accurate and realistic internal combustion engine simulation using ANSYS Fluent. They are crucial in describing how the engine interacts with its environment and behaves.

Table 3.2. Boundary conditions.

| Name | Type | Value |
|---|---|---|
| ice-sector-top-faces | Wall temperature | 602 K |
| ice-piston | Wall temperature | 645 K |
| ice-cyl-piston | Wall temperature | 567 K |
| ice-cyl-chamber-top | Wall temperature | 567 K |
| ice-cyl-chamber-bottom | Wall temperature | 567 K |

The engine speed will be changed from 1150, 1400, 1600, and 1800 RPM. Biodiesel and Nanoparticle $Al_2O_3$ will also be added at 50, 100, and 150 ppm, depending on the properties reviewed in tables 3.3, 3.4, and 3.5.

### 3.3.2. Fuel Properties

Table 3.3. Fuel properties.

| No. | Property | Unit | Diesel | Biodiesel | Biodiesel (D80B20) |
|---|---|---|---|---|---|
| 1 | Density at 15 °C | g/cm³ | 0.823 | 0.8794 | 0.8325 |
| 2 | Carbon Residue (on 10 % Residue) | % m/m | 0.08 | 2.145 | 0.036 |
| 3 | Flash point | °C | 62.5 | Flammable | Flammable |
| 4 | Pour point | °C | < -21 | -3 | -21 |
| 5 | Cetane Index | ---- | 52.6 | 44.3 | 52.2 |
| 6 | Calorific Value (**Gross**) | Kcal/Kg | 10976 | 10774 | 10945 |
| 7 | Calorific Value ( **Net** ) | Kcal/Kg | 10288.6 | 10129 | 10262 |
| 8 | Viscosity @ 40 °C | Mm²/s | 2.16 | 7.6 | 8 |

Table 3.4. $Al_2O_3$ property.

| NO | Property | $Al_2O_3$ |
|---|---|---|
| **1** | Density(g/cm³) | 3.97 |
| **2** | Assay % | 99.5 % |
| **3** | Grain size(nm) | 50 |
| **4** | Color | White |
| **5** | Melting point | 2040 |
| **6** | Molar weight(g/mol) | 101.96 |
| **7** | CAS Number | 1344-28-1 |

Table 3.5. Calorific value of the sample.

| NO. | Sample | Density @ 15 °C | Sp. Gr. @15.6 °C | Calorific value(Kcal/Kg) Net | Calorific value(Kcal/Kg) Gross | Cetane Index |
|---|---|---|---|---|---|---|
| **3** | D80B20N50($AL_2O_3$) | 0.8315 | 0.8319 | 10265.5 | 10946.679 | 52.4 |
| **6** | D80B20N100($AL_2O_3$) | 0.8318 | 0.8322 | 10264.7 | 10945.63 | 52.7 |
| **7** | D80B20N150($AL_2O_3$) | 0.8326 | 0.8330 | 10262.5 | 10942.833 | 52.9 |

### 3.3.3. Combustion Modelling

Continuity equation:

$$\nabla \cdot \vec{V} = 0 \tag{3.1}$$

Momentum equation:

$$\frac{\partial \vec{\mathrm{V}}}{\partial \mathrm{t}} + \vec{\mathrm{V}} \cdot \nabla \vec{\mathrm{V}} = \frac{1}{\rho}\left(-\nabla \mathrm{P} + \mu \nabla^2 \vec{\mathrm{V}} + \rho \vec{\mathrm{g}} \beta (\mathrm{T} - \mathrm{T}_{\mathrm{ref}})\right) + S_m \tag{3.2}$$

Energy equation:

$$\frac{\partial h_{\text{sens}}}{\partial t} + \frac{\partial h_{\text{lat}}}{\partial t} + \nabla \cdot \left(\vec{V} h_{\text{sens}}\right) = \nabla \cdot \left(\frac{k}{\rho c_p} \nabla h_{\text{sens}}\right) \quad (3.3)$$

In CFD simulations, sparks are often blurred due to their relatively small initial size relative to the grid cell size. Modelling ignition by burning a few cells near the spark location can introduce significant grid and time step sensitivity, as it introduces inaccuracies in flame velocity and flame brush propagation due to insufficient spatial and temporal resolution. However, ignition may occur prematurely when the initial spark size is smaller than the grid cell.

ANSYS IC Engine Fluent calculates a sub-grid equation for spark evolution to reduce this sensitivity. The spark's flame front is assumed to be an infinitely thin, perfectly spherical shape, with its radius (r) expanding over time, t,

$$\frac{dr}{dt} = \frac{\rho_u}{\rho_b} S_t \quad (3.4)$$

Here, $\rho_b$ represents the density of the burned fluid behind the flame, $s_t$denotes the turbulent flame speed, and $\rho_u$ refers to the density of the unburned fluid ahead of the flame front.

The sub-grid spark model is mapped onto the CFD grid using a representative volume of CFD cells. A fixed-diameter spherical container determines the local turbulent length scale at the spark location. To ensure an appropriate size that is neither excessively large relative to the combustor nor too small in comparison to the cell size, the radius of the representative sphere, $r_t$, is calculated as follows,

$$r_t = \max\left(r_0 + 34{,}3\, r_0, \min\left(\frac{1}{2} l_t, r_0 + 10\Delta\right)\right) \quad (3.5)$$

Where $l_t$ is the turbulent length scale, and $r_0$ is the initial spark radius that the user specifies.

It is also important to note that the provided time only determines the rate of spark energy input and when this input ceases to occur. At this point, Ansys Fluent disables the spark flame speed model and applies the flame speed model selected in the Species dialog box to simulate flame propagation throughout the domain. The temperature and species composition of the usual spherical volume, denoted by, are calculated as follows:

$$\varphi = c\varphi^{b} + (1 - c)\varphi^{\mu} \tag{3.6}$$

where $\varphi^{\mu}$ is the unburned composition and $\varphi^{b}$ is the equilibrium burnt composition. These musical arrangements are constant in time and consistent in space.

Spark energy is unnecessary to ignite the mixture because the thermo-chemical condition behind the spark flame front is quickly equilibrated as the spark propagates. Every combustion model begins with the burned temperature as the equilibrium temperature and the spark energy set to zero. On the other hand, the equilibrium temperature will be higher if the temperature behind the spark is altered to a positive value through the user interface.

Using the Turbulent Curvature model, the turbulent flame speed is calculated as follows:

$$S_{\mathrm{t}} = \max\left(S_l - \frac{2D}{r}, S_t(r) - \frac{2D_t}{r}\right) \tag{3.7}$$

Here, $S_{\mathrm{t}}$ presents the turbulent flame speed, representing how fast the flame propagates through a turbulent medium, $S_l$ illustrates the laminar flame speed, which is the flame propagation speed in a quiescent (non-turbulent) gas. D and $D_t$ represent diffusion coefficients, with D likely for molecular diffusion and $D_t$ for turbulent diffusion; $r$ is the radius or local radius of curvature of the flame front; and $S_t(r)$ reveals to a radius-dependent turbulent flame speed from a local or previously computed profile.

The turbulent flame speed is determined using the Turbulent Length model as follows:

$$S_t = \max(S_l S_t(r)) \tag{3.8}$$

In other words, the Turbulent Length model disregards how flame curvature influences flame speed. The Herweg and Maly model is used to compute the turbulent flame velocity.

$$S_\varepsilon = \max\left(S_l, S_l\left(I_0 + I_0^{\frac{1}{2}}\left(\frac{u}{u+S_l}\right)^{\frac{1}{2}}\left[1-\exp\left(-\frac{r}{l_t}\right)\right]^{\frac{1}{2}}\left[1-\exp\left(-\frac{t-t_0}{\tau_s}\right)\right]^{\frac{1}{2}}\left(\frac{u}{S_l}\right)^{\frac{5}{6}}\right)\right) \tag{3.9}$$

Where, $I_0$ It is a function of the influence of strain on the laminar burning velocity.

$$I_0 = \max\left(0{,}1 - \left(\frac{\delta}{15 l_t}\right)^{\frac{1}{2}}\left(\frac{u}{S_l}\right)^{\frac{3}{2}} - 2\frac{\delta}{\Gamma}\frac{\rho_u}{\rho_b}\right) \tag{3.10}$$

and

$t =$ current time
$t_0 =$ start time
$u =$ turbulent velocity scale
$\tau_s = \dfrac{l_t}{u + S_i}$
$\delta =$ laminar flame thickness $= \dfrac{D}{S_i}$

### 3.3.4. Ansys Package

The stream conditions are addressed by utilizing two modules:

- The pre-processor module is the crucial component; it is a program structure that creates the matrix and calculation as shown in the accompanying:
    - Modelling of calculation.
    - Mesh number.
    - Boundary condition.

- The second module is the Solution module, for settling Navier-Stokes conditions (which incorporates flow rate, force, and energy conditions), as well as the violent stream model.

### 3.3.5. Problem Solution

The volume of the control depends on the technique that comprises the accompanying advances, which can be utilized for arrangement:

- On the field, a network is established.
- Each control volume of the administering conditions is combined to create mathematical sets of conditions such as pressure, velocity, and preserved scalars.
- The Discretized Equations are linearized and tackled iteratively.

### 3.3.6. Solution Parameters

The solution parameters include the following:

#### 3.3.6.1. Precision Solver Type

Typically, single- and two-fold methods are used to find accurate solutions. As the arrangement merges, residuals would go to zero on a PC with infinite accuracy. The residuals of a real PC deteriorate to a point of little value ("adjust") and then change ("level out").

#### 3.3.6.2. Number of Iterations

This is the maximum number of iterations completed before the solver ends. Figure 3.9 illustrates the location of the two processors that will be connected for simulation purposes.

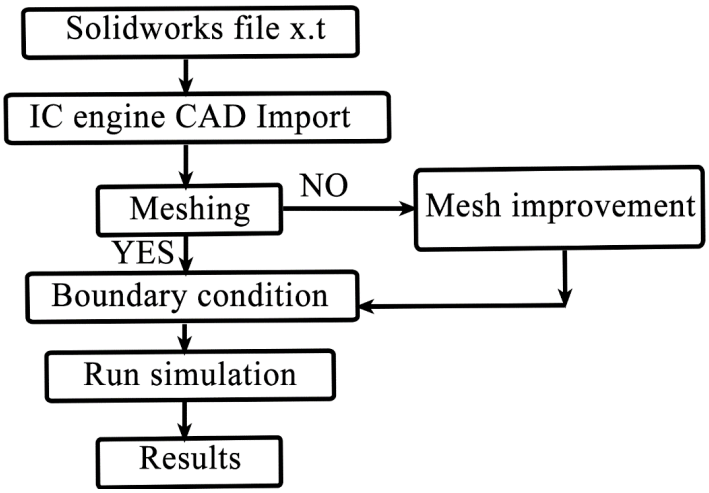


Figure 3.9. Flow chart of CFD.

### 3.3.7. Convergence Criteria

It should be emphasized that the flow conditions of the internal combustion process parameters are regulated according to the CFD approach to ensure proper recognition and simulation. When the order of the materials involved in the reaction remains within the accuracy of the specified mixing models, a complete simulation is obtained without errors. The error residuals, which compare the positive aspects of a variable at two continuous concentrations, are considered. For all flow conditions mentioned previously, the ranking is assumed to be uniform when the error percentage is less than the outcome difference value of $10^{-6}$.

### 3.3.8. Theoretical Calculation of Engine Parameters.

Several factors affect internal combustion engines, including combustion chamber design, cetane number, fuel, injection timing, compression ratio, adding biodiesel, and improving fuel quality. All of these factors affect engine performance. Here, we can improve engine performance by reducing the amount of fuel and adding biodiesel to pure fuel, as this affects combustion efficiency, emissions, and cetane number, to reach peak brake thermal efficiency at all loads for a mixture of conventional fuel and biodiesel.

### 3.3.8.1. Brake Power

The braking power is measured using a diameter, and the braking power is calculated using this equation [6]:

$$BP = \frac{2\pi NT}{60.000} \quad (3.11)$$

So that:
BP is the braking power (KW)
N is the spinning speed (rpm)
T is the torque (Nm)

### 3.3.8.2. Brake Thermal Efficiency

Thermal efficiency is the ratio of braking power to the energy available due to fuel combustion. There are two definitions of thermal efficiency, one is based on the graphical power, called thermal efficiency, and the other is inferred from braking capacity and is called braking thermal efficiency.

The braking thermal efficiency is calculated through the following equation[117,118]:

$$\eta_{bth} = \frac{BP}{mf * LCV} \quad (3.12)$$

Where:
$\eta_{bth}$ is the thermal efficiency (%)
LCV is the thermal value (KJ/Kg)
Where: -
$BP_{NU}$ =T*ƓƆ

$$T_{NU} = F_{total} * r \quad (3.13)$$

$F_{total} = F_L + F_I$

Where the force acting on the piston is due to fuel pressure

$$F_L = \rho * \frac{\pi d N}{4} \quad (3.14)$$

$$F_I = M_R * Ɗ^2 * r * \left(cos2\theta + \frac{\mathbf{cos2\theta}}{n}\right) \quad (3.15)$$

These marks can be used when the piston moves inside the cylinder from top dead center to the bottom dead center, and are symbolized by (TDC, BDC):

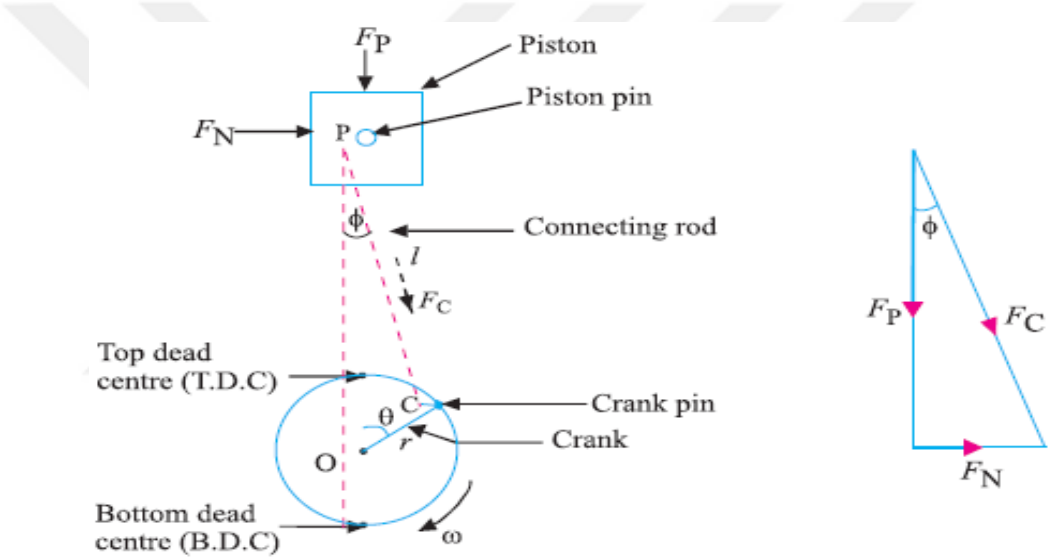


Figure 3.10. presents the force acting on the piston when the piston moves inside the cylinder from top dead center to bottom dead center, (TDC from BTC) and the theoretical calculations.

# PART 4

# EXPERIMENTAL WORK

## 4.1. OVERVIEW

This experiment was conducted at Al-Musayyab Technical Institute, one of the formations of Al-Frat Middle Technical University. It is located 67 km south of Baghdad, equipped with a four-stroke engine, and runs on pure diesel fuel as its main fuel. A mixture of ammonium trioxide with pure diesel fuel at different ratios (50, 100, 150) ppm was used with (B20%) biodiesel, and the engine was operated at different speeds (1150, 1400, 1600, and 1800) and constant loads (40) Newton. Performance effects on engine brake consumption, noise intensity, friction force, exhaust gas temperature, carbon monoxide, carbon dioxide, and nitrogen oxides were studied. And also smoke.

## 4.2. EXPERIMENTAL IMPLEMENTATION

### 4.2.1. Compression Ignition Engine

Figure 4.1 shows the experimental computational model of a four-stroke, four-cylinder CI engine. The base engine used in the experiment was a four-stroke, four-cylinder engine (8041 i40, direct injection), with the exact specifications shown in Table 4.1.

Table 4.1. Technical qualifications of the test engine.

| | |
|---|---|
| Model | 8041 i40 |
| Type | DI, 4 cylinder, diesel natural aspirated |
| Combustion types | Direct injection |
| Bore x stroke | 104 mm x 115 mm |
| Cylinder Number | 4 |
| Compression ratio | 17.1 |
| Maximum speed | 2940 RPM |
| Maximum torque | 266 Nm/2300 RPM |
| Stand-by(Maximum) rating | 64 kW(87HP)/2940 RPM |
| Flywheel & Has | SAE/11.5 |
| Dry weights | 415 Kg |
| Dimension L*W*H | 1094 * 680*885mm |
| Fuel consumption | 296 g/kw.h(198g/HP.h)/2940 r.p.m |
| Displacement | 3,9 it |

Figure 4.1. Engine tests

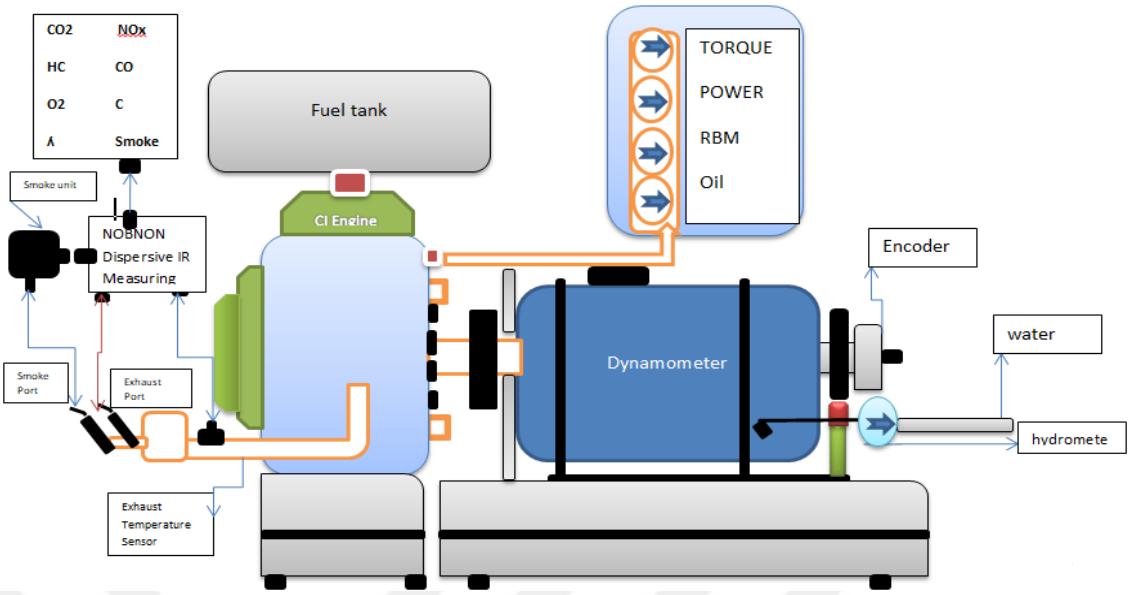


Figure 4.2. Experimental setup

### 4.2.2. Preparation for Fuel Samples

#### 4.2.2.1. Diesel and Biodiesel Fuel

Diesel fuel is used to operate internal combustion engines and is a complex mixture of hydrocarbons (paraffin, naphthalene, and aromatics) obtained from crude oil, with the molecular formula ($C_{12}H_{23}$). Its refining method also consists of hydrocarbon compounds and lubricating oils. Good fuel has three main characteristics: ease of transportation, storage, smoothness, ignition efficiency, and continuity of cleanliness during ignition. Diesel fuel is more thermally efficient and is used in various applications, including heavy machinery, freight vehicles, ships, and agricultural equipment. The physical properties of pure diesel are shown in Table 3.1. Here, the fuel was purchased from Babel Petroleum Products Company. There are types of biofuels whose fuel was manufactured in a laboratory experiment using 20% water hyacinth at the Musayyib Institute. Mixing with 80% pure diesel fuel and four conventional fuels, as shown in Figure 4.3. The pure fuel and biofuel (from water hyacinth) were mixed with three different concentrations of ammonium trioxide. It was also purchased from the local market, and its concentration is 50, 100, and 150 ppm, respectively, of ammonium trioxide $AL_2O_3$, as shown in Table 4.2.

Figure 4.3. Diesel with biodiesels

Because of growing environmental concerns and the depletion of global petroleum sources, alternative fuels have garnered a lot of attention. An appealing processed vegetable oil substitute for use as fuel in compression ignition engines is biodiesel. Crude oil and petroleum products will become extremely rare and expensive to locate and produce at some point in the twenty-first century. There will probably be a rise in cars and other internal combustion engine numbers concurrently. Even if engine fuel efficiency has significantly increased over the years and will continue to rise, the number alone indicates that fuel demand will be high in the upcoming ten years. Biodiesel is a component of the biofuel idea, which is an essential contraction of bio-organic fuel. This is the scientific term for any material that burns, be it plant or animal. Renewable liquid fuels derived from plant matter as opposed to fossil fuels are called biofuels. Ethanol and biodiesel are the two main biofuels used today.

The usage of biofuels can lessen reliance on imported oil, greenhouse gas accumulation, and emissions of air toxics. The aquatic freshwater plant known as water hyacinth colonizes bodies of water and offers a variety of benefits and drawbacks for both users and the bodies of water. It impairs fishing, marine transportation, and irrigation systems by blocking water intakes, which results in severe damage and a negative impact on water resources. Additionally, it makes the water less light and oxygenated, alters its chemistry, impacts the life of plants and animals, increases water loss by transpiration, and threatens biodiversity. However, the plant is thought to be an excellent source of feedstock for the synthesis of biofuels since it has high levels of hemicellulose (49%), moderate levels of cellulose (approximately 28%), and low

levels of lignin (10%). Water hyacinths are also attractive for fuel generation because of their high biomass yield and availability. Water hyacinth has been used to produce a variety of biofuels, including direct combustion, biogas, biodiesel, bioethanol, bioethanol gel, biochars, and other possible non-energy uses.

The B20 found in water hyacinth, scientifically known as Eichhornia crassipes, is the primary subject of this investigation. This study will combine nano additives into a biodiesel-diesel blend (D80B20), which has better density, carbon residue, flash point, and calorific value than plain diesel. Table 4.2 enumerates the specifications of the three blends.

Table 4.2. The physical properties of Biodiesel blend.

| No. | Property | Unit | Diesel | Biodiesel | Biodiesel (D80B20) |
|---|---|---|---|---|---|
| **1** | Density at 15 °C | g/cm³ | 0.823 | 0.8794 | 0.8325 |
| **2** | Carbon Residue (on 10 % Residue) | % m/m | 0.08 | 2.145 | 0.036 |
| **3** | Flash point | °C | 62.5 | Flammable | Flammable |
| **4** | Pour point | °C | < -21 | -3 | -21 |
| **5** | Cetane Index | ---- | 52.6 | 44.3 | 52.2 |
| **6** | Calorific Value ( Gross ) | Kcal/Kg | 10976 | 10774 | 10945 |
| **7** | Calorific Value ( Net ) | Kcal/Kg | 10288.6 | 10129 | 10262 |
| **8** | Viscosity @ 40 °C | Mm²/s | 2.16 | 7.6 | 8 |

Table 4.3. Biodiesel blend

| No. | Prperty | Unit | Biodiesel (D80B20) |
|---|---|---|---|
| **1** | Density at 15 °C | g/cm³ | 0.8325 |
| **2** | Carbon Residue (on 10 % Residue) | % m/m | 0.036 |
| **3** | Flash point | °C | Flammable |
| **4** | Pour point | °C | -21 |
| **5** | Cetane Index | ---- | 52.2 |

| | | | |
|---|---|---|---|
| **6** | Calorific Value ( **Gross** ) | Kcal/Kg | 10945 |
| **7** | Calorific Value ( Net ) | Kcal/Kg | 10262 |

#### 4.2.2.2. Nanoparticles Additive

Nanoparticles (a powder-based metal base) are added to the fuel to improve performance. Physical properties, such as density, certain numbers, flash points, pour points, and Calorific values, are also improved, and so are the thermal properties of fuel. Nanoparticles used are Aluminum oxide nanoparticles ($AL_2O_3$), it was produced in the United States of America and received from a special chemical agent in Baghdad. As shown in Figure 3.2, the properties of the nanoparticles used are shown in Table 4.4. Here, the nanomaterial was weighed by a sensitive electronic weighing device, as shown in Figures 4.4a and b.

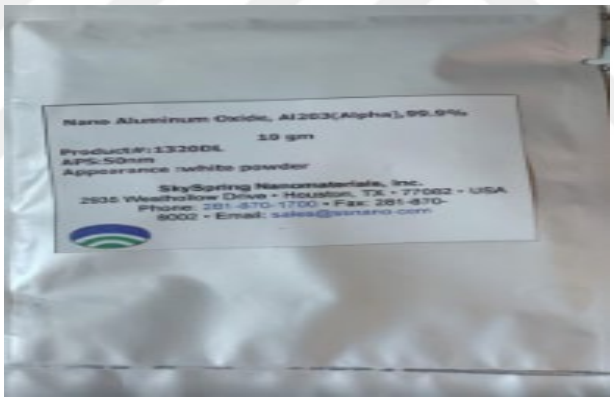


(a)

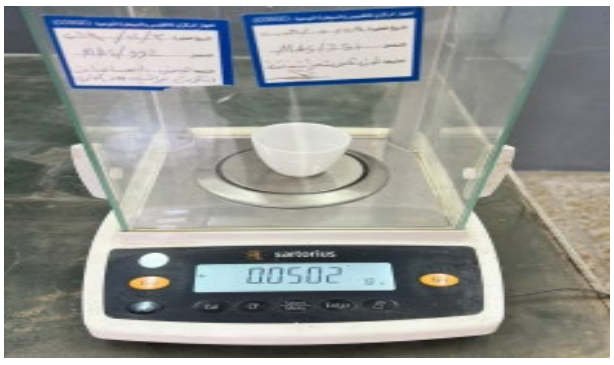


(b)

Figure 4.4. (a) Nanoparticles, and (b) Electronic weighing device.

Table 4.4. Properties of the nanoparticle $AL_2O_3$

| **Properties** | |
|---|---|
| Chemical formula | $Al_2O_3$ |
| Molar mass | 101.960 $g.mol^{-1}$ |
| Appearance | white solid |
| Odor | odorless |
| Density | 3.987$g/cm^3$ |
| Melting point | 2,072 °C (3,762 °F; 2,345 K) |
| Boiling point | 2,977 °C (5,391 °F; 3,250 K) insoluble |
| Solubility in water | insoluble |
| Solubility | in all solvents |
| log *P* | 0.31860 |
| Magnetic susceptibility (*X*) | $-37.0\times10^{-6}$ $cm^3/mol$ |
| Thermal conductivity | 30 $W.m^{-1}.K^{-1}$ |
| Refractive index ($n_D$) | n=1.768-1.772<br>n=1.760-1.763<br>Birefringence 0.008 |

The performance and emission parameters of the experimental diesel engine were evaluated using these samples. All fuel samples' physical and chemical properties under investigation (D80B20N50, D80B20N100, and D80B20N) were analyzed under ASTM guidelines. The specific criteria and results for these evaluations are presented in Table 4.4. Separate nano mixtures were prepared using a biodiesel blend of 80% clean diesel and 20% biodiesel (D80 B20). Doses of $AL_2O_3$ nanoparticles of 50, 100, and 150 ppm were extracted from the biodiesel derived from the water hyacinth plant. The mass fractions were determined using an ultrasonic instrument and an electric mixer, as shown in the accompanying figure. At a dose of 50 ppm, the nanoparticles were accurately measured. Ultrasound was also used to facilitate the uniform distribution of nanoparticles throughout the biodiesel blends. A Model 504 processor, operating at 50 kHz and 60 W output power, was used to generate biofuel-containing nanoparticles (D80B20 + 50 ppm) for 30 min, thus ensuring the homogeneity of the mixture. The same process was carried out for 100 ppm and 150 ppm mass fractions.

All the fuel samples were evaluated for their physical and chemical properties, as shown in Table 4.4.

To assess the stability properties of biodiesel, it is placed in test tubes and kept in a controlled environment. Their identification remained unchanged for over a month after profiling tests revealed it. Three nanoparticles are added to the biodiesel blend during production to ensure optimal engine performance. In the experiment, nanoparticles at different ratios (50, 100, 150) ppm were combined with pure diesel and biodiesel (D80B20) as base fuel using biodiesel blends and testing performance parameters. We can also see the water hyacinth oil as in Figure 4.5

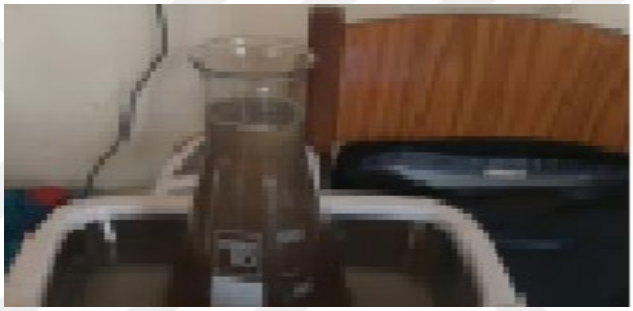

Figure 4.5. Water hyacinth.

### 4.2.3. Ultrasound Measuring

Nanomaterials are mixed with fuel by ultrasound using a (power sonic 405) device with technical specifications. Ultrasound was used for its great effectiveness in mixing solutions well, as documented by sound. Collecting a sample from groups published by seventeen sounds, as shown in Figure 4.6.


Figure 4.6. Ultrasound process.

### 4.2.4. Experimental Measurement Setup

#### 4.2.4.1. Engine Speed

Engine speed is measured electronically by the number of pulses and an optical head directed to the rotating disk in the engine using an infrared transceiver. It also has a rotating disc with two radial slots between the light source and the sensor. Electronic processing: The engine speed is read to ensure the speed is accurate in the existing device and also with a crankshaft, as shown in Figure 4.7 (a and b). The main specifications of the digital tachometer employed are provided in Table 4.5.


Figure 4.7. Engine speed measurement: (a) engine speed reader, (b) digital tachometer.

Table 4.5. Digital tachometer properties.

| | |
|---|---|
| Range | 5 to 9999RPM (± 0.05%+1digit) |
| Resolution | ±0.1RPM (1RPM above 1000) |
| Power Supply | 4*AA size batteries (not supplied) |
| Precision | ±1.75 RPM@1500 |
| Size | (HxWxD)3.7*19*7cm |
| Weight | 250 g |
| manufacturing | Made in China |

#### 4.2.4.2. Measurement Of Fuel Consumption

Figure 4.8 shows a glass burette with a marked tube and a fixed capacity of 200 mL used to measure the engine's fuel consumption. A stopwatch measured how long it took to consume so much fuel. Equation (4.4) was utilized to calculate fuel consumption [17]:

$$\dot{m}_f = \frac{V_f \times \rho_f}{t \times 10^6} \quad (4.1)$$

Where: $V_f$ is the volume of fuel consumption (m3), and $\rho_f$ is the fuel density (kg/m3); t is the time (sec).

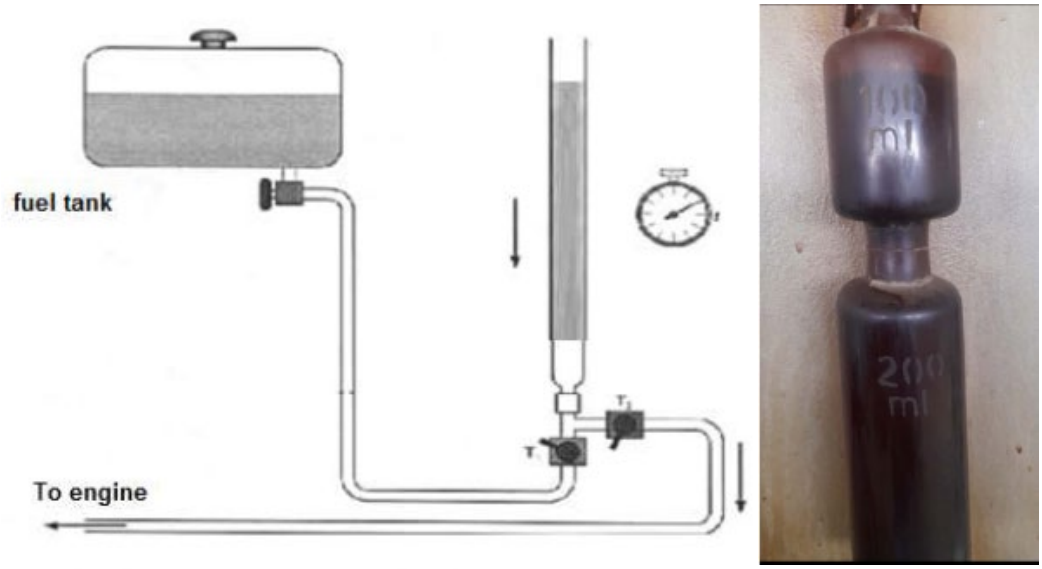


Figure 4.8. Fuel consumption measurement.

#### 4.2.4.3. Measurement of Air Consumption

Using this air box to feed air into the engine intake manifold, as shown in Figure 4.9, here, the air mass consumption rate is measured using the orifice device. The inclined pressure gauge measures the pressure difference between the inside and outside of the air box. The air intake orifice monitors the pressure difference between the atmosphere and the intake pressure. Calculate the air mass flow rate using Equation (4.2).

$$\dot{m}_a = 4.78 A_o \sqrt{\frac{P_a h}{T_a}} \tag{4.2}$$

where $P_a$ is the atmospheric pressure (mbar), $T_a$ is the temperature (K), h is the manometer reading ($mmH_2O$), and $A_o$ is the area of the orifice ($m^2$).

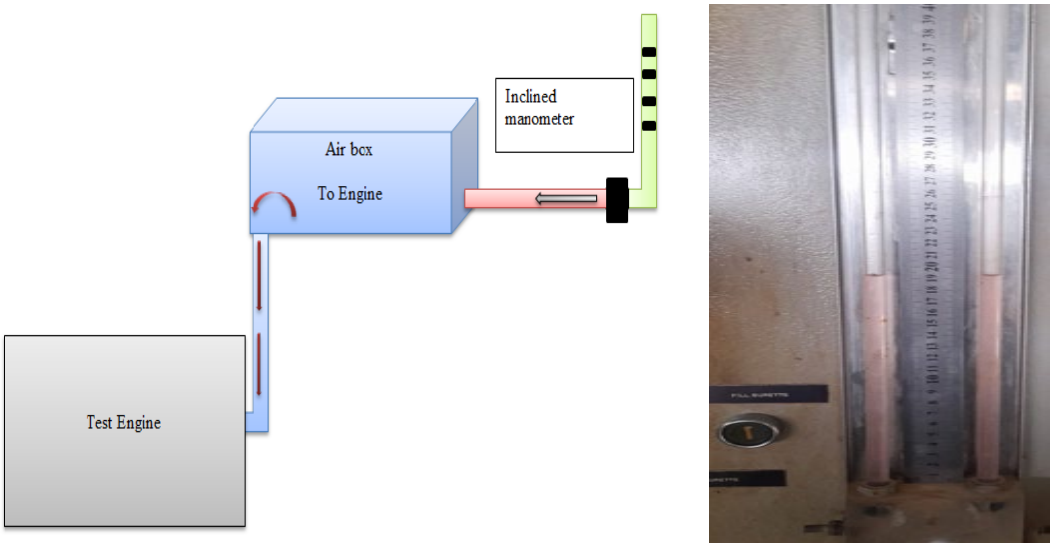


Figure 4.9. Schematic diagram of the manometer of the test engine.

#### 4.2.4.4. Measurement of Brake Torque

A water pump dynamometer was used to measure brake torque. It works on an oscillating field. It also has enough capacity to absorb the maximum power produced by the engine at all speeds and can run the engine. The mass balance connected to the dynamometer of the water pump, as shown in Figure 4.10, determines the load applied by the dynamometer.

Figure 4.10. The dynamometer.

#### 4.2.4.5. Exhaust Gas Temperature

There is a unit for measuring the temperature of the exhaust gases, where the exhaust temperature is measured using a thermocouple. It is made of brass and is placed inside the exhaust pipe near the engine cylinder block. The thermocouple is connected to a coded system and communicates with the Chinese-made measuring unit, type 6675Max. Readings are displayed directly on the meter from 0 to 1000°C, as shown in Figure 4.11.

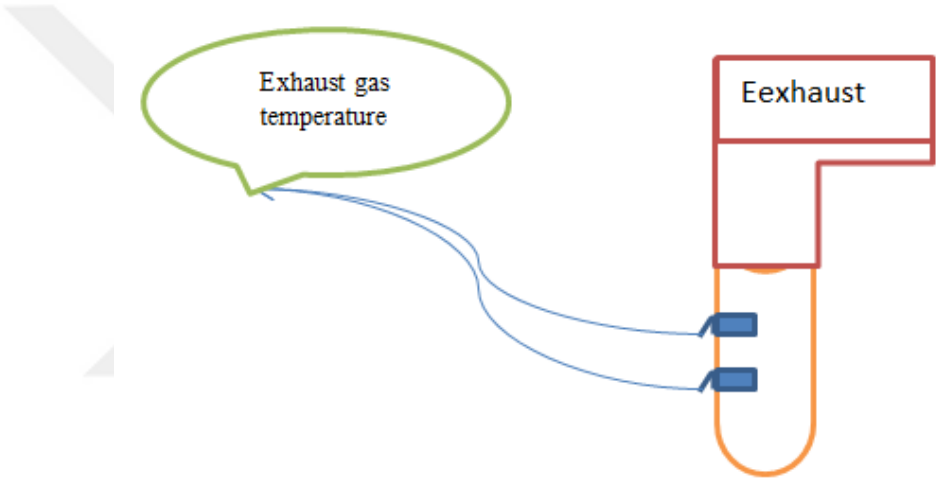


Figure 4.11. Exhaust gas temperature.

#### 4.2.4.6. Analyzer Gas Exhaust

The exhaust gases of a four-stroke and four-cylinder engine were analyzed using an experimentally used exhaust gas analyzer, a Korean-made AIRREX, HG-540L, as shown in the figure. The device is used to measure the density of vehicle exhaust according to the technical specifications of the exhaust gas analysis device ($CO_2$, CO, HC, NOx). Exhaust gases were measured by placing the instrument tube inside the pipe, as shown in Figure 4.12.

Figure 4.12. The analyzer of the inside exhaust gas in our experiment.

## 4.3. ENGINE PERFORMANCE PARAMETERS

### 4.3.1. Brake Power

The braking power is measured using a diameter, and the braking power is calculated using this equation:

$$BP = \frac{2\pi NT}{60.000} \tag{4.3}$$

Where:

BP is the braking power (kW)

N is the spinning speed (rpm)

T is the torque (Nm)

### 4.3.2. Brake Specific Fuel Consumption

$$m°f = \frac{Sgf*100*0.001}{t} * 3600 \tag{4.3}$$

Where:

$m°f$ is the Brake specific fuel consumption (Kg/hr)

Sgf is the fuel specific gravity

Brake-specific fuel consumption is calculated by using the following equation:

$$\mathrm{BSFC} = \frac{\mathrm{m}^{\circ}f}{\mathrm{BP}} \tag{4.4}$$

Where:

BSFC is the Brake specific fuel consumption (Kg/kW.h)

$\mathrm{m}^{\circ}f$ Is the Fuel consumption (Kg/hr)

BP is the Brake power (KW)

### 4.3.3. Break Specific Fuel Consumption

Fuel is provided through the 10-liter fuel tank above the metering unit, and the fuel flows downward, as shown in Figure 4.13, and comes out through the tube size (200 ml). Then, the fuel consumption rate is determined using the time from the tube to the engine[119].

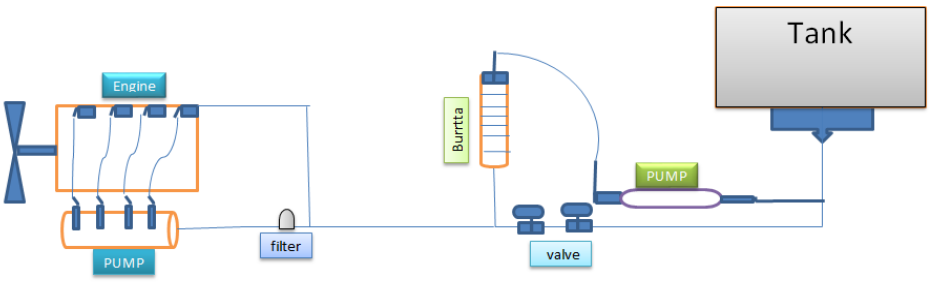


Figure 4.13. Brake specific fuel consumption.

### 4.3.4. Brake Thermal Efficiency

Thermal efficiency is the ratio of braking power to the energy available due to fuel combustion. There are two definitions of thermal efficiency: one is based on the graphical power, called thermal efficiency, and the other is inferred from braking capacity, which is called braking thermal efficiency.

The braking thermal efficiency is calculated through the following equation:

$$\eta_{bth} = \frac{\text{BP}}{\text{m}*\text{LCV}} \quad (4.5)$$

Where $\eta_{bth}$ is the thermal efficiency (%)

## 4.4. TEST SYSTEM

The test kit includes a gauge with a fuel consumption measuring tube, an engine speed step gauge, an engine temperature gauge, an exhaust temperature gauge, and a diameter load gauge. It also includes exhaust gases and opacity gauges, as shown in Figure 4.2.

### 4.4.1. Practical Tests

Where was it conducted in this experiment?

- The oil and water levels in the internal combustion engine's radiator and fuel delivery pipes are checked.

Using a load of 40 Nm.

Using traditional fuel, which is the basis for mixing with biodiesel, ensure there is no air gap inside, and start the engine. It gradually increases the speed at low speeds until it stabilizes at 1150 rpm. We wait until the engine temperature stabilizes at 35 degrees Celsius. Then, we start by adding the first speed, 1150 rpm, to each load operation of the engine for a full hour.

Four times, the engine temperature readings, exhaust gas temperature, pressure, and temperature entering and leaving the engine were recorded.

Take these readings for each speed distributed as follows: the first 10 minutes, after half an hour, and at the end of a full hour.

We change the second speed to 1400 and repeat the same previous steps four times.

When the variable speed engine is finished running, we bring the fuel mixed with Nano material at a certain concentration after emptying the tank and all the pipes and connections and filling it with Nano fuel.

## 4.5. DATA COLLECTION

The experimental procedure used for a four-cylinder four-stroke diesel engine was used on a mixture of biodiesel with nanomaterial ($AL_2O_3$) in different proportions (50, 100, 150 ppm, and the doses and different loads 40, 80, 120, 160, and 200 N.m were changed to obtain the ideal results of the break power, fuel consumption rate, air mass rate and fuel mass rate. as mentioned in Tables 4.6 and 4.7, respectively.

Table 4.6. Data collected for the effect of a mixture of biodiesel with nanomaterials

| Fuel | 1150 rpm | | | 1400 rpm | | | 1600 rpm | | | 1800 rpm | | |
|---|---|---|---|---|---|---|---|---|---|---|---|---|
| | Ma kg/s | Mf kg/s | Torque N.m | Ma kg/s | Mf kg/s | Torque N.m | Ma kg/s | Mf kg/s | Torque N.m | Ma kg/s | Mf kg/s | Torque N.m |
| D100 | 0.746 | 0.503 | 40 | 0.76 | 0.688 | 40 | 0.867 | 0.800 | 40 | 0.944 | 0.851 | 40 |
| D80B20 | 0.782 | 0.510 | 80 | 0.817 | 0.612 | 80 | 0.883 | 0.832 | 80 | 0.912 | 0.860 | 80 |
| D80B20N50 | 0.80 | 0.522 | 120 | 0.782 | 0.742 | 120 | 0.867 | 0.815 | 120 | 0.927 | 0.880 | 120 |
| D80B20N100 | 0.782 | 0.504 | 160 | 0.817 | 0.736 | 160 | 0.850 | 0.777 | 160 | 0.944 | 0.891 | 160 |
| D80B20N150 | 0.764 | 0.594 | 200 | 0.800 | 0.756 | 200 | 0..883 | 0.858 | 200 | 0.967 | 0.897 | 200 |

Table 4.7. Data collected for the effect of a mixture of biodiesel with nanomaterials

| load | D100 | | D80B20 | | D80B20N50 | | D80B20N100 | | D80B20N150 | |
|---|---|---|---|---|---|---|---|---|---|---|
| | 40N.m | | 80 N.m | | 120 N.m | | 140 N.m | | 200 N.m | |
| speed | BP kw | PSFC kg/kw.s | BP kw | PSFC kg/kw.s | BP kw | PSFC kg/kw.s | BP kw | PSFC kg/kw.s | BP kw | PSFC kg/kw.s |
| 1150 | 4.81 | 0.104 | 9.62 | 0.053 | 6.69 | 0.075 | 7.53 | 0.066 | 24.07 | 0.024 |
| 1400 | 5.86 | 0.117 | 11.72 | 0.0435 | 17.72 | 0.0223 | 23.4 | 0.021 | 29.30 | 0.0258 |
| 1600 | 6.69 | 0.120 | 13.39 | 0.062 | 20 | 0.040 | 26.79 | 0.029 | 33.43 | 0.00265 |
| 1800 | 7.535 | 0.125 | 15.2 | 0.065 | 22.6 | 0.0417 | 30.14 | 0.0306 | 37.68 | 0.0245 |

## 4.6. UNCERTAINTY ANALYSIS

The error analysis in the experiments was required to determine the repeatability and reproducibility of the findings. The experiment was performed three times, and the fluctuations in performance, combustion characteristics, and exhaust emissions were utilized to compute the uncertainty using the percent relative standard error (RSE), as shown in Equation (4.6) [77].

$$RSE\ (\%) = \frac{E_{st}}{\delta} \times 100 \tag{4.6}$$

Where $E_{st}$ is the standard error, $\delta$ is the mean of the collected data. The standard error is calculated using Equation (4.7).

$$E_{st} = \frac{\gamma}{\sqrt{n}} \tag{4.7}$$

Where $\gamma$ is the standard deviation, and $n$ is the repeatable readings of performance, combustion characteristics, and emissions parameters. Overall experimental uncertainty, $\gamma_k$ was calculated using Equation (4.8).

$$\gamma_k = \sqrt{{\gamma_{q1}}^2 + {\gamma_{q2}}^2 + \cdots .. + {\gamma_{qn}}^2} \tag{4.8}$$

Where $\gamma_k$ is the total uncertainty and $\gamma_{q1}$, $\gamma_{q2}$, and $\gamma_{qn}$ are the uncertainties of individual parameters.

Table 4.8 comprehensively summarizes the measurement limits, instrument accuracy, and associated uncertainties for various parameters measured in an engine-related experimental setup. High uncertainty-to-accuracy ratios were observed, particularly for temperature and gas concentration parameters, likely due to dynamic environmental conditions. Mechanical parameters (torque, speed) have lower relative uncertainties, indicating better control or calibration. BSFC stands out as having low uncertainty compared to a relatively broad accuracy range. Parameters related to emissions (CO, $CO_2$, HC, NOx) generally show higher uncertainties due to the

complexities in sampling and real-time analysis. The torque measurement in this experiment has a defined limit of 200 Nm, with an instrument accuracy of ±0.25 Nm. This indicates a high-precision measuring device capable of capturing small variations in torque. However, the reported uncertainty is significantly larger at ±0.76 Nm, suggesting that the actual measured values may be influenced by factors beyond the device's intrinsic accuracy. The engine speed measurement is defined by a limit of 2000 rpm with an accuracy of ±1 rpm, indicating a high degree of precision in the instrument used. The uncertainty associated with this measurement is ±1.21 rpm, which is only slightly higher than the stated accuracy. On the other hand, the Brake Specific Fuel Consumption (BSFC) measurement has a limit of 511 g/kWh with a stated accuracy of ±3.11 g/kWh. Interestingly, the uncertainty is significantly lower at ±0.88 g/kWh. The exhaust temperature measurement, with a limit of 350.7°C and an accuracy of ±0.33°C, demonstrates high instrument sensitivity. However, the associated uncertainty is much larger at ±3.11°C—nearly ten times the stated accuracy. For carbon monoxide (CO), the measurement limit is 23 vol% with a very tight accuracy of ±0.002 vol%. Despite this precision, the uncertainty stands at ±1.44 vol%, indicating significant variability. Similarly, the carbon dioxide ($CO_2$) measurement, with a limit of 14.9 vol% and an accuracy of ±0.015 vol%, shows an uncertainty of ±1.1 vol%. This again highlights the challenge of achieving consistent and stable readings in exhaust gas analysis. Hydrocarbons (HC) measurement in the exhaust is capped at a limit of 73 ppm, with an accuracy of ±1.5 ppm and an uncertainty of ±2.88 ppm. This indicates a moderate level of uncertainty relative to the measurement range. For NOx emissions, the measurement limit is 1005 ppm with an accuracy of ±1 ppm and an uncertainty of ±1.63 ppm. This represents a relatively reliable measurement, especially given the wide measurement range. The low uncertainty relative to the overall limit makes this data suitable for emissions studies, where precise monitoring of nitrogen oxides is critical for regulatory compliance and environmental impact assessments. Finally, the overall experimental uncertainty is given as ±4.98. This value is a composite reflection of all measurement tools and procedures used in the experiment. It encompasses the cumulative effect of individual uncertainties from each parameter and represents the potential deviation in the final experimental results. A total uncertainty of ±4.98 suggests a reasonably controlled setup.

Table 4.8. The accuracies and uncertainties of the measured parameters.

| **Parameters** | **Measurement Limit** | **Accuracy** | **Uncertainty** |
|---|---|---|---|
| Torque | 200 Nm | ±0.25 Nm | ±0.76 |
| Engine speed | 2000 rpm | ±1 rpm | ±1.21 |
| BSFC | 511 g/kWh | ±3.11 g/kWh | ±0.88 |
| T exhaust | 350.7ºC | ±0.33ºC | ±3.11 |
| CO | 23 vol% | ±0.002 vol% | ±1.44 |
| $CO_2$ | 14.9 vol% | ±0.015 vol% | ±1.1 |
| HC | 73 ppm | ±1.5 ppm | ±2.88 |
| NOx | 1005 ppm | ±1 ppm | ±1.63 |
| Overall experimental uncertainty | | | ±4.98 |

# PART 5

# RESULTS AND DISCUSSION

## 5.1. INTRODUCTION

This chapter presents the experimental results obtained from tests conducted on an Italian-made Fiat 8041i40 diesel engine, a four-stroke, four-cylinder engine with a compression ratio 17.1. The experiment aimed to evaluate the physical properties of the fuel and assess engine performance under varying conditions. Detailed information is provided regarding the fuel parameters used, the quantities applied during testing, and the corresponding analytical methods.

The combustion process involved using 100% pure diesel fuel blended with 20% biofuel, tested under varying loads (100 and 200) and speeds up to 1800 rpm. Additionally, aluminum oxide ($Al_2O_3$) nanoparticles were introduced at concentrations of 50, 100, and 150 ppm to examine their effect on engine behavior. The resulting exhaust emissions, namely $NO_x$, HC, CO, and $CO_2$, were measured and analyzed to assess the environmental impact and efficiency of the fuel blends.

## 5.2. EXPERIMENT RESULTS

### 5.2.1. Performance of Diesel Engines

#### 5.2.1.1. Effect of Biodiesel Blends

Figure 5.1 illustrates the variation in Brake Specific Fuel Consumption (BSFC) with respect to engine load at a constant speed of 1800 rpm for two fuel types: pure diesel (D100) and a biodiesel blend consisting of 80% diesel and 20% biodiesel (D80B20). The findings present that while D80B20 is a cleaner alternative fuel, its higher BSFC

values highlight a trade-off between fuel economy and environmental sustainability, especially at medium to high engine loads. The figure shows that BSFC decreases progressively as the engine load increases for both fuel types. However, throughout all load conditions, the BSFC of the D80B20 blend remains consistently higher than that of pure diesel (D100). The difference is more pronounced at lower and medium load conditions (e.g., 20% to 60% load), where the biodiesel blend exhibits higher fuel consumption per unit of energy produced. At higher engine loads (above 80%), the difference between D100 and D80B20 narrows, though D80B20 still records slightly higher BSFC.

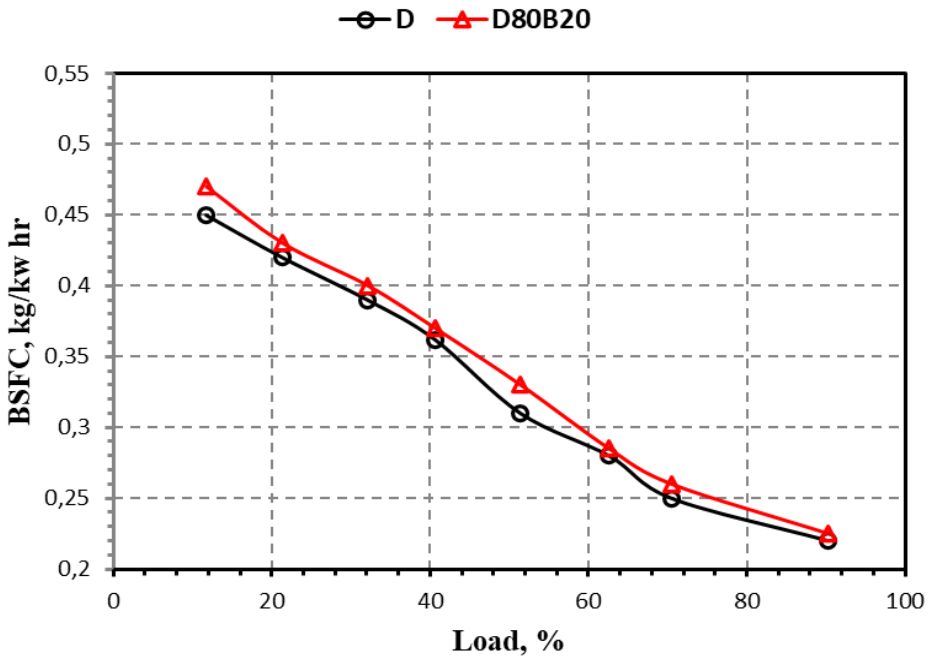


Figure 5.1. Variation of brake specific fuel consumption (BSFC) with engine load for diesel and biodiesel blends (D100, D80B20) at 1800 rpm.

Figure 5.2 illustrates the variation of Brake Thermal Efficiency (BTE) with respect to engine load for two fuels: conventional diesel (D100) and a biodiesel blend consisting of 80% diesel and 20% biodiesel (D80B20), tested at a constant engine speed of 1800 rpm. These results are consistent with previous research findings [120], which indicate that blending diesel with 20% biodiesel not only improves the combustion process but can also offset the disadvantages of biodiesel's lower calorific value at higher loads. The findings show that while D100 demonstrates marginally higher BTE at low loads

due to its superior combustion properties under light demand, D80B20 delivers comparable, and even superior, thermal efficiency under medium and high-load conditions. As observed, BTE increases progressively with engine load for both fuels, rising from approximately 16% at 10% load to around 28% at 100% load. At low loads, a significant portion of the fuel energy is lost as heat to the cylinder walls or through incomplete combustion, resulting in lower thermal efficiency. At 10% load, the BTE for D100 is approximately 16.5%, while D80B20 records a lower value of 15.5%, indicating that pure diesel performs slightly better under light load conditions. At 40% load, both fuels converge at nearly 22% BTE, suggesting similar combustion characteristics at this intermediate range. Beyond 60% load, the biodiesel blend (D80B20) begins to outperform pure diesel. For instance, at 80% load, D100 achieves a BTE of 26.5%, while D80B20 reaches 27.5%. Similarly, at full load (100%), D100 peaks at around 28%, while D80B20 slightly exceeds it at approximately 28.5%. Moreover, biodiesel's better lubricating properties may contribute to reducing mechanical losses, especially under heavy engine operation.

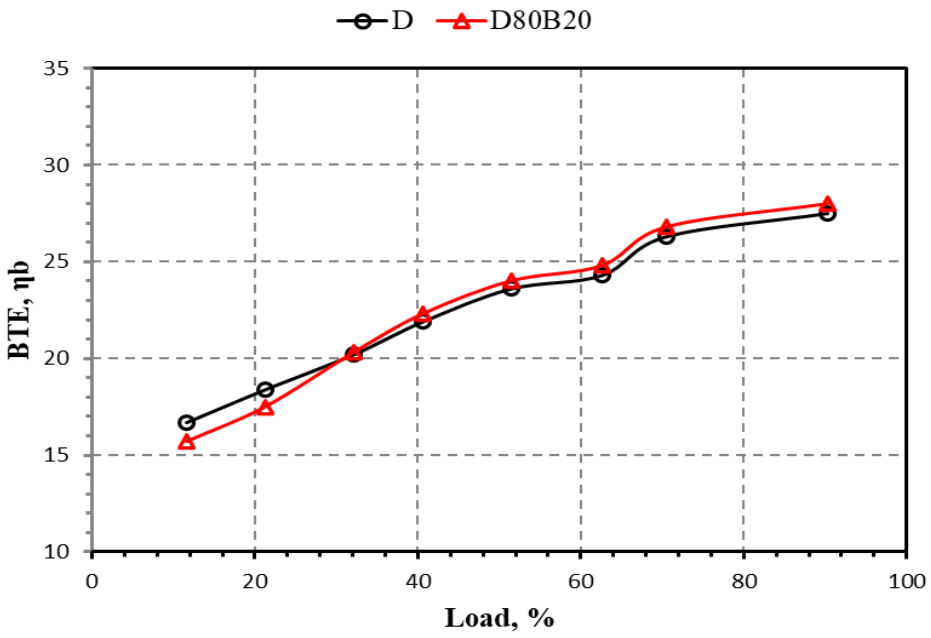


Figure 5.2. Effect of engine load on brake thermal efficiency (BTE) using diesel and 20% biodiesel blend (D100, D80B20) at 1800 rpm.

Figure 5.3 illustrates the variation in maximum exhaust gas temperature (in Kelvin) as a function of engine load for two fuel types: pure diesel (D100) and a biodiesel blend (D80B20, referred to as B20). The engine loads are 40, 60, and 90 N·m. The figure confirms that D100 yields higher exhaust gas temperatures than D80B20 across all load conditions. The temperature difference diminishes at high loads, as combustion efficiency improves for both fuels. The maximum temperature rise with load is a direct result of increased chemical energy released and the greater need for power output from the engine. At each load level, the exhaust temperature for D100 is consistently higher than that of D80B20, indicating differences in combustion characteristics between the two fuels. At 40 N·m, the temperature for D100 is approximately 315 K, whereas for B20, it is around 290 K—a difference of nearly 8%. This gap decreases slightly at higher loads: at 60 N·m, D100 reaches around 350 K compared to 330 K for B20; and at 90 N·m, D100 shows 375 K, while B20 records 365 K, narrowing the difference to approximately 3%, as noted. This pattern is consistent with findings in prior studies [121], where biodiesel blends generally produced lower exhaust temperatures at low and medium loads due to incomplete combustion and slower ignition delays.

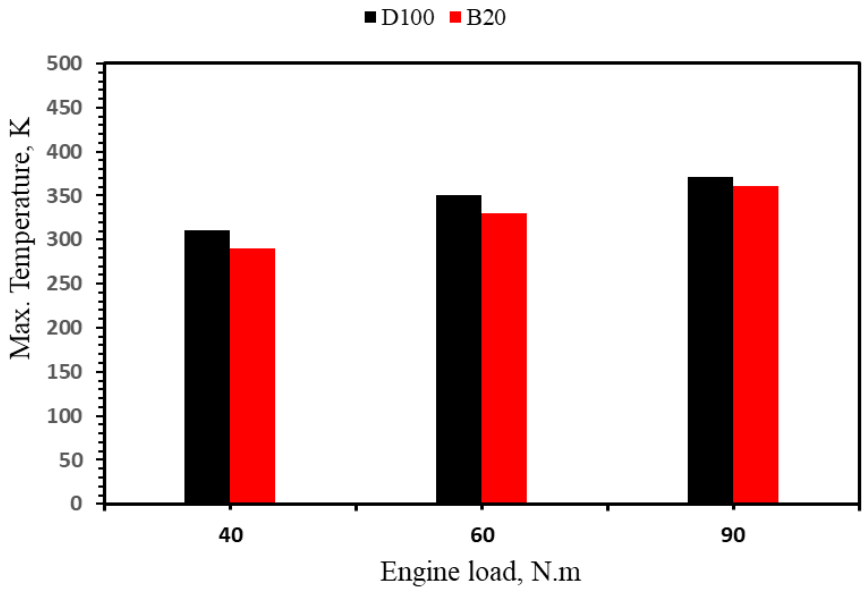


Figure 5.3. Comparison of exhaust gas temperature at varying engine loads for diesel and biodiesel blends (D100, D80B20).

Figure 5.4 presents the variation of Brake Specific Fuel Consumption (BSFC) with engine speed for two types of fuel: pure diesel (D100) and a biodiesel blend consisting of 80% diesel and 20% biodiesel (D80B20) over a speed range from 1100 rpm to 1800 rpm under no-load conditions. The results show that D80B20 shows higher BSFC across all speeds, indicating lower fuel efficiency than D100. The BSFC gap decreases with speed, particularly at 1800 rpm, where both fuels show nearly identical performance. Also, these results support the use of biodiesel blends in high-speed, light-load applications where their efficiency is comparable to diesel. At the lower end of the speed spectrum (1100 rpm), the BSFC values are approximately 0.21 kg/kWh for D80B20 and 0.185 kg/kWh for D100, indicating that the biodiesel blend requires more fuel to produce the same unit of power at low speeds. This trend persists through intermediate speeds, where D80B20 maintains a consistently higher BSFC than pure diesel. For example, at 1300 rpm, the BSFC for D100 is about 0.17 kg/kWh, while D80B20 records roughly 0.195 kg/kWh. As engine speed rises, the BSFC for both fuels follows a U-shaped curve, initially decreasing and then increasing again after reaching the optimal combustion speed. The lowest BSFC for D100 appears near 1300–1400 rpm, while D80B20's minimum occurs slightly earlier but remains consistently higher. At the maximum tested speed of 1800 rpm, the BSFC values for both fuels begin to converge. At this point, D100 reaches about 0.225 kg/kWh, while D80B20 closely follows at 0.23 kg/kWh. The gap narrows to just 0.005 kg/kWh, or about 2.2%. This observation aligns with findings from the literature [122], which suggest that the combustion efficiency of biodiesel blends improves with increasing engine speed, thereby reducing the efficiency gap compared to diesel.

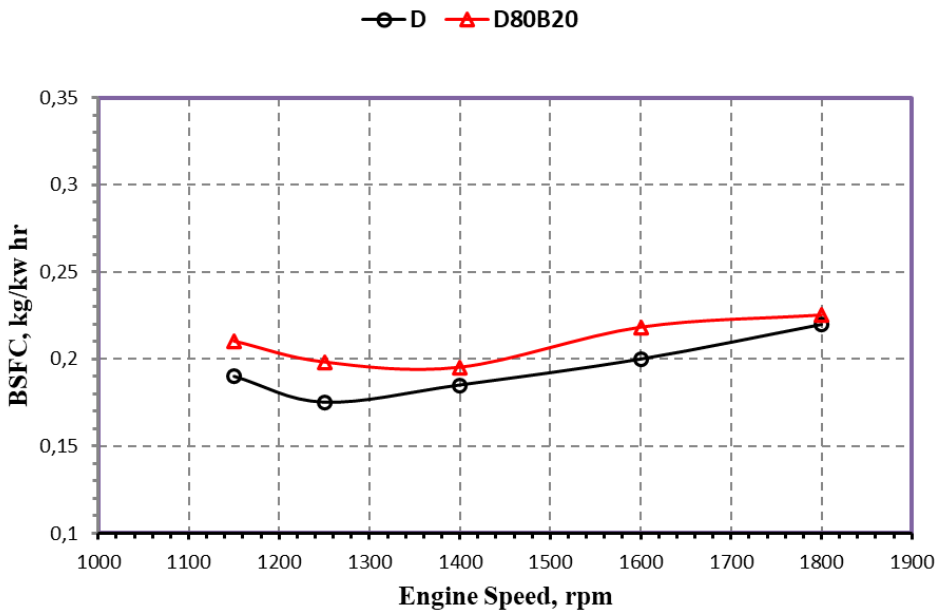


Figure 5.4. Effect of engine speed on brake specific fuel consumption (BSFC) for diesel and biodiesel blend (D100, D80B20) under No-Load conditions.

Figure 5.5 displays the variation of BTE with engine speed for pure diesel (D100) and a biodiesel blend containing 20% biodiesel (D80B20), under no-load conditions. The data demonstrates that BTE improves both fuels with engine speed. D80B20 consistently shows higher BTE values, peaking at 29% at 1800 rpm, the highest in the test range. As engine speed increases from 1100 rpm to 1800 rpm, both fuels steadily increase BTE, indicating enhanced combustion efficiency and improved engine operating conditions. At the lower speed of 1100 rpm, D100 records a BTE of approximately 18.5%, while D80B20 begins slightly higher at 19.3%. For instance, at 1300 rpm, BTE values are about 23.5% for D80B20 and 23% for D100. At 1500 rpm, D80B20 reaches 26%, while D100 is at around 25%. Finally, at 1800 rpm, D80B20 achieves the maximum observed BTE of 29%, compared to 28% for D100. This performance advantage is attributed to biodiesel's faster burning and enhanced evaporation characteristics due to its intrinsic oxygen content. Moreover, the slightly higher cetane number of biodiesels contributes to shorter ignition delay, enabling better pressure development within the cylinder and increasing thermal efficiency. These factors combined to allow D80B20 to outperform D100 even at high speeds, which aligns with previously published experimental findings [123].

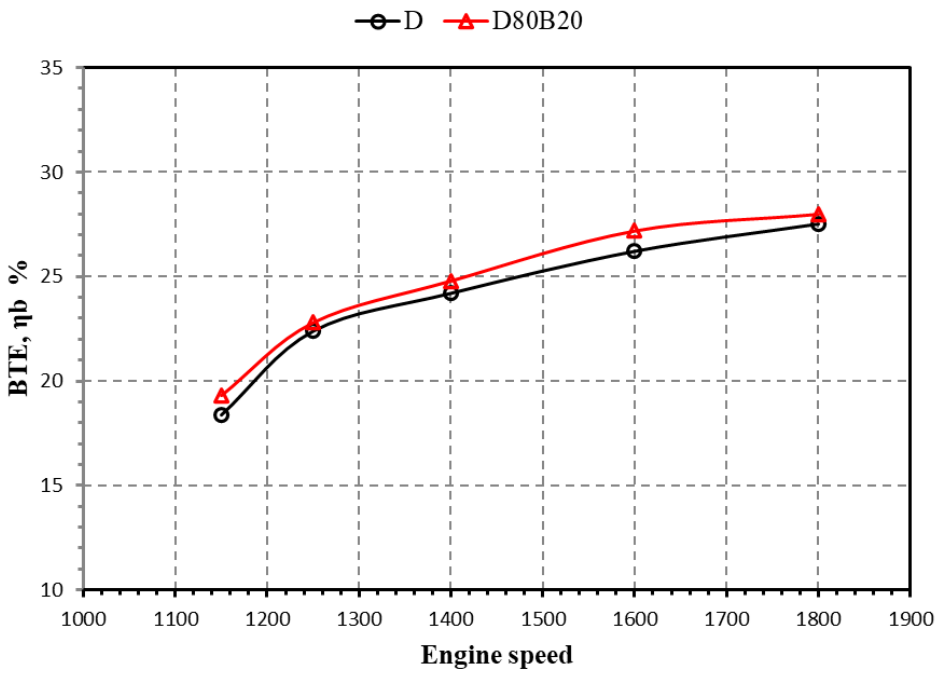


Figure 5.5. Influence of engine speed on brake thermal efficiency (BTE) for diesel and biodiesel blend (D100, D80B20) under no-load conditions.

Figure 5.6 illustrates the variation in volumetric efficiency as a function of engine speed for pure diesel (D100) and a biodiesel blend with 20% biodiesel (D80B20). The graph shows that volumetric efficiency decreases with increasing engine speed for both fuel types. This decline is typical in naturally aspirated engines, where higher speeds reduce the available time for the intake process, thus limiting the amount of air that can enter the combustion chamber. Across all engine speeds, D100 consistently maintains higher volumetric efficiency compared to the biodiesel blend. The average difference ranges from 2% to 3%, which can be attributed to the higher density and viscosity of biodiesel, which can alter the air–fuel mixing dynamics. Also, it is possible that incomplete vaporization of biodiesel at lower cylinder temperatures slightly hinders intake air movement. Reduced intake air temperature with diesel-only fuel leads to denser charge and better cylinder filling than biodiesel blends, which may increase intake temperatures due to their oxygen content and fuel spray characteristics. At the lowest tested speed of 1100 rpm, D100 exhibits a volumetric efficiency of approximately 74%, whereas D80B20 starts slightly lower at around 71.8%. As speed increases to 1400 rpm, volumetric efficiency drops to about 71.5% for D100 and 68% for D80B20. At the highest speed of 1800 rpm, D100 records about 66.8%, while

D80B20 falls further to around 65.5%. These findings are consistent with prior studies [121], showing that engine speed negatively affects volumetric efficiency for diesel and biodiesel blends.

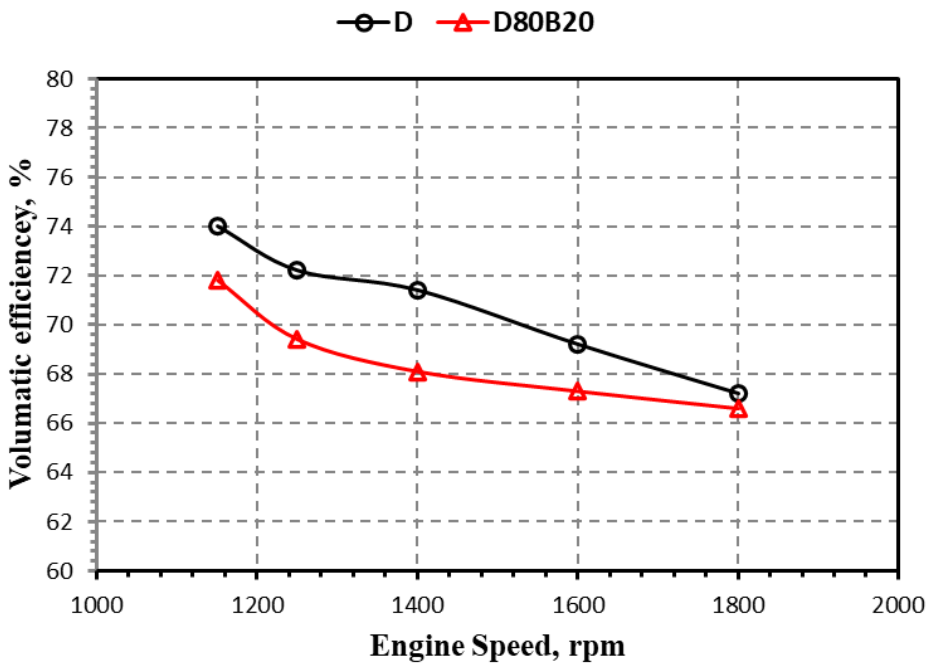


Figure 5.6. Effect of engine speed on volumetric efficiency for diesel and biodiesel blend (D100, D80B20).

Figure 5.7 demonstrates the variation of exhaust gas temperature with respect to engine speed for two fuel types: pure diesel (D100) and a biodiesel blend containing 20% biodiesel (D80B20). At low engine speeds, the exhaust temperature is lower for both fuels, with D100 slightly exceeding D80B20. For example, at 1150 rpm, the exhaust temperature for D100 is approximately 225 K, while B20 records around 215 K, representing a difference of about 2–3%. By 1400 rpm, D100 reaches around 240 K and B20 approximately 235 K. At 1600 rpm, both temperatures rise further to 260 K for D100 and 255 K for B20, and at the maximum speed of 1800 rpm, D100 peaks near 355 K, while B20 follows closely at about 348 K. The consistently higher exhaust temperature for D100 can be attributed to its lower cetane number and slower combustion characteristics, while biodiesel has a higher cetane number, promoting earlier and more complete combustion, resulting in slightly lower exhaust temperatures. The temperature gap between D100 and D80B20 remains small

(approximately 2%), even at high speeds, suggesting that biodiesel blends can achieve similar thermal behavior to pure diesel.

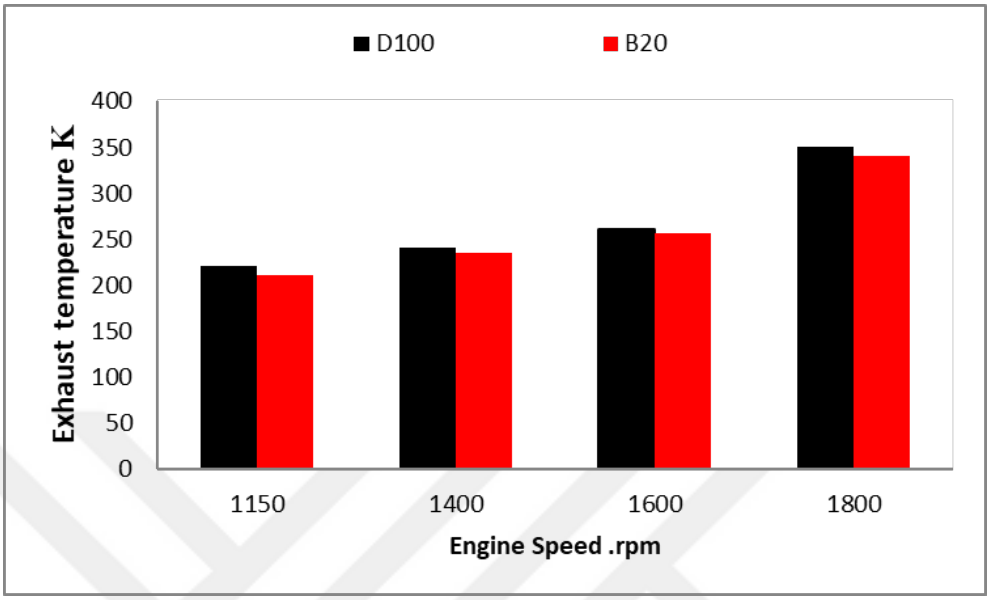


Figure 5.7. Effect of engine speed on exhaust gas temperature for diesel and biodiesel blends (D100, D80B20).

### 5.2.1.2. Effect of $AL_2O_3$ Nanoparticle Blends

Figure 5.8 illustrates the variation in BSFC as a function of engine load (% for five different fuel types: Pure diesel (D100), Biodiesel blend (D80B20), and biodiesel blends enhanced with nano-additives at different concentrations: D80B20N50, D80B20N100, and D80B20N150. All fuel types show improved BSFC at higher loads. D100 remains the most efficient, but biodiesel blends with nanoparticles perform increasingly well under high-load conditions. These trends affirm the potential of nano-additive technology in narrowing the efficiency gap between diesel and renewable fuel alternatives. Across all tested fuels, BSFC exhibits a general decreasing trend as engine load increases, starting from around 0.50 kg/kWh at 10% load and declining to nearly 0.22 kg/kWh at 90% load. Pure diesel (D100) consistently demonstrates the lowest BSFC values across all load levels, indicating superior combustion characteristics. For example, at 40% load, D100 shows a BSFC of approximately 0.37 kg/kWh, whereas D80B20 and the nano-enhanced blends (especially D80B20N50 and D80B20N100) exhibit slightly higher values ranging

from 0.39 to 0.41 kg/kWh. The higher BSFC of biodiesel and nano-additive blends compared to D100 can be attributed to the higher density and viscosity, which affect atomization quality and mixing with air, and Lower calorific value, meaning more fuel mass is needed to produce the same energy output. At high engine loads (above 70%), the gap in BSFC narrows. For instance, at 90% load, D100 and D80B20N150 both reach BSFC values around 0.22–0.23 kg/kWh.

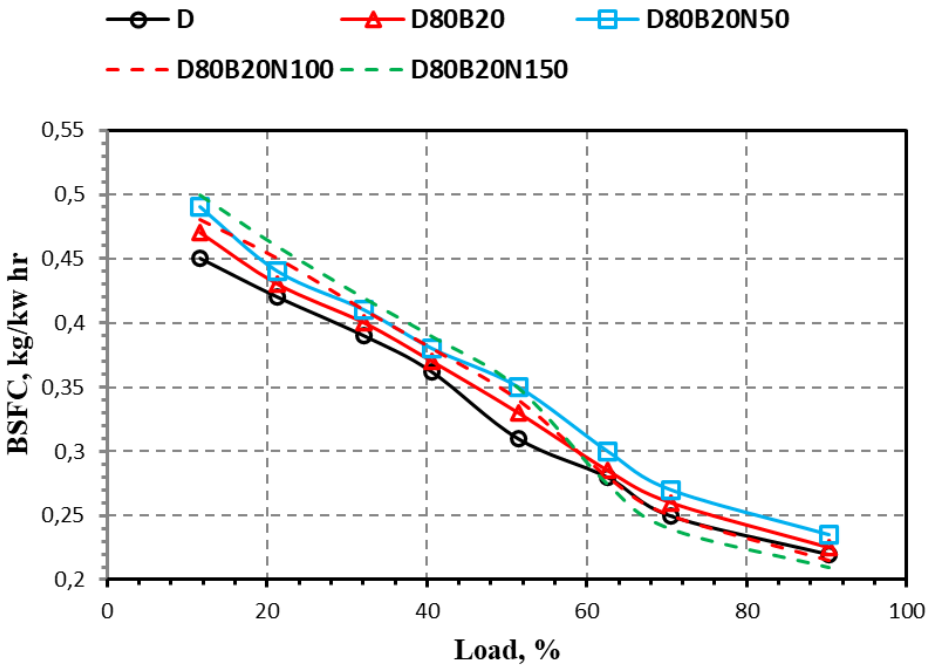


Figure 5.8. Effect of engine load on brake specific fuel consumption (BSFC) for diesel and biodiesel-nanoparticle blends (D100, D80B20, D80B20N50, D80B20N100, D80B20N150).

Figure 5.9 illustrates the BTE performance of various fuel samples, D100, D80B20, and biodiesel blends with $AL_2O_3$ nanoparticles (D80B20N50, D80B20N100, D80B20N150), across increasing engine loads, from 0% to 100%. The findings present that the BTE improves steadily with load across all samples. D80B20 without nanoparticles shows the highest efficiency. Higher nanoparticle doses reduce BTE at full load, likely due to increased viscosity and reduced effective energy content. Across all fuels, BTE increases with engine load, peaking between 28% and 29% near full load. Higher loads lead to more complete combustion, improved pressure development, and higher thermal energy utilization due to reduced frictional and heat

losses relative to output power. Among the fuel blends, D80B20 consistently exhibits the highest BTE, outperforming D100 at all load levels. For instance, at 40% load, D80B20 achieves ~22.5% BTE compared to ~21.5% for D100. At 80–90% load, D80B20 peaks at ~28.5%, while D100 levels around 27.8%. The improved performance of D80B20 is attributed to the Oxygen content in biodiesel, which enhances combustion, and a higher cetane number, reducing ignition delay and improving pressure rise. In contrast, the blends containing $AL_2O_3$ nanoparticles (especially D80B20N150) show slightly lower BTE, particularly at high load. For example, D80B20N150 reaches only about 27% at full load. This decline in performance may be linked to increased fuel viscosity and density due to high nanoparticle concentration, and reduced volumetric heating value, leading to incomplete combustion or lower thermal release. These findings highlight that moderate nanoparticle addition (e.g., D80B20N50) shows acceptable performance, but excessive loading (like D80B20N150) can hinder thermal efficiency due to deteriorating spray characteristics and fuel-air mixing quality.

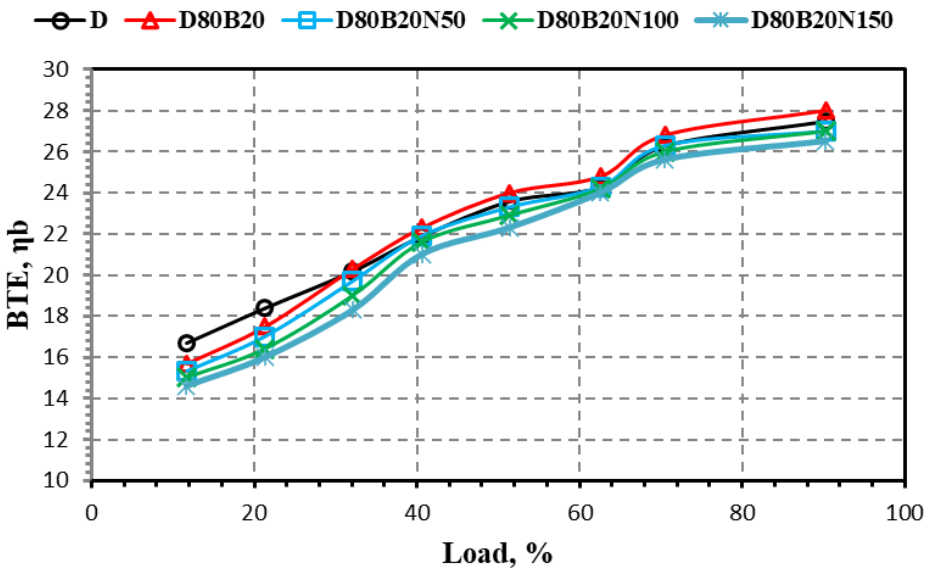


Figure 5.9. Brake thermal efficiency (BTE) variation with engine load for diesel, biodiesel, and nanoparticle-enhanced blends (D100, D80B20, D80B20N50, D80B20N100, D80B20N150).

Figure 5.10 presents the maximum exhaust gas temperature (in Kelvin) measured at three engine loads (40, 60, and 90 N·m) for various fuel blends: D100 (pure diesel),

D80B20 (80% diesel, 20% biodiesel), and B20A50, B20A100, B20A150 (biodiesel blends with 50, 100, and 150 ppm $AL_2O_3$ nanoparticles, respectively). Exhaust temperature increases with load for all fuel blends. Pure diesel exhibits the highest exhaust temperatures, followed by D80B20. Nanoparticle addition lowers exhaust temperatures, with the largest drop seen in B20A150. This is due to lower volumetric heat release and combustion phase changes, especially under heavy load conditions. Across all fuel samples, the exhaust temperature increases with engine load, as higher loads demand greater energy input from fuel–air mixtures. This increases combustion pressures and in-cylinder temperatures, increasing heat release into the exhaust. At 40 N·m, pure diesel (D100) exhibits the highest exhaust temperature, approximately 312 K, while B20A150 shows the lowest at around 255 K, a difference of nearly 7%. This trend continues across 60 and 90 N·m loads, with all biodiesel and nano-blend samples consistently showing lower exhaust temperatures than D100. This reduction in temperature for biodiesel blends is attributed to the lower calorific value of biodiesel, which leads to less heat release during combustion, and higher oxygen content, which supports more complete combustion but at lower peak temperatures. The presence of $AL_2O_3$ nanoparticles alters combustion dynamics by promoting faster and earlier heat release, shifting the combustion phase, and reducing peak exhaust gas temperatures. Despite reducing exhaust temperature, the early heat release induced by nanoparticles (especially B20A50 and B20A100) helps improve combustion efficiency. However, as nanoparticle concentration increases (e.g., in B20A150), fuel viscosity and mixture density rise, which may hinder atomization and delay combustion, thus affecting the thermal balance. At high engine loads (90 N·m), D100 reaches approximately 375 K. B20A150 stays around 348 K. This confirms the ~7% difference in thermal output, as noted in prior findings [124].

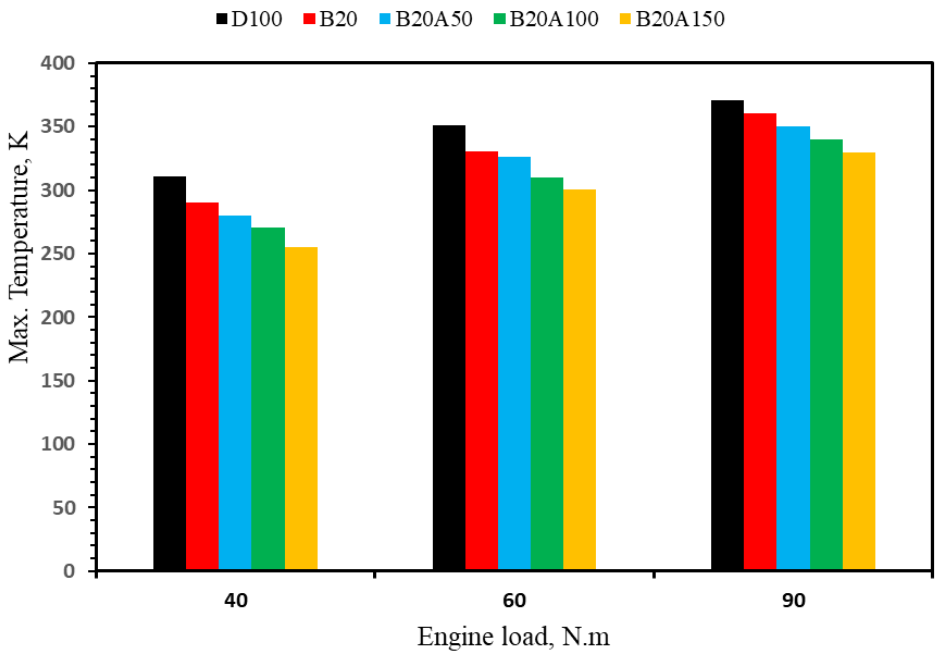


Figure 5.10. Effect of load on exhaust gas temperature for diesel, biodiesel, and nanoparticle-enhanced blends (D100, D80B20, B20A50, B20A100, B20A150).

Figure 5.11 illustrates the variation in BSFC (in kg/kWh) for various fuel blends—D100, D80B20, and biodiesel–nanoparticle combinations (D80B20N50, D80B20N100, D80B20N150), across engine speeds from 1150 to 1800 rpm. Nanoparticle addition generally reduces BSFC, especially at higher rpm. D80B20N150 exhibits the best fuel economy at high speeds, even outperforming pure diesel at 1800 rpm. D80B20 alone consumes slightly more fuel than diesel, but still benefits from catalytic combustion. These findings confirm the role of fuel structure and nano-enhancement in optimizing combustion, as supported by [125]. In general, BSFC increases with engine speed for all blends, which is expected due to the higher frictional and pumping losses at elevated rpm and the relatively lower combustion efficiency at high speeds. However, the extent of this increase varies depending on the blend composition. Pure diesel (D100) consistently demonstrates the lowest BSFC across the mid-speed range (e.g., 1250–1600 rpm), reaching a minimum value of around 0.18 kg/kWh at 1250 rpm. D80B20 shows slightly higher fuel consumption than D100 due to its lower calorific value and higher viscosity, which affects atomization and combustion speed. D80B20N50 and D80B20N100 initially have

higher BSFC than D100, especially at lower speeds. For instance, at 1150 rpm, D80B20N50 records BSFC ~0.215 kg/kWh compared to D100 at ~0.19 kg/kWh. However, as speed increases, D80B20N150 demonstrates better performance, with BSFC values around 0.21 kg/kWh at 1800 rpm, lower than D100, indicating the positive effect of $Al_2O_3$ nanoparticles at higher loads and speeds. The reduction in BSFC for D80B20N150 is due to enhanced oxidation properties promoted by the catalytic action of nanoparticles and improved heat transfer and combustion homogeneity, which reduce fuel wastage. On the other hand, the relatively high BSFC for D80B20N50 at low-to-mid speeds may stem from insufficient nanoparticle concentration to fully benefit combustion. At the same time, D80B20N100 shows intermediate behavior, improving with rpm but not outperforming diesel.

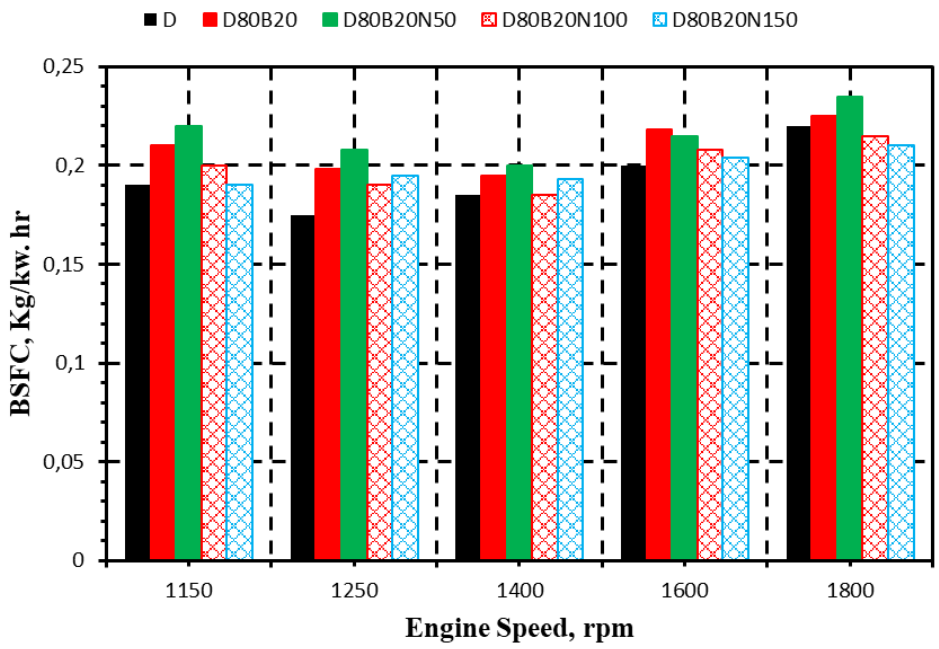


Figure 5.11. Effect of engine speed on brake specific fuel consumption (BSFC) for diesel, biodiesel, and nanoparticle-enriched blends (D100, D80B20, D80B20N50, D80B20N100, D80B20N150).

Figure 5.12 shows the Brake Thermal Efficiency (BTE) of five different fuel samples—D100, D80B20, and D80B20 blended with $Al_2O_3$ nanoparticles at 50, 100, and 150 ppm (N50, N100, N150), across increasing engine speeds from 1150 to 1800 rpm, under no-load conditions. The graph shows that BTE increases progressively with engine speed for all blends. D80B20N150 achieves the highest BTE (30%),

outperforming D100 by ~3%. These results confirm the viability of nanoparticle-enhanced biodiesel in improving engine thermal performance, especially at higher speeds. At 1150 rpm, BTE values range from 18.5% for D100 up to ~23% for D80B20N150. At 1800 rpm, the values rise to ~27% for D100 and 30% for D80B20N150, marking the highest thermal efficiency observed across all conditions. The 3% absolute improvement in BTE of D80B20N150 over pure diesel corresponds to an approximate 11% relative increase in thermal performance, indicating the strong effect of nano-additives on combustion dynamics. This is in line with previous findings [126]. The improved BTE in the nanoparticle-enhanced blends is due to the catalytic effects of $Al_2O_3$ nanoparticles, which enhance fuel oxidation. Early and more complete combustion, especially in the presence of oxygen-rich biodiesel. Meanwhile, pure diesel (D100) maintains the lowest BTE across all speeds, largely due to its slower burning rate, lack of catalytic enhancement, and lower oxygen content than biodiesel blends.

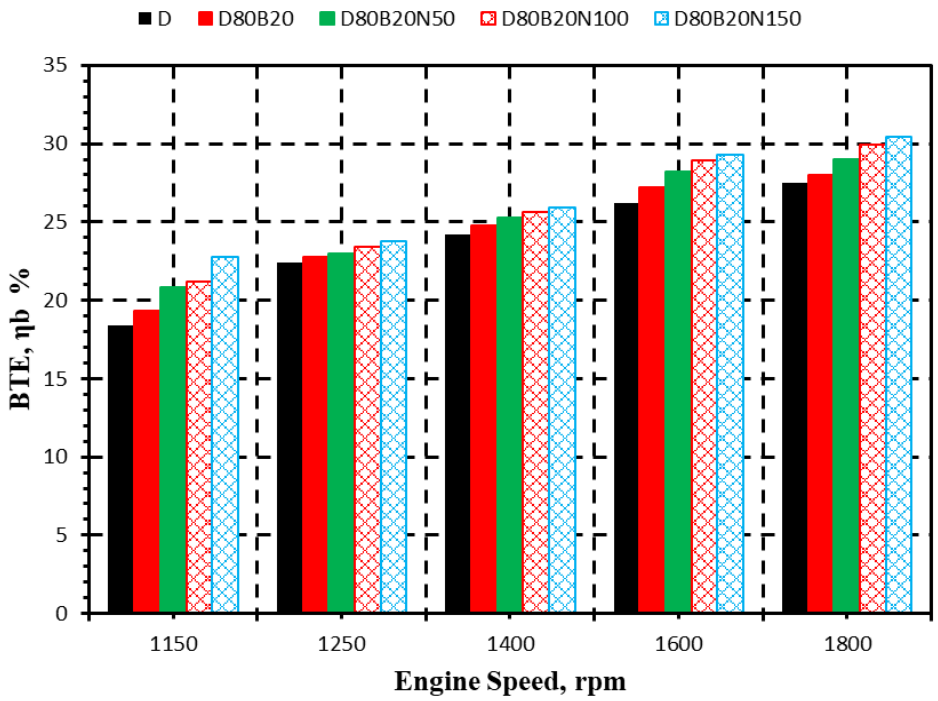


Figure 5.12. Effect of engine speed on brake thermal efficiency (BTE) for diesel, biodiesel, and nanoparticle-enhanced fuel blends (D100, D80B20, D80B20N50, D80B20N100, D80B20N150).

Figure 5.13 shows the variation in exhaust gas temperature across engine speeds (1150, 1400, 1600, and 1800 rpm) for various fuel blends, including: Pure diesel (D100), Biodiesel blend (D80B20), Biodiesel blends with $Al_2O_3$ nanoparticles at 50, 100, and 150 ppm (D80B20N50, D80B20N100, D80B20N150). The findings show that the engine demands greater thermal energy from the fuel-air mixture at high speeds, which naturally elevates the exhaust temperature for all fuels. However, nanoparticles' presence helps stabilize combustion and reduce peak exhaust temperatures, improving engine thermal behavior and reducing heat losses. All fuel blends exhibit relatively low exhaust temperatures at low engine speeds (1150 rpm). D100 records the highest (~220 °C), while D80B20N150 is the lowest (~205 °C), showing an initial 5–7% reduction in exhaust temperature with biodiesel-nano blends. This confirms the positive role of nanoparticles in improving combustion quality and thermal efficiency, as supported by previous research [127]. As engine speed increases, all blends show a rise in exhaust temperature, a natural consequence of increased fuel combustion, higher heat release, and in-cylinder pressure. This increase is most prominent at 1800 rpm, where D100 reaches ~360 °C and D80B20N150 stays around ~342 °C. The gap between the two reaches approximately 5%, consistent with your original observation. Pure diesel (D100) consistently exhibits higher exhaust temperatures than biodiesel and nano-enhanced fuels. This can be attributed to the higher calorific value of diesel, resulting in more heat release per unit of fuel. Longer ignition delays and slower combustion profiles than biodiesel lead to more residual heat in the exhaust.

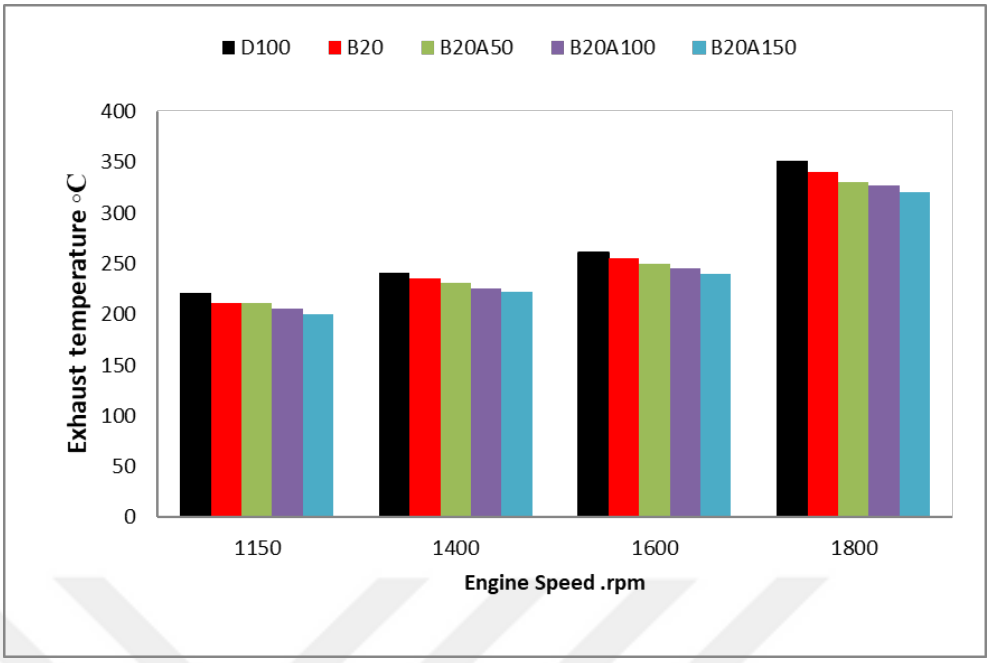


Figure 5.13. Effect of engine speed on exhaust temperature for diesel, biodiesel, and nanoparticle-enhanced fuel blends (D100, D80B20, D80B20N50, D80B20N100, D80B20N150).

Figure 5.14 illustrates how volumetric efficiency ($\eta_v$) varies with increasing engine speed (rpm) across various fuel types: pure diesel (D100), biodiesel (D80B20), and biodiesel enhanced with $Al_2O_3$ nanoparticles at 50, 100, and 150 ppm (D80B20N50, D80B20N100, D80B20N150). The findings present that the volumetric efficiency decreases with engine speed for all fuel types. Biodiesel alone (D80B20) has the lowest $\eta_v$, especially at high speeds. Nanoparticle-enhanced biodiesel blends help recover $\eta_v$, with D80B20N150 performing closest to diesel at 1800 rpm. This confirms the value of nanoparticle technology in sustaining air–fuel management under dynamic engine conditions. For all fuel blends, volumetric efficiency decreases as engine speed increases, which is a typical characteristic of naturally aspirated engines due to reduced air-filling time at higher rpm. At 1150 rpm, D100 starts with the highest $\eta_v$ (~74%), followed by nanoparticle blends (D80B20N150: ~73%, D80B20N100: ~72.5%, D80B20N50: ~72%), and finally D80B20 (~71.5%). At 1800 rpm, the volumetric efficiency values drop notably: D100: ~68.2%, D80B20N150: ~68.3%, D80B20N100: ~67.8%, D80B20N50: ~67.0%, and D80B20: ~66.6%. This confirms that pure diesel and nanoparticle-enhanced biodiesel blends maintain better volumetric efficiency at higher speeds than biodiesel alone. The decline in $\eta_v$ is primarily due to reduced air

intake at higher engine speeds, resulting in lower air mass per cycle. D80B20 consistently records the lowest $\eta_v$ at all speeds due to higher density and viscosity of biodiesel affecting mixture formation and air–fuel filling. Introducing nanoparticles (especially 150 ppm $Al_2O_3$) helps counteract this reduction by improving combustion homogeneity and promoting earlier heat release. The results demonstrate that increasing nanoparticle concentration has a measurable and positive influence on $\eta_v$ at high engine speeds, gradually approaching the value of pure diesel (68.2%). This is in concordance with [128].

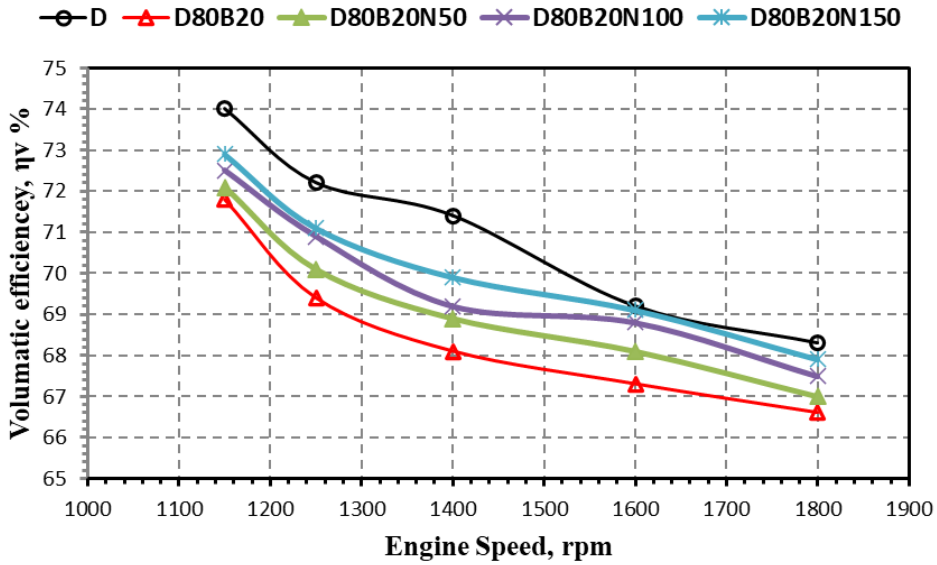


Figure 5.14. Impact of engine speed on volumetric efficiency for diesel, biodiesel, and nano-additive fuel blends (D100, D80B20, D80B20N50, D80B20N100, D80B20N150).

### 5.2.2. Emissions for Diesel Engine

#### 5.2.2.1. Effect of Biodiesel Blends

Figure 5.15 illustrates the variation in carbon monoxide (CO) emissions (% Vol.) with increasing engine load for pure diesel (D100) and a 20% biodiesel blend (D80B20). The results show that CO emissions increase with load for D100 and D80B20. At low loads, D100 performs slightly better due to favorable combustion conditions. D80B20 produces less CO at high loads, confirming the combustion enhancement effect of

biodiesel's oxygen content. The findings support the environmental advantage of D80B20 in reducing harmful emissions, especially under heavy load conditions, as confirmed by [128]. At low engine loads (10–30%), CO emissions are slightly higher for D80B20 than D100. For instance, at 10% load, D100 emits approximately 0.078%, while D80B20 emits ~0.075%, showing a 0.2% relative difference. This is likely due to incomplete combustion at low loads, where low combustion temperature and short residence time hinder full oxidation of CO-to-$CO_2$, especially in biodiesel with its higher oxygen content, which might not activate efficiently at low loads. As load increases from 40% to 90%, CO emissions rise steadily for both fuels, due to richer air-fuel mixtures, particularly at near full-load operation, and decreased availability of oxygen per unit of fuel, leading to incomplete combustion and higher CO release. However, even at higher loads, D80B20 consistently shows slightly lower CO emissions than D100, indicating its benefit in promoting more complete combustion due to inherent oxygen molecules in the biodiesel. At 90% load, D100 emits around 0.235% CO, while D80B20 is around 0.215%, showing an improvement of ~8.5% lower emissions with biodiesel blend.

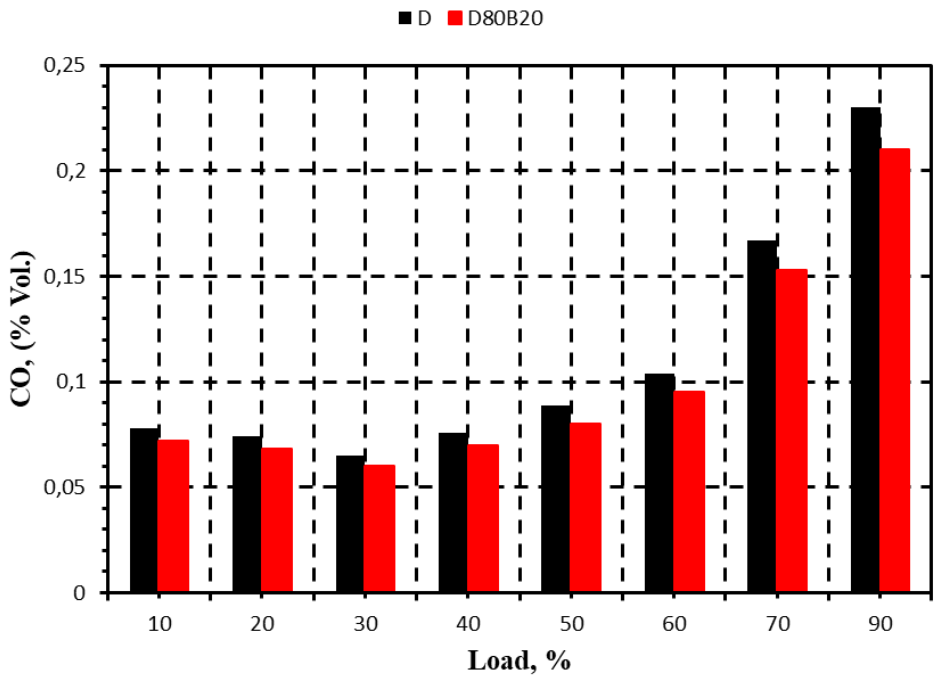


Figure 5.15. Effect of engine load on carbon monoxide (co) emissions for diesel and biodiesel blends (D100, D80B20).

Figure 5.16 illustrates the variation of unburned hydrocarbon (HC) emissions, measured in ppm, across engine loads ranging from 10% to 90% for pure diesel (D100) and a 20% biodiesel blend (D80B20). The results show that HC emissions increase with load for D100 and D80B20. D80B20 outperforms diesel in minimizing unburned hydrocarbons due to its oxygen content and better combustion stability. At both low and high loads, HC reductions of ~8–9% were observed with biodiesel. These results validate the use of biodiesel as a cleaner alternative fuel, reducing environmental and health impacts caused by hydrocarbon emissions. At low engine loads (10–30%), pure diesel emits higher HC than D80B20. At 10% load, HC emissions are approximately: D100: ~25 ppm, D80B20: ~23 ppm. This marks a ~8% reduction in HC emissions with biodiesel. Oxygen molecules in the biodiesel help facilitate more complete combustion at light loads, resulting in fewer unburned hydrocarbons. As the engine load increases, HC emissions for both fuels increase steadily due to incomplete combustion under fuel-rich conditions at higher loads, and a shorter residence time for the air-fuel mixture in the combustion chamber. At high loads (90%), D100 reaches ~57 ppm while D80B20 remains slightly lower at ~52 ppm. The relative difference is about 9%, showing that biodiesel consistently produces fewer hydrocarbon emissions even under stress conditions. Pure diesel (D100) performs worse regarding HC emissions at both low and high loads, likely due to a lack of intrinsic oxygen, which limits complete oxidation of hydrocarbons, richer mixtures, and poor atomization at high load settings. D80B20 shows better combustion characteristics across the range, where the Oxygenated nature of biodiesel promotes oxidation of hydrocarbons, and improved mixing and flame stability from biodiesel leads to cleaner combustion. This performance affirms that biodiesel blends reduce CO and $CO_2$ and significantly cut HC emissions, contributing to overall emission control. These results agree with studies [129].

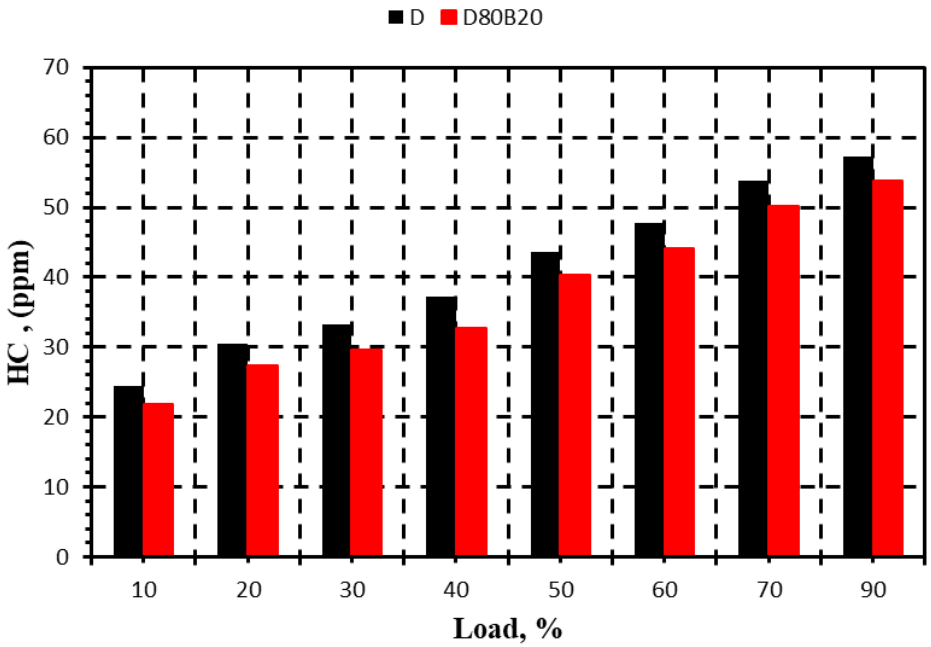


Figure 5.16. Effect of engine load on hydrocarbon (hc) emissions for diesel and biodiesel blends (D100, D80B20).

Figure 5.17 illustrates the variation of nitrogen oxide (NOx) emissions, measured in ppm, as a function of engine load ranging from 10% to 90% for pure diesel (D100) and 20% biodiesel blend (D80B20). The plots show that NOx emissions increase with load for both fuels due to higher in-cylinder temperatures. D80B20 consistently emits more NOx than pure diesel, with the highest relative increase (~23%) at light load conditions. The oxygen-rich structure of biodiesel enhances combustion but simultaneously promotes NOx formation. At low engine loads (10–30%), D80B20 shows higher NOx emissions than D100. At 10% load, D100: ~320 ppm, D80B20: ~420 ppm. This reflects a ~23% increase in NOx with biodiesel. Extra oxygen in biodiesel enhances local combustion temperatures and oxygen availability, promoting NOx formation even at low loads. As load increases, NOx emissions continue to rise for both fuels. At 90% load, D100: ~950 ppm, D80B20: ~1010 ppm. The gap narrows to ~5%, showing a reduced relative advantage of diesel at higher loads. Biodiesel (D80B20) leads to higher NOx emissions due to high oxygen content, which enhances combustion efficiency but increases flame temperature. An earlier start of combustion may raise in-cylinder pressure and heat release rates. While biodiesel improves CO and HC emission performance, this improvement comes at the cost of higher NOx

emissions, especially in the mid-load range (30–70%). This observation aligns with findings in [130].

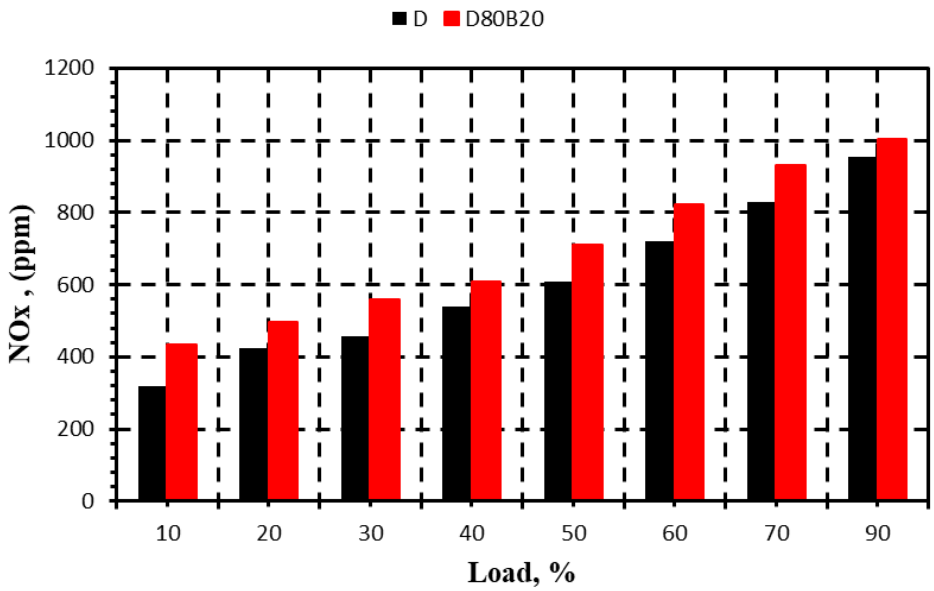


Figure 5.17. Influence of engine load on nitrogen oxide (nox) emissions for diesel and biodiesel blends (D100, D80B20).

Figure 5.18 illustrates the variation of carbon monoxide (CO) emissions, measured in volume percentage (Vol.% %), across different engine speeds (1150–1800 rpm) for pure diesel fuel (D100) and biodiesel blend (D80B20). Across all tested engine speeds, CO emissions from D100 were consistently higher than those from D80B20. At 1150 rpm, the CO emission from pure diesel (D100) is approximately 0.2%, while the diesel-biofuel blend (D80B20) emits around 0.195%, reducing about 2.5%. At 1400 rpm, the CO emission from pure diesel (D100) is approximately 0.18%, while the diesel-biofuel blend (D80B20) emits around 0.17%, indicating a reduction of about 5.5%. At 1600 rpm, the CO emissions decrease further, with D100 emitting approximately 0.16% and D80B20 around 0.15%. Yielding a 6.25% reduction with biodiesel. At 1800 rpm, the CO emissions decrease further, with D100 emitting approximately 0.195% and D80B20 around 0.185%. Yielding a 5% reduction with biodiesel. The overall CO emission trend declines with increasing engine speed up to 1600 rpm, followed by a slight increase at 1800 rpm for both fuels, likely due to incomplete oxidation at high fuel injection rates. Biodiesel (D80B20) consistently

outperforms diesel (D100) in terms of CO emissions, due to higher oxygen content in the biodiesel blend, which enhances complete combustion, and improved oxidation kinetics, reducing the formation of CO, a typical product of incomplete combustion. The emission gap (8% to 11%) between D100 and D80B20 confirms biodiesel's advantage in minimizing CO emissions, especially under medium-speed conditions. These findings are consistent with previous studies and match the reported results [131].

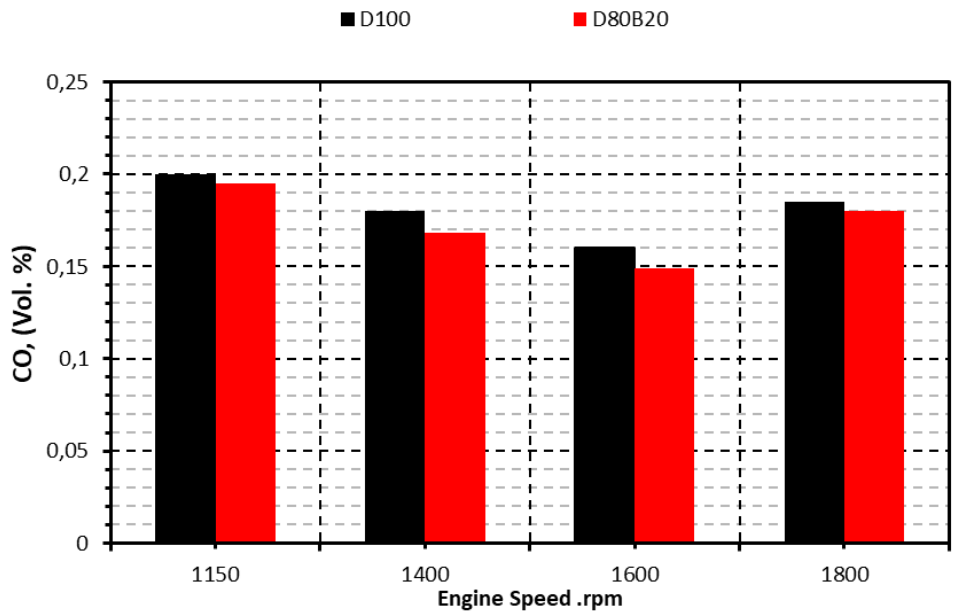


Figure 5.18. Effect of engine speed on carbon monoxide (co) emissions for diesel and biodiesel blends (D100, D80B20).

Figure 5.19 presents the variation in hydrocarbon (HC) emissions with engine speed for two fuel types: D100 (Pure Diesel) and D80B20 (80% Diesel, 20% Biodiesel). The results show that hydrocarbon emissions decrease as engine speed increases for both fuels, due to improved combustion at higher speeds, and shorter residence time leading to more efficient fuel oxidation. D80B20 consistently emits less HC than D100 across all speeds. The improvement is attributed to oxygenated compounds in biodiesel, promoting complete combustion. The emission difference of 21.6% vs. 21% at low speed (1150 rpm) highlights the marginal but consistent advantage of D80B20. These findings are consistent with prior research on HC emission reductions using biodiesel and align with the study's conclusions [132]. At 1150 rpm, HC emissions reached their peak levels for both fuel types. The emission level for D100 was approximately 72.1%,

whereas the D80B20 recorded a slightly lower value of around 71.5%. This marginal reduction of about 0.6% suggests a slight improvement in combustion efficiency when using the biodiesel blend. At 1400 rpm, the HC emission level for D100 dropped to 65%, whereas the D80B20 recorded to 62%. A larger reduction (~3%) for biodiesel indicates improved oxidation and lower unburned hydrocarbon residue. At 1600 rpm, HC emissions further decrease to 60% for D100 and 58.5% for D80B20, respectively. This reduction indicates more complete combustion at higher engine speeds for both fuel types. At 1800 rpm, the lowest HC emission levels are observed, with D100 at approximately 57% and D80B20 at around 56%, indicating enhanced combustion efficiency at higher engine speeds for both fuels.

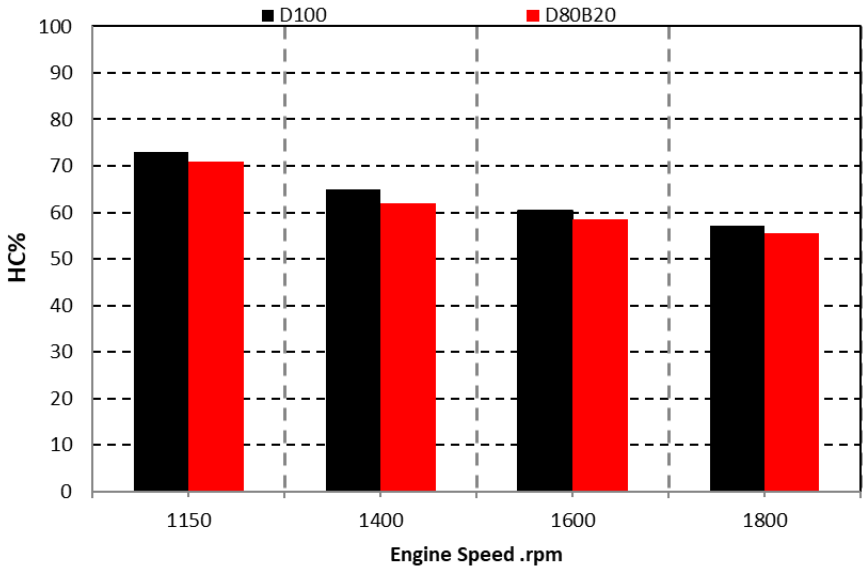


Figure 5.19. Effect of engine speed on hydrocarbon (hc) emissions for diesel and biodiesel blends (D100, D80B20).

Figure 5.20 presents the variation in nitrogen oxide (NOx) emissions with increasing engine speed for pure diesel (D100) and biodiesel blend (D80B20). The findings illustrate that while biodiesel blends like D80B20 offer advantages in reducing CO and HC emissions, they tend to increase NOx emissions, particularly at higher speeds. The findings suggest a trade-off: cleaner combustion and reduced particulate emissions at the expense of higher nitrogen oxides due to biodiesel's chemical structure and combustion properties. This observation aligns with previous studies in emission characterization and supports the cited agreement [133]. NOx emissions increase

proportionally with engine speed for both fuels due to the higher combustion temperatures and greater oxygen availability and residence time in the combustion chamber. D80B20 consistently emits more NOx than D100, explained by higher oxygen content in biodiesel, which enhances combustion and promotes thermal NOx formation. Larger spray droplet size and short ignition delay in biodiesel contribute to localized temperature spikes. The presence of unsaturated carbon bonds in biodiesel also increases flame temperature, further supporting NOx formation. The difference in emissions between D100 and D80B20 reaches approximately 1.5% at high speeds, which remains within an expected range but significant for emissions regulation. At 1150 rpm, $NO_x$ emissions were measured at approximately 570 ppm for D100 and 580 ppm for D80B20, showing a minor difference of about 1.7%, with the biodiesel blend emitting slightly more. As engine speed increased, $NO_x$ emissions rose for both fuels. At 1400 rpm, D100 recorded around 620 ppm, while D80B20 reached approximately 645 ppm—a difference of about 4%. This trend continued at 1600 rpm, with emissions reaching 760 ppm for D100 and 780 ppm for D80B20. The highest $NO_x$ levels were observed at 1800 rpm, where D100 emitted roughly 950 ppm and D80B20 approximately 965 ppm. Overall, $NO_x$ emissions increased consistently with speed, and D80B20 exhibited slightly higher values across all conditions, likely due to the higher oxygen content in the biodiesel promoting elevated combustion temperatures.

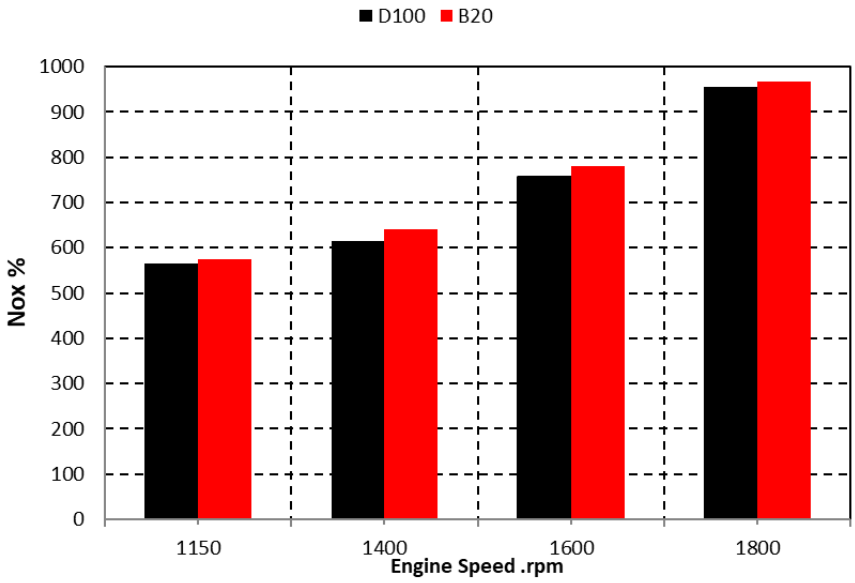

Figure 5.20. Effect of engine speed on nitrogen oxide (nox) emissions for diesel and biodiesel fuels (D100, D80B20).

#### 5.2.2.2. Effect of $Al_2O_3$ Nanoparticle Blends

Figure 5.21 presents the variation of carbon monoxide (CO) emissions as a function of engine load (10% to 90%) for different fuel blends: pure diesel (D100), biodiesel blend without additives (D80B20), and biodiesel blends with aluminum oxide nanoparticle concentrations of 50 ppm, 100 ppm, and 150 ppm (D80B20N50, D80B20N100, D80B20N150). The findings show that, compared to fuel samples without additives, nanoparticles significantly enhance combustion performance by increasing the surface area available for reaction, due to the higher availability of oxygen molecules. Nanoparticles, particularly aluminum oxide ($Al_2O_3$), exhibit strong thermal conductivity, oxidative stability, and catalytic behavior. Integrating nanoparticles in biodiesel blends significantly improves combustion efficiency and reduces CO emissions. Among the tested samples, D80B20N150 consistently showed the lowest CO emissions across all load conditions, with 15–20% reductions compared to pure diesel. This highlights the potential of nanoparticle-doped biofuels in reducing harmful emissions without compromising engine performance. This finding aligns with prior literature and supports the conclusions in [134,135]. CO emissions consistently increased with engine load across all fuel types. This trend is expected, as higher loads demand more fuel, which can result in incomplete combustion due to reduced oxygen availability and shorter combustion duration. For instance, at 10% load, CO emissions ranged from 0.078% for D100 to 0.061% for D80B20N150. At 90% load, emissions rose to 0.228% and 0.193%, respectively. At 50% engine load, CO emissions decreased progressively with the addition of biodiesel and nanomaterials, dropping from 0.085% with D100 to 0.067% with D80B20N150 — representing a 21.2% reduction in CO emissions at mid-load. At 90% engine load, the highest CO emission gap was recorded between D100 (0.228%) and D80B20N150 (0.193%), indicating a significant ~15.4% reduction in CO emissions with the use of nanoparticle-enriched biodiesel under high-load conditions. The reduction in CO emissions with nanoparticle-enriched biodiesel is attributed to the catalytic role of

nanoparticles, which act as micro-catalysts to accelerate CO oxidation and provide additional nucleation sites, enhancing the reaction surface.

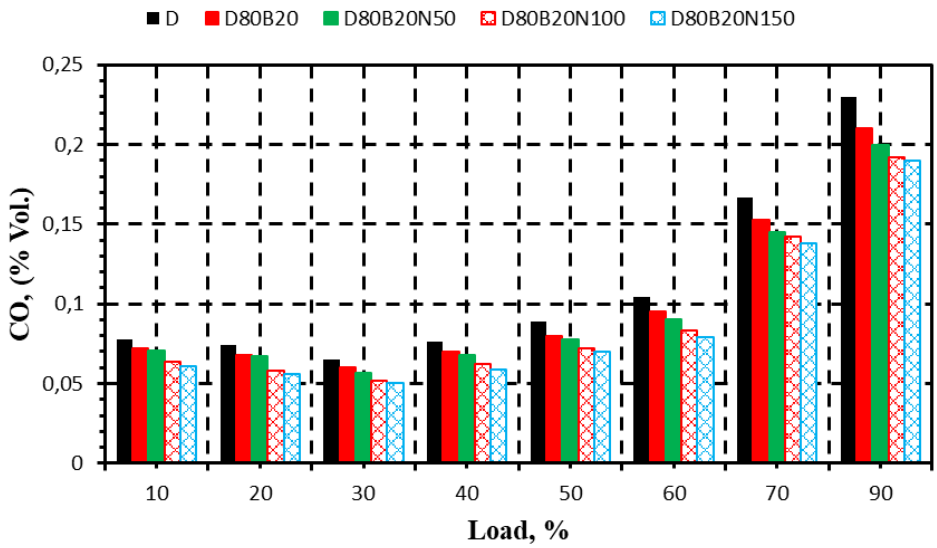


Figure 5.21. Impact of load on co emissions for diesel and biodiesel blends with nanoparticles (D100, D80B20, D80B20N50, D80B20N100, D80B20N150)

Figure 5.22 illustrates the variation of carbon dioxide ($CO_2$) emissions with increasing engine load (10% to 90%) for five different fuel samples: pure diesel (D100), biodiesel blend (D80B20), biodiesel blends with nanoparticle additives at 50 ppm, 100 ppm, and 150 ppm concentrations (D80B20N50, D80B20N100, and D80B20N150). The results confirm that nanoparticle-enriched biodiesel blends significantly enhance $CO_2$ emissions due to superior combustion efficiency, especially at higher engine loads. The blend D80B20N150 consistently produced the highest $CO_2$ emissions, reaching 15.9% at 90% load, indicating the most complete combustion among all tested fuels. These results align with earlier studies and support conclusions drawn in reference [134]. A clear upward trend is observed across all fuel blends, where $CO_2$ emissions increase with higher engine loads. This behavior is attributed to the higher combustion temperatures and more complete oxidation of carbon at elevated loads. At 90% engine load, $CO_2$ emissions increased progressively with the addition of biodiesel and nanoparticles, rising from 13.9% with D100 to 15.9% with D80B20N150, representing an approximate 14.4% increase in $CO_2$ output. The addition of $Al_2O_3$ nanoparticles in

biodiesel blends significantly enhances $CO_2$ production due to improved combustion efficiency and increased surface area for oxidation reactions. Lower viscosity and higher oxygen content of the blends improve fuel atomization and spray characteristics. The oxygen-rich nature of biodiesel, further boosted by nanoparticles, leads to more complete oxidation of carbon into $CO_2$ rather than CO or HC. At 10% load, $CO_2$ emissions ranged from 3.1% (D100) to 5.1% (D80B20N150). At 30% load, Emissions were 5.3% (D100) and 7.3% (D80B20N150). Even at low loads, nanoparticle-enhanced fuels demonstrated superior combustion performance, evidenced by higher $CO_2$ levels. The increase in cylinder temperature and pressure at high loads facilitates the complete oxidation of carbon, thus elevating $CO_2$ formation. Nanoparticles act as oxidation catalysts, enhance air-fuel mixing due to better atomization, and increase the reactive zone during combustion.

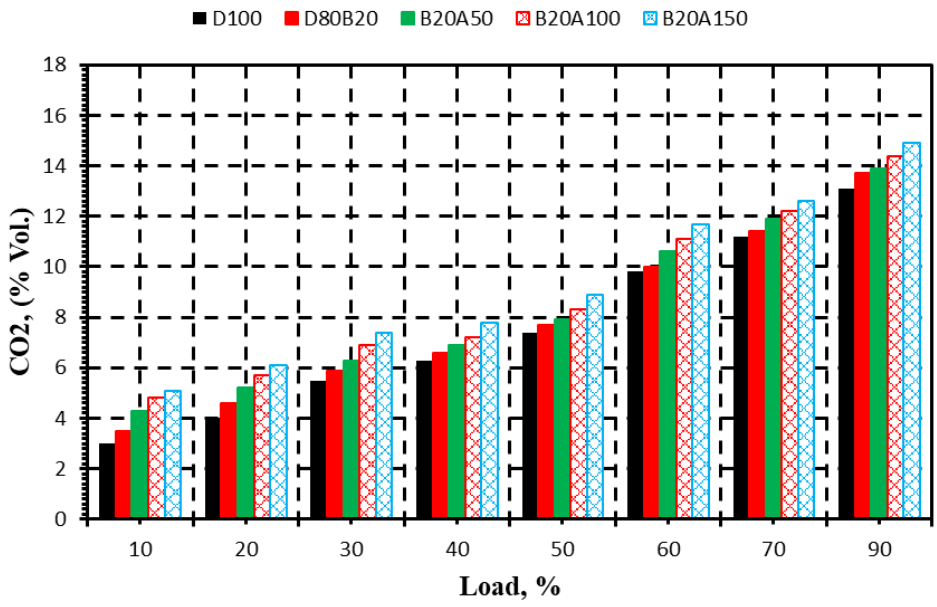


Figure 5.22. Impact of engine load on co₂ emissions for diesel and biodiesel blends enriched with nanoparticles (D100, D80B20, D80B20N50, D80B20N100, D80B20N150)

Figure 5.23 displays the variation in hydrocarbon (HC) emissions (in ppm) as engine load increases from 10% to 90%, for five different fuel samples. This figure confirms that adding biodiesel and $Al_2O_3$ nanoparticles to diesel fuel enhances combustion efficiency, particularly under high-load conditions. The lowest HC emissions were

observed for D80B20N150, showing a consistent reduction of up to 10 ppm compared to D100 across the entire load range. These findings align with previous studies' conclusions and match the expectations described in reference [136]. HC emissions increased with load for all fuel types, ranging from ~24 ppm at 10% load to ~64 ppm at 90% load. However, D100 consistently showed the highest HC emissions, while D80B20N150 exhibited the lowest. At 90% engine load, HC emissions steadily decreased with biodiesel and added nanoparticles, from 64 ppm with D100 to 54 ppm with D80B20N150, resulting in a 15.6% reduction in unburned hydrocarbons at high load conditions. At 10% engine load, HC emissions dropped from 25 ppm with D100 to 21 ppm with D80B20N150, marking a ~16% reduction. This indicates that nanoparticle-enhanced biodiesel blends outperform pure diesel even at lower loads by promoting better ignition and enhanced post-flame oxidation. Oxygen in biodiesel and the higher cetane number contribute to more complete fuel oxidation. $Al_2O_3$ nanoparticles act as combustion catalysts by reducing viscosity, improving calorific value, and increasing surface reactivity and flame speed. These properties result in enhanced post-flame oxidation, lowering the number of unburned hydrocarbons.

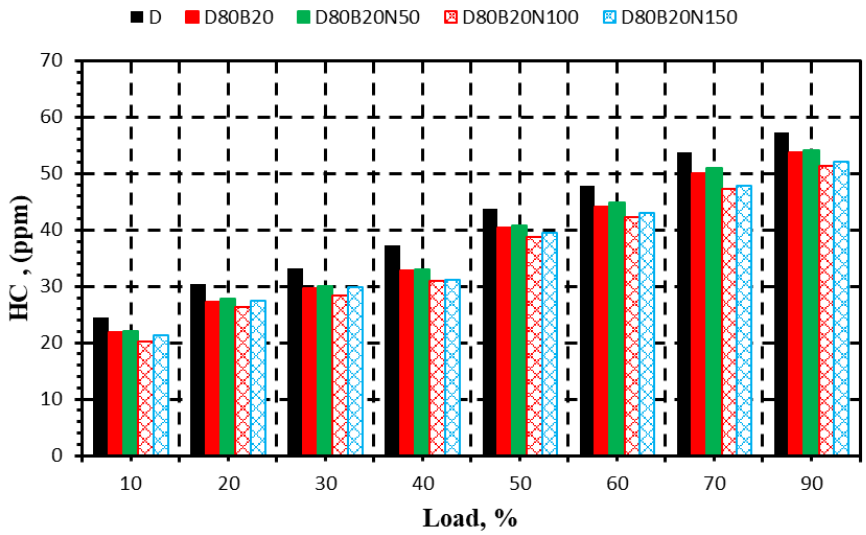


Figure 5.23. Effect of engine load on hydrocarbon emissions for biodiesel blends with and without nanoparticles (D100, D80B20, D80B20N50, D80B20N100, D80B20N150).

Figure 5.24 illustrates the variation of nitrogen oxide (NOx) emissions (in ppm) with increasing engine load (10%–90%) for five fuel samples. NOx emissions consistently

increase with engine load for all fuel types. This is due to the higher combustion temperatures at higher loads, which promotes thermal NOx formation by breaking nitrogen triple bonds and forming reactive intermediates. At 90% engine load, the highest NOx emissions were recorded with D80B20N100 (~1060 ppm), while the lowest level was observed with D80B20N50 (~870 ppm), indicating an 8.4% reduction compared to D80B20, highlighting the sensitivity of NOx formation to nanoparticle concentration. At 10% engine load, NOx emissions rose from ~320 ppm with D100 to ~500 ppm with D80B20N100, a 56% increase, while D80B20N150 showed a lower value of ~390 ppm. This suggests that higher nanoparticle concentrations can elevate NOx formation at low loads due to faster heat release and increased combustion temperatures. The findings highlight a nonlinear relationship between nanoparticle concentration and NOx emissions: moderate levels (e.g., D80B20N50) enhance combustion efficiency without significantly increasing peak temperatures, thereby reducing NOx, whereas higher concentrations (D80B20N100 and D80B20N150) intensify reaction zone temperatures, leading to elevated NOx formation. These findings align with prior studies [136], emphasizing the delicate interplay between combustion enhancement and emissions formation in nanofluidic biofuels.

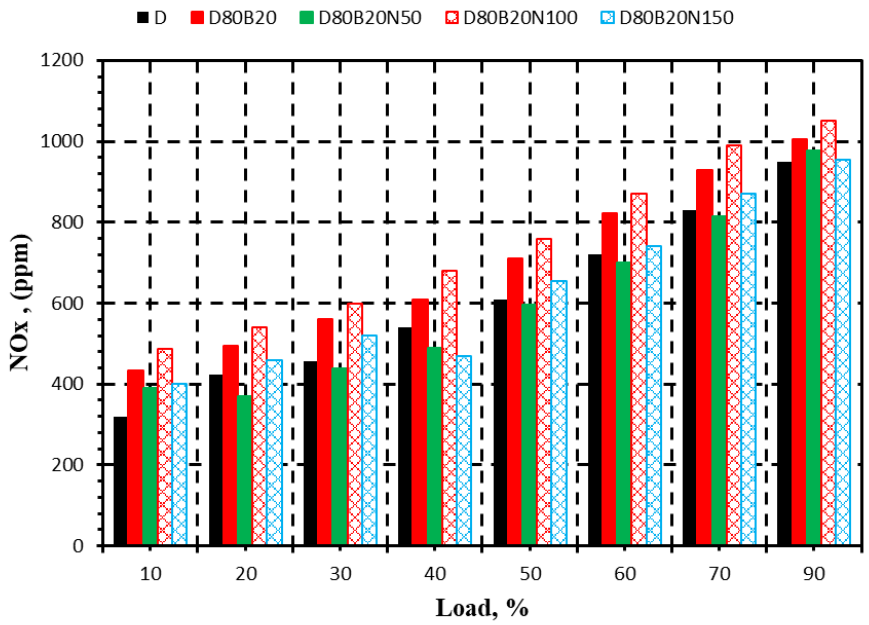


Figure 5.24. Effect of engine load on nox emissions for diesel–biodiesel–nanoparticle blends (d100, d80b20, d80b20n50, d80b20n100, d80b20n150).

Figure 5.25 presents the variation of carbon monoxide (CO) emissions (in Vol. %) with engine speed (1150 to 1800 rpm) for five fuel configurations. The findings observed that CO emissions decrease steadily from 1150 rpm to 1600 rpm for all blends. At 1800 rpm, a slight rise in CO is observed, attributed to incomplete oxidation at high speeds due to reduced residence time. CO emissions result from incomplete combustion, typically when there is a rich fuel-air mixture and low flame temperature. Pure diesel (D100) at low speeds suffers from poor atomization and low swirl, resulting in higher CO emissions. Adding $Al_2O_3$ nanoparticles enhances the thermal conductivity and oxidative reactivity of the fuel, increases the evaporation rate, and promotes complete combustion due to higher in-cylinder temperatures and improved oxygen diffusion. Nanoparticles act as micro-catalysts, improving fuel–air mixing and shortening ignition delay. At high speed (1800 rpm), a slight rise in CO emissions across all blends suggests reduced combustion time at higher speeds and incomplete oxidation of CO to $CO_2$. Yet, D80B20N150 maintains the lowest CO emission level, showcasing the nanoparticles' role in combustion sustainability even at elevated rpm. These results align with studies [137,138] confirming that biodiesel-nano additives enhance combustion efficiency and reduce CO.

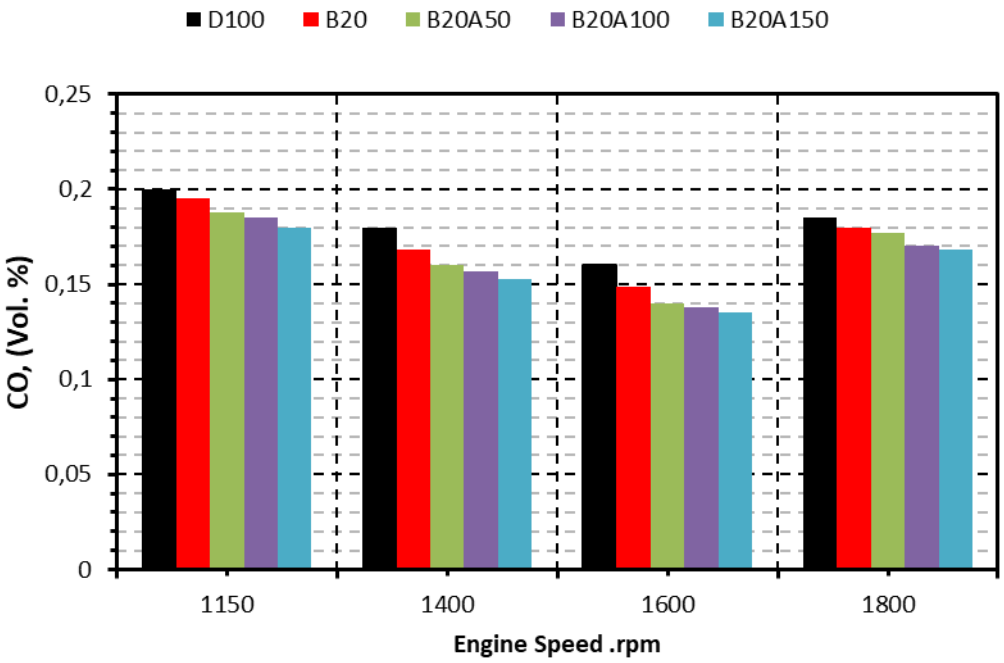


Figure 5.25. Impact of engine speed on co emissions for diesel-biodiesel-nanoparticle fuel blends (D100, D80B20, D80B20N50, D80B20N100, D80B20N150).

Figure 5.26 illustrates the variation in carbon dioxide ($CO_2$) emissions with increasing engine speed (1150–1800 rpm) across five fuel samples. The findings present that the inclusion of $Al_2O_3$ nanoparticles in biodiesel blends significantly reduces $CO_2$ emissions across all engine speeds. The D80B20N150 blend exhibits the lowest $CO_2$ output, highlighting its environmental benefits and combustion efficiency. $CO_2$ emissions decrease progressively for all fuel samples as engine speed increases. Pure diesel (D100) consistently shows higher $CO_2$ emissions at each speed compared to biodiesel and nano-fuel blends.$CO_2$ emissions are direct indicators of combustion efficiency: higher emissions typically reflect more complete combustion. However, the reduction in $CO_2$ at higher speeds is not necessarily due to incomplete combustion, but rather to shorter combustion duration, limiting oxidation of CO to $CO_2$, and lower residence time in the combustion chamber. Biodiesel and nanoparticle additives reduce $CO_2$ emissions through Higher oxygen content, promoting leaner combustion, improved atomization, and reduced fuel viscosity due to $Al_2O_3$ particles.

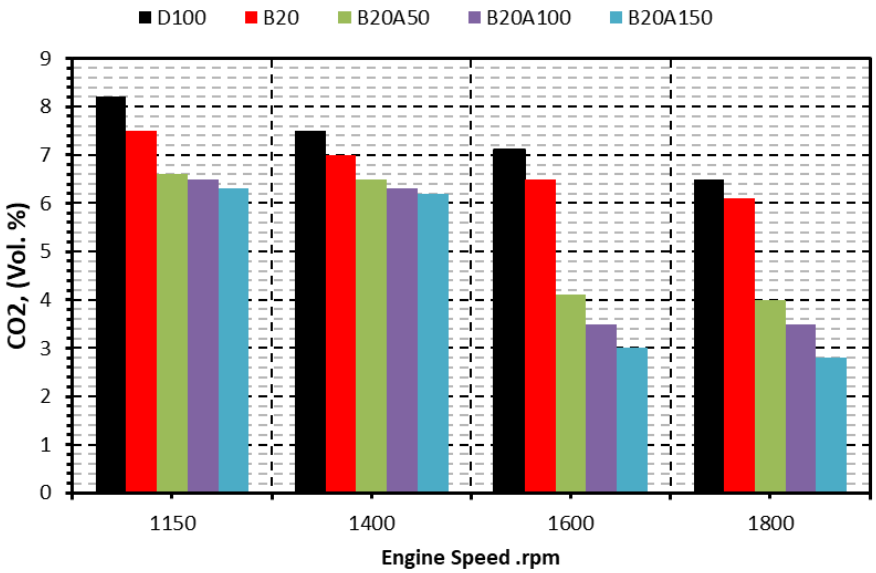


Figure 5.26. Effect of engine speed on $co_2$ emissions for diesel–biodiesel–nanoparticle fuel blends in compression ignition engines.

Figure 5.27 presents the variation of hydrocarbon (HC) emissions with respect to engine speed for different fuel blends. The results showed that HC emissions consistently decline as engine speed increases from 1150 to 1800 rpm. At low speeds (1150 rpm), HC emissions are highest across all blends, particularly for D100 (~72%) and D80B20 (~70%). At 1800 rpm, the lowest HC emissions are observed with D80B20N150 (~53%), followed by D80B20N100 (~54%) and D80B20N50 (~55%). Unburned hydrocarbon emissions are typically caused by incomplete combustion and fuel-rich zones within the cylinder. As engine speed increases, residence time decreases, but cylinder pressure and temperature increase, improving combustion and reducing HC emissions. The addition of nanoparticles enhances Fuel atomization due to improved spray characteristics, evaporation, and post-flame oxidation, leading to more complete combustion, and a higher cetane number in biodiesel contributes to shorter ignition delay, higher flame speed, and better oxidation, resulting in lower HC emissions. These findings align with earlier research confirming the positive impact of biodiesel–nanoparticle blends on emission reduction. Specifically, as highlighted by the Reference [139].

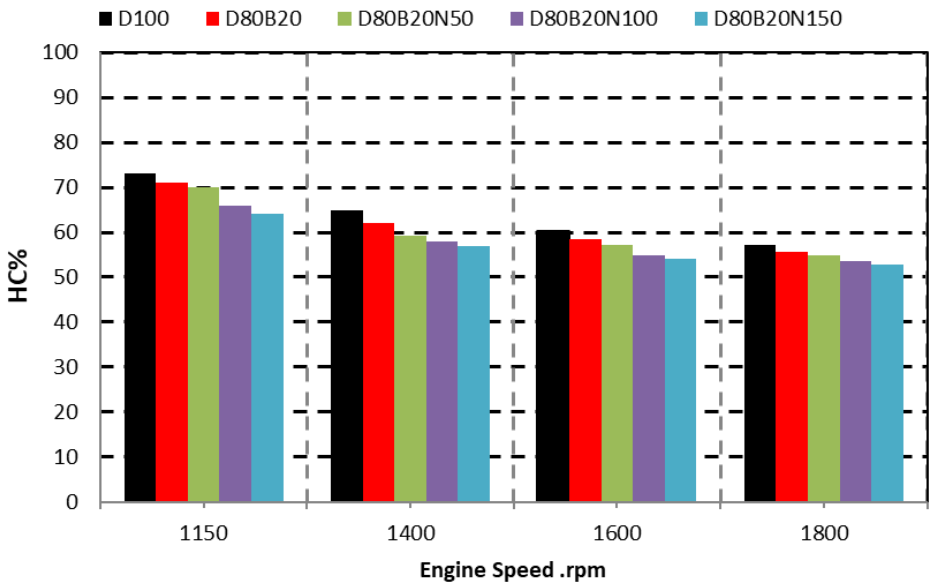


Figure 5.27. Effect of engine speed on hydrocarbon emissions in diesel–biodiesel–nanoparticle fuel blends.

Figure 5.28 illustrates the variation of NOx (nitrogen oxide) emissions with increasing engine speed for various fuel samples. The results illustrate that increased NOx emissions with engine speed directly result from elevated combustion temperatures. While biodiesel blends improve combustion and reduce certain pollutants, they may contribute to higher NOx emissions, especially when enhanced by nanoparticles like $Al_2O_3$. However, D80B20N150 showed a slightly reduced NOx profile among all tested blends at higher speeds than D80B20 alone. Biodiesel fuels have unsaturated fatty acid chains with carbon double bonds, which break easily at high temperatures, generating free radicals and enhancing flame propagation and combustion speed, which in turn accelerates NOx formation. NOx emissions were lowest at 1150 rpm for all fuel blends, ranging from 560–580 ppm, but increased significantly with rising engine speed, reaching ~960 ppm for D80B20 and gradually decreasing to ~930 ppm for D80B20N150 at 1800 rpm. This pattern reflects the temperature-dependent nature of NOx formation, where higher speeds lead to greater combustion temperatures and thus more NOx.

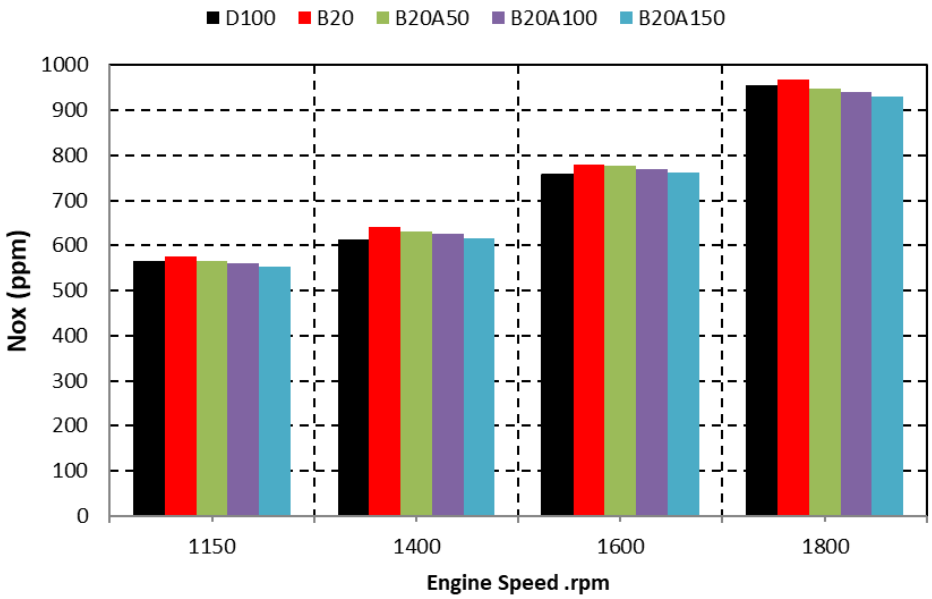


Figure 5.28. Effect of engine speed on nitrogen oxide (NOx) emissions in diesel–biodiesel–nanoparticle blends.

## 5.3. NUMERICAL SIMULATION RESULTS

This study uses a numerical approach to correctly analyze the release and distribution of heat within the cylinder, simulating fuel injection phenomena and improving the performance of a four-cylinder, four-stroke internal combustion engine. The 3D ANSYS FLUENT application simulates numerical operating conditions and compares results to experimental data. The aim is to evaluate the validity of the CFD model. While the software delivers computational fluid dynamics within the engine, utilizing the physical and chemical characteristics of pure diesel, biodiesel, and nanomaterials, it also saves time and accuracy while doing experiments. Data and computations can also be collected rapidly and reliably under ideal engine operating conditions.

### 5.3.1. Performance of Diesel Engines

#### 5.3.1.1. Effect of Additive Blends with Diesel

Figure 5.29 shows the cylinder pressure contours at different crank angles (CA 700, CA 720, and CA 740) for various biodiesel-nano fuel blends. This figure demonstrates

that increasing nanoparticle concentrations in biodiesel blends significantly alter combustion dynamics by increasing peak cylinder pressure, particularly around TDC (CA 720). This is attributed to improved ignition properties, thermal behavior, and catalytic effects of the nanoparticles. The cylinder pressure is comparatively lower across all blends at CA 700 (before top dead center). Pressure distribution remains concentrated in the upper combustion chamber, with dominant green/blue zones (~6.0–7.0 MPa). As nanoparticle concentration increases, slight pre-combustion activity is evident, especially for B20A150. At CA 720 (top dead center), peak combustion occurs with rapid pressure buildup. B20 shows pressure up to ~8.0 MPa. B20A50 and B20A100 demonstrate improved combustion characteristics with a wider spread of high-pressure zones (orange to red, ~8.3–8.5 MPa). B20A150 reaches the highest peak pressure, clearly showing a more intense combustion event — a direct result of nanoparticle-enhanced ignition. At CA 740 (after top dead center), pressure drops rapidly as expansion begins. All blends show diminished pressure fields. However, B20A150 maintains a slightly higher-pressure tail, which implies better post-combustion energy utilization. Nanoparticles ($Al_2O_3$) enhanced thermal conductivity and catalytic activity accelerate the combustion rate and increase the surface-area-to-volume ratio, improving fuel-air mixing and atomization. Higher cetane number from biodiesel + nano blends contributes to shorter ignition delays, leading to earlier combustion and increased peak cylinder pressure. The B20A150 blend consistently demonstrates superior combustion characteristics across all crank angles.

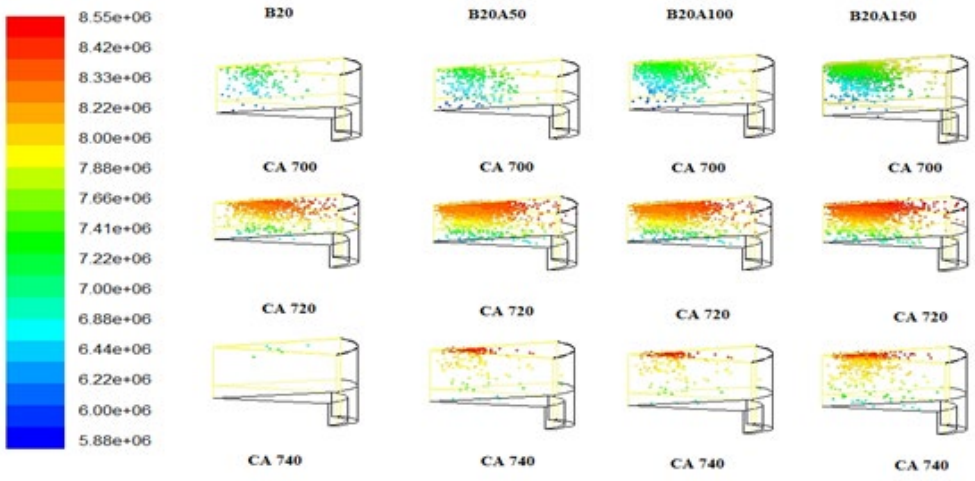


Figure 5.29. Impact of nanoparticle-enriched biodiesel blends on cylinder pressure profiles at 200 n·m load across crank angles.

Figure 5.30 illustrates the variation of cylinder pressure (P<sub>cy</sub>) with crank angle (CA) during the combustion cycle for five tested fuel samples. The results demonstrate the superior combustion performance of biodiesel–nanoparticle blends compared to pure diesel and standard biodiesel. D80B20N150 exhibits one of the highest and most stable cylinder pressure curves. All fuel types reach peak pressure close to TDC, around CA 718–720°. D100 shows the highest peak pressure (~82 Pa), closely followed by B20A150, B20A100, and B20A50. The pressure curve for B20 is notably lower than that of both D100 and the nano-enhanced biodiesel blends. The inclusion of $Al_2O_3$ nanoparticles enhances combustion efficiency, resulting in higher cylinder pressures, and pressure rises progressively with increasing nanoparticle concentration. The pressure build-up starts around CA 700° and rapidly rises to its peak at ~CA 720°, then falls until CA 750–760°. Nano-blended fuels maintain a slightly longer high-pressure zone, indicating sustained energy release.

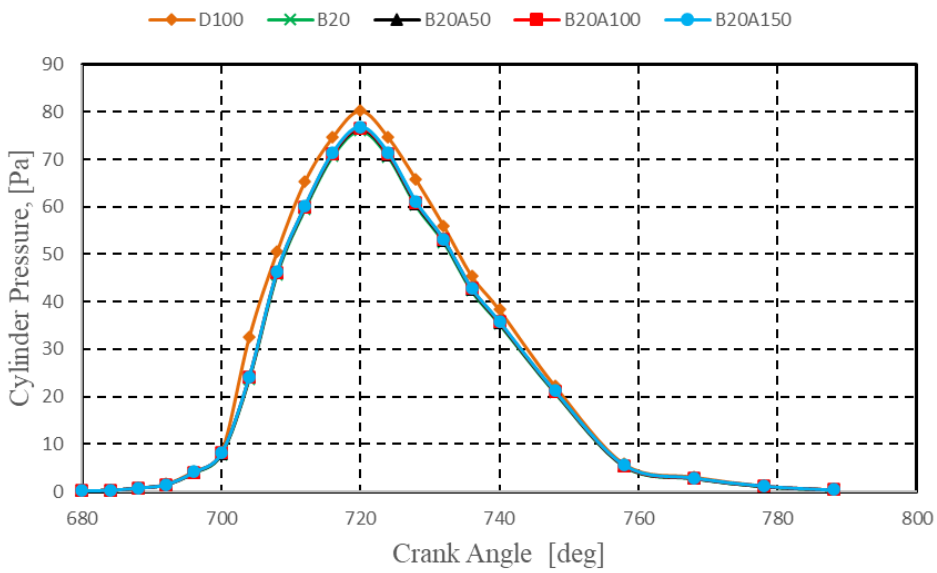


Figure 5.30. Comparative cylinder pressure trends across crank angles for diesel and nano-biodiesel fuel blends at 200 N·m.

Figure 5.31 illustrates the variation in peak cylinder pressure across three engine load conditions (0, 100, and 200 N·m) for five fuel types. The findings demonstrate the positive influence of $Al_2O_3$ nanoparticles on improving the peak cylinder pressure of biodiesel blends under different loading conditions. The rise in pressure is consistent with enhanced combustion characteristics, validating previous research findings [140,141]. The increased surface area and catalytic behavior of $Al_2O_3$ nanoparticles facilitate enhanced combustion. Their thermal conductivity accelerates heat transfer, reducing ignition delay and promoting faster fuel oxidation, which boosts peak pressure. At higher loads, fuel injection quantity increases, leading to more energetic combustion and naturally higher cylinder pressures. Normally, biodiesel alone (B20) produces lower peak pressure due to its higher viscosity and oxygen content. With the addition of nanoparticles, the combustion phase advances, making the performance closer to that of D100.Among the nano-blends, D80B20N150 shows the highest improvement in pressure. At 0 N·m Load (No Load), pure diesel (D100) records the highest peak pressure (~65 bar). Among the biodiesel variants, nano-enhanced blends (B20A50, B20A100, B20A150) show slightly higher pressure than plain biodiesel (B20), ranging from ~59 to 61 bar, confirming the initial enhancement even under unloaded conditions. At 100 N·m load, peak cylinder pressure increased for all fuels, with D100 reaching the highest at ~72 bar, while nano-biodiesel blends gradually rose,

from ~66 bar (B20A50) to ~68 bar (B20A150). All samples exhibited maximum peak pressures at 200 N·m load, indicating stronger combustion intensity under higher load conditions.

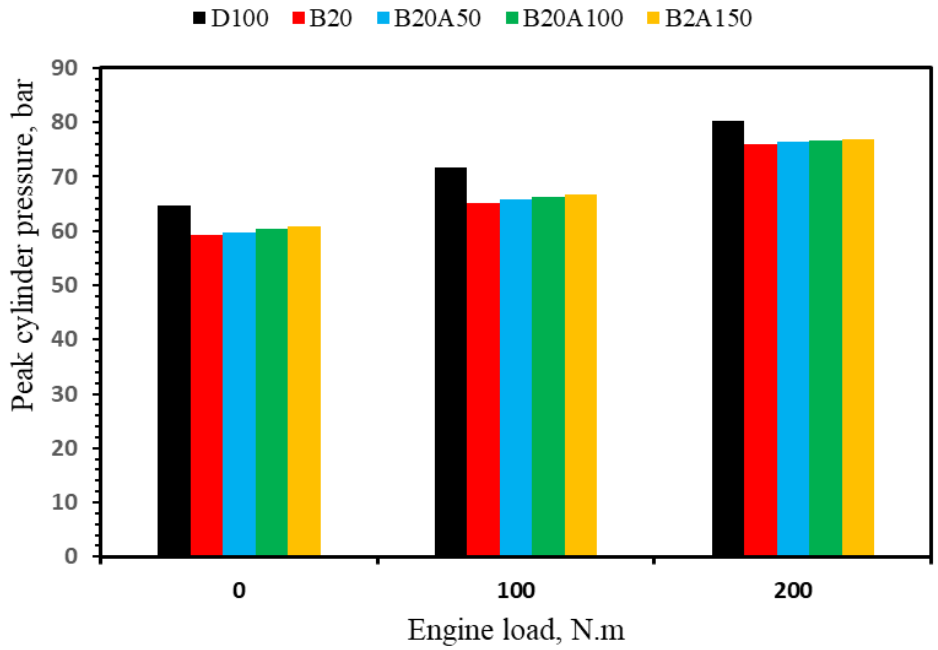


Figure 5.31. Peak cylinder pressure response to load for diesel-biodiesel blends with nano-additives

Figure 5.32 presents the variation of numerical Brake Thermal Efficiency (BTE) with increasing engine load for five different fuel types. The numerical simulation confirms that $Al_2O_3$ nanoparticle-doped biodiesel blends significantly improve engine thermal efficiency, especially under higher loads. D80B20N150 stands out with the best BTE performance, proving the viability of nanotechnology in biofuel applications. The findings observed that pure diesel (D100) consistently yields the lowest BTE values among the tested fuels, especially at high loads. D80B20 (biodiesel alone) exhibits a 4.8% reduction in thermal efficiency compared to D100, indicating that biodiesel lowers combustion efficiency when used without enhancement. Nano-enhanced blends (D80B20N50, D80B20N100, D80B20N150) outperform both D100 and D80B20. D80B20N50 shows slight improvement over D80B20, D80B20N100 improves further, and D80B20N150 achieves the highest BTE, particularly at 90% load, where it records a 2.8% improvement over pure diesel. $Al_2O_3$ nanoparticles enhance thermal efficiency because nanoparticles possess high surface-to-volume

ratios, increasing the contact area for combustion reactions, and the catalytic behavior of $Al_2O_3$ promotes better atomization, faster fuel-air mixing, and shorter ignition delay, all of which improve combustion efficiency. The fuel injection rate increases as load increases, leading to higher in-cylinder temperatures and pressures. This favors nano-blended fuels because they ignite and evaporate more efficiently under such thermal conditions. Biodiesel has higher viscosity and lower volatility than diesel, which hinders atomization and slows down ignition, resulting in incomplete combustion. The 150-ppm concentration of nanoparticles offers an optimal balance: high catalytic activity, improved oxidation, and faster flame propagation. This blend mitigates the negative effects of biodiesel while enhancing its strengths.

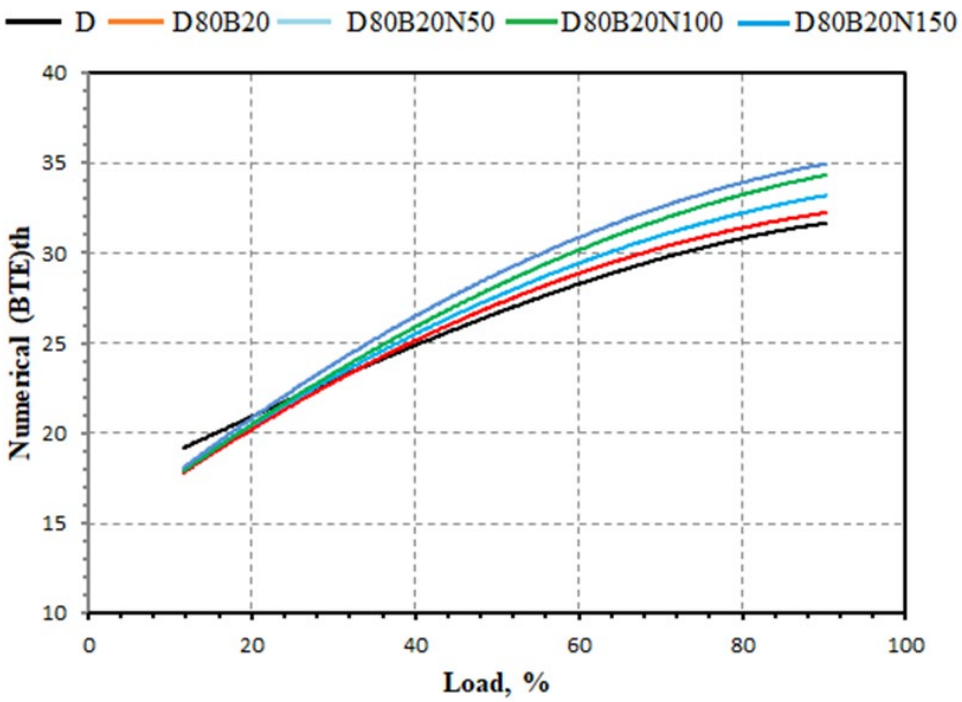


Figure 5.32. Effect of engine load on numerical brake thermal efficiency (BTE) of diesel-biodiesel-nanoparticle blends.

Figure 5.33 illustrates the contours of cylinder temperature fluctuation across different crank angles for the B20A150 fuel blend (a mix of 80% diesel, 20% biodiesel, and 150 ppm $Al_2O_3$ nanoparticles) under an engine load of 200 Nm, using computational fluid dynamics (CFD) simulations. The thermal contours of this figure provide strong evidence that B20A150 significantly improves combustion quality. The increase in peak in-cylinder temperature to nearly 1188 K, particularly at CA 720, confirms that

the $Al_2O_3$ nanoparticles at 150 ppm enable a more vigorous and efficient combustion process. When compared to baseline fuels such as pure diesel (D100) or biodiesel blends without nanoparticles, the D80B20N150 blend exceeds average peak temperatures by 5–10%. This improvement correlates with enhanced combustion efficiency and higher brake thermal efficiency, as evidenced in earlier figures (e.g., Figures 5.30–5.32). The findings present a sequential thermal map of combustion temperature at various crank angles, including CA 640, 680, 700, 720, 740, 784, 800, and 833. The highest combustion temperature reaches approximately 1188 K, which is observed near crank angle CA 720, signifying the peak combustion phase. At earlier crank angles (e.g., CA 640 to CA 700), the temperature remains relatively low, dominated by shades of blue and cyan, indicating temperatures of 500–800 K. As combustion initiates and proceeds, especially between CA 720 and CA 740, a sharp temperature rise is evident, shifting the color spectrum toward green, yellow, and red, corresponding to temperatures approaching and exceeding 1000 K. Post-combustion phases (CA 784, CA 800, and CA 833) show a return to cooler temperatures, indicating dissipation and completion of the combustion cycle.

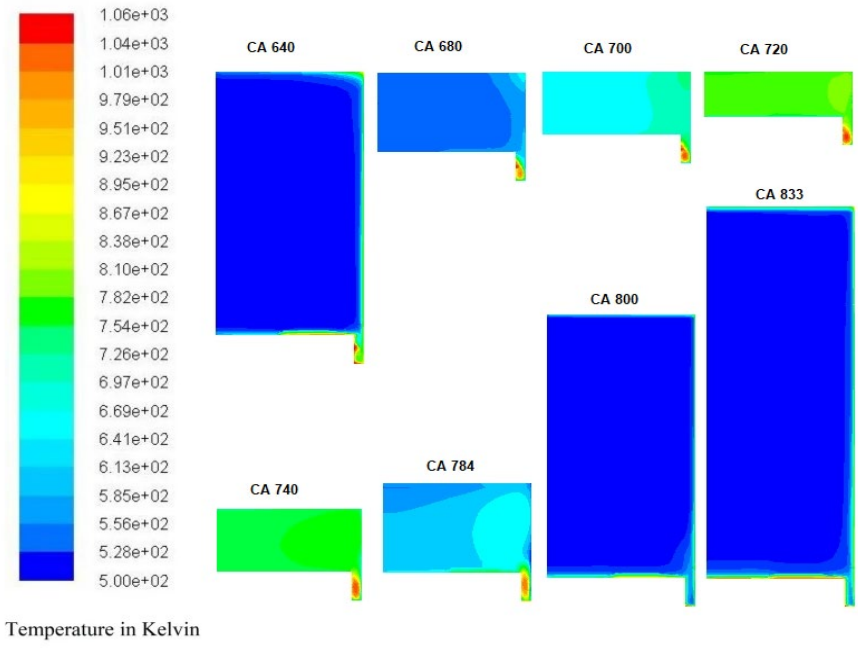


Figure 5.33. Effect of crank angle on in-cylinder temperature distribution for B20A150 fuel at full load.

Figure 5.34 presents the maximum in-cylinder temperature recorded for various fuel samples (D100, B20, B20A50, B20A100, and B20A150) under three engine load conditions: 0, 100, and 200 N·m. The findings observed that at 0 N·m, the highest temperature recorded was for B20, approximately 1090 K, while D100 showed the lowest temperature at around 1010 K. With increased load to 100 N·m, all fuel samples exhibited higher peak temperatures, with B20 reaching nearly 1170 K and the nano-additive blends (B20A50–B20A150) slightly lower in the range of 1140–1155 K. At the maximum load of 200 N·m, the peak temperature further increased, with B20 approaching 1200 K, while the nano-fuels stabilized at a slightly lower thermal range (1170–1180 K), still above D100 (~1160 K). The higher peak temperatures observed in B20 compared to D100 are attributed to its higher oxygen and hydrocarbon content, promoting more complete and vigorous combustion.

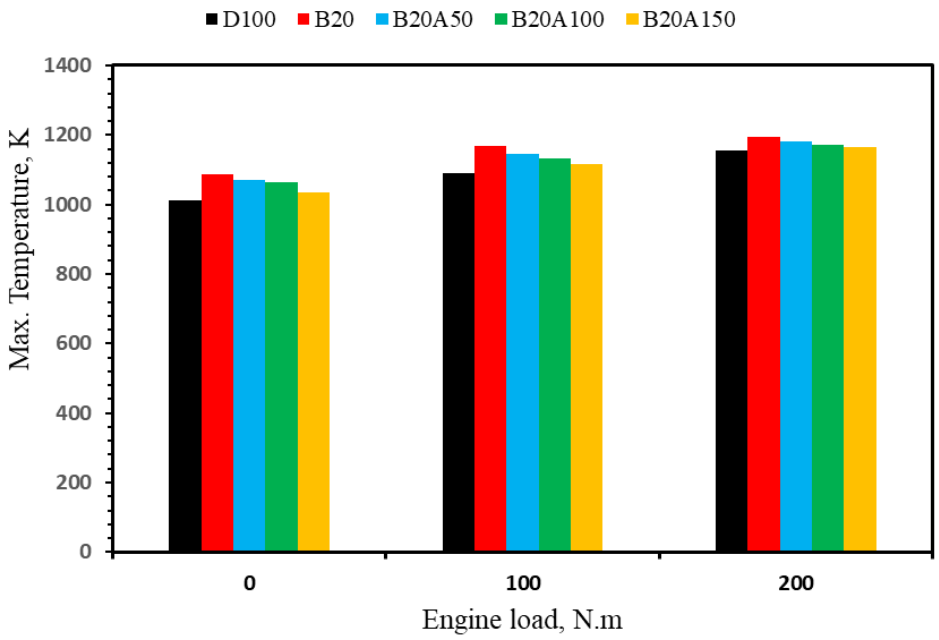


Figure 5.34. Effect of engine load on maximum combustion temperature in diesel-biodiesel blends with nano-additives.

Figure 5.35 displays the velocity distribution contours inside the combustion chamber of a diesel engine running on the B20A150 (biodiesel + $Al_2O_3$ nanoparticles at 150 ppm) fuel blend under a constant load of 200 N·m, across multiple crank angles ranging from CA 640 to CA 833. The results reveal that at early crank angles (CA

640–CA 700), velocity magnitudes are relatively low and mostly concentrated around the periphery of the combustion chamber, near the piston bowl edges, while the central zone remains calm with minimal turbulence. Between CA 720 and CA 740, the velocity distribution becomes more uniform due to fuel injection and subsequent diffusion, which enhances air-fuel mixing. From CA 784 to CA 833, a distinct stratification of velocities appears, with higher values (up to ~8.6 m/s) near the piston surface and side walls, while the upper central region maintains lower velocities. The high velocity zones near the walls play a pivotal role in fuel breakup and atomization, while the low velocity center acts as a buffer region for flame development. The presence of $Al_2O_3$ nanoparticles improves combustion dynamics by increasing swirl intensity and enhancing charge turbulence, which shortens ignition delay and supports faster flame propagation. As a result, this leads to more complete combustion, which positively impacts thermal efficiency and reduces unburnt hydrocarbons (HC). The findings also demonstrate that lower velocities at the cylinder center during combustion are attributed to diminished swirl motion, which is common during the compression and combustion strokes. In contrast, swirl velocity peaks during the intake stroke due to the strong inflow momentum, then decays as the piston compresses the charge. The swirl is reenergized after fuel injection due to momentum transfer and turbulence caused by fuel droplet dispersion, which nano-additives enhance. Swirl flow, defined as the rotation of air about the cylinder axis, is a critical mechanism to promote rapid air-fuel mixing, enhance flame propagation, and support a more homogenous and efficient combustion process.

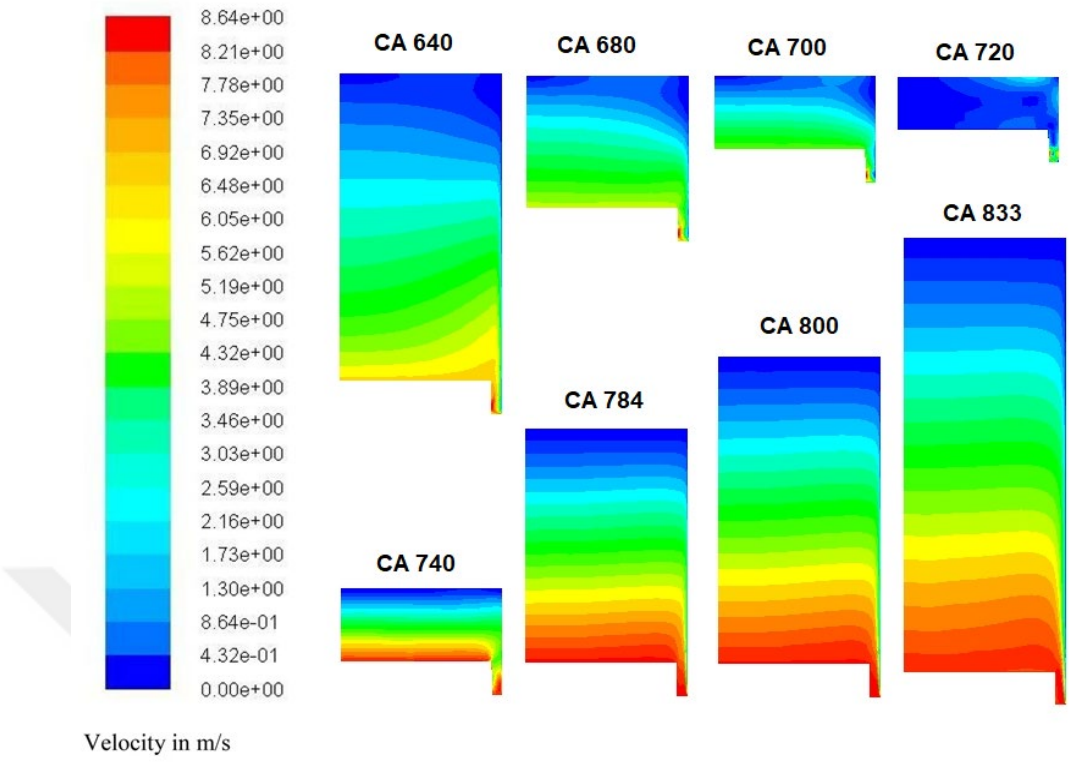


Figure 5.35. Velocity field evolution in B20A150 fuel blend at 200 N·m load across crank angles.

### 5.3.2. Emissions for Diesel Engine

#### 5.3.2.1. Effect of Biodiesel and $Al_2O_3$ Nanoparticle Blends

Figure 5.36 illustrates the contours of $CO_2$ mass fraction for four biodiesel blends, D80B20, D80B20N50, D80B20N100, and D80B20N150, under identical engine conditions: a load of 200 N·m and a speed of 1150 rpm. The findings present that the $CO_2$ mass fraction for the baseline biodiesel blend (D80B20) was approximately 4.41%. With the introduction of $Al_2O_3$ nanoparticles at 50 ppm (D80B20N50), the $CO_2$ mass fraction increased by 8.45% relative to pure diesel. Further enhancement with 100 ppm (D80B20N100) raised the $CO_2$ output to 14.47% above diesel. The highest recorded increase was observed with 150 ppm nanoparticles (D80B20N150), resulting in an 18.7% boost in $CO_2$ emissions compared to D100. The gradual increase in $CO_2$ mass fraction across the nano-blended fuel samples reflects improved combustion efficiency, attributable to enhanced oxygen content from both the biodiesel and the

metal-oxide ($Al_2O_3$) additives, and improved fuel-air mixing due to nanoparticles' catalytic and thermal properties. The variation of the CO2 mass fraction increases percentages for all fuel samples compared to pure diesel D100, as shown in Table 5.1.

Table 5.1. Variations of CO2 mass friction percentages for all fuel samples compared to pure diesel.

| | **Engine speed** | | | |
|---|---|---|---|---|
| Fuel samples | 1150 rpm | 1400 rpm | 1600 rpm | 1800 rpm |
| D80B20 | 4.41% | 4.28% | 2.53% | 2.6% |
| D80B20N50 | 8.45% | 8.21% | 3.75% | 5.1% |
| D80B20N100 | 14.47% | 10.6% | 6.1% | 7.4% |
| D80B20N150 | 18.7% | 12.8% | 8.33% | 9.67% |

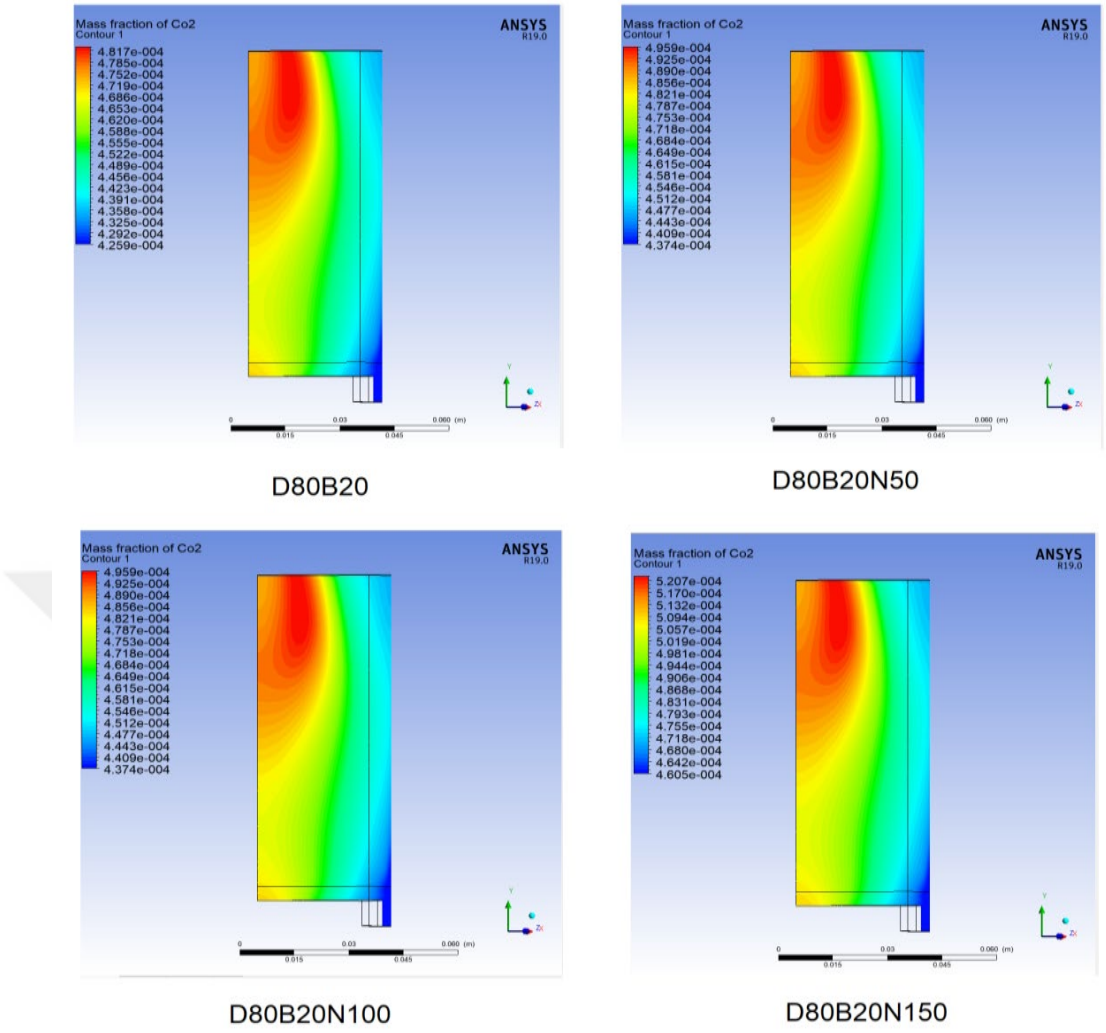


Figure 5.36. $CO_2$ mass fraction distribution for nanoparticle-enriched biodiesel blends at 1150 rpm and 200 N·m load

Figure 5.37 displays the $CO_2$ mass fraction contours for biodiesel blends with and without $Al_2O_3$ nanoparticles, namely D80B20, D80B20N50, D80B20N100, and D80B20N150, under engine conditions of 1400 rpm speed and 200 N·m torque. This figure reinforces the trend observed at 1150 rpm (Figure 5.36), confirming that increasing $Al_2O_3$ nanoparticle concentrations in biodiesel blends leads to higher $CO_2$ mass fractions, improved combustion characteristics, and greater emission efficiency. The improvements, especially for D80B20N150, demonstrate the significant potential of nanotechnology-enhanced biofuels in boosting environmental and thermal performance. D80B20 (baseline blend) exhibits a $CO_2$ mass fraction of approximately $4.80\times10^{-4}$. With 50 ppm nanoparticles (D80B20N50), the $CO_2$ fraction increases

slightly to about $4.86\times10^{-4}$, representing a ~1.25% rise. D80B20N100 shows a more substantial increase, reaching $5.00\times10^{-4}$, indicating a ~4.2% improvement in combustion efficiency over D80B20. D80B20N150, the highest nanoparticle concentration, peaks at $5.11\times10^{-4}$, yielding a ~6.4% rise in $CO_2$ emissions compared to the baseline blend.

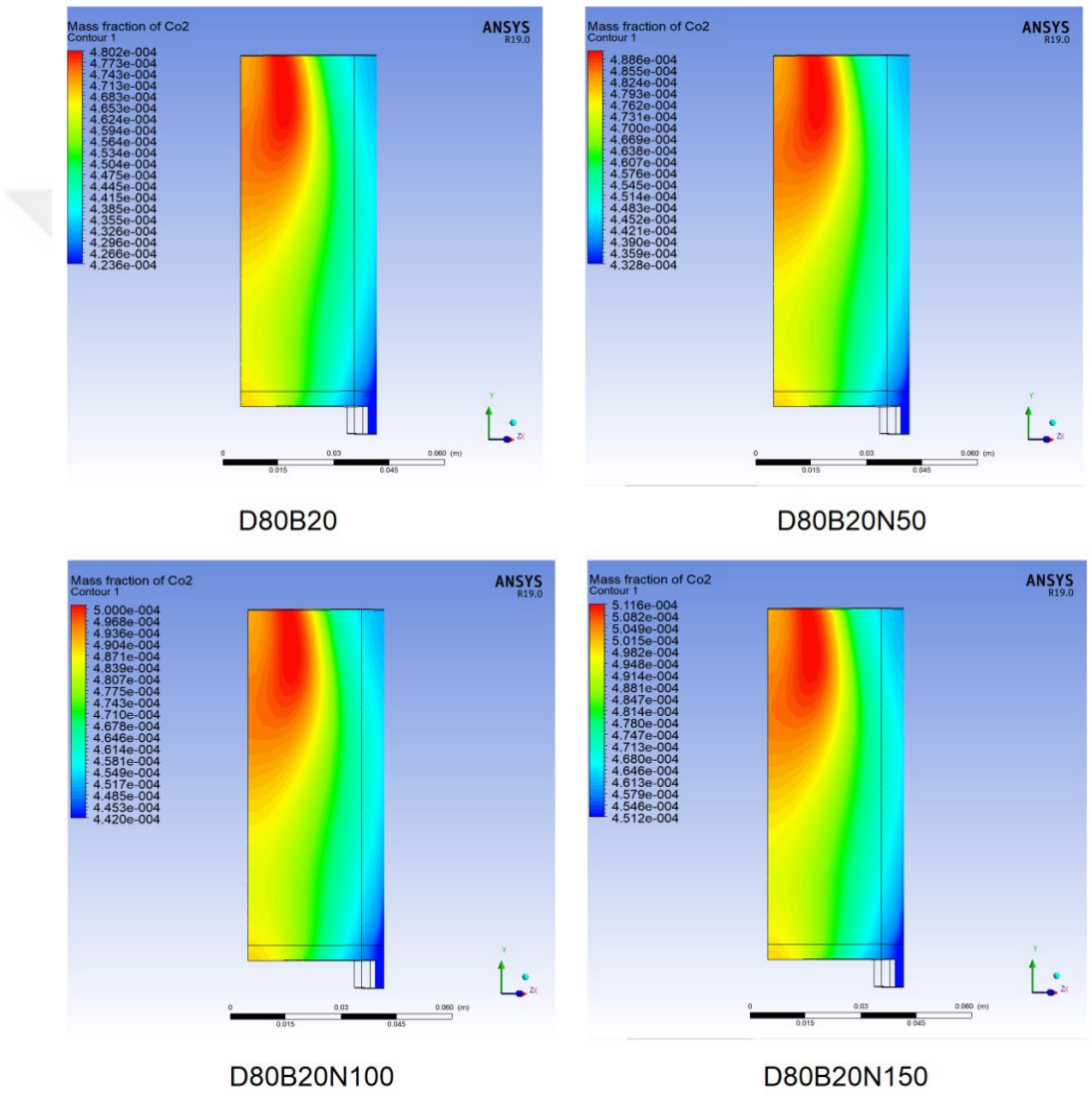


Figure 5.37. $CO_2$ mass fraction distribution for biodiesel-nanoparticle blends at 1400 rpm and 200 N·m load.

Figure 5.38 illustrates the $CO_2$ mass fraction contours for four fuel blends—D80B20, D80B20N50, D80B20N100, and D80B20N150, under operating conditions of 1600

rpm engine speed and 200 N·m engine load. These contours depict how effectively each blend facilitates combustion, as reflected by the distribution of carbon dioxide across the combustion chamber. At 1600 rpm, the use of $Al_2O_3$ nanoparticles in biodiesel blends significantly improves combustion quality, as demonstrated by the progressive increase in $CO_2$ mass fraction. The improvement is not only quantitative but also reflected in the spatial distribution of combustion efficiency across the chamber. D80B20 baseline shows a $CO_2$ mass fraction peak of approximately $4.47\times10^{-4}$, slightly higher than previous rpm levels, consistent with increased combustion intensity at higher speed. D80B20N50 achieves ~$4.60\times10^{-4}$, reflecting a ~2.9% rise over D80B20. D80B20N100 increases further to ~$4.77\times10^{-4}$, yielding a ~6.7% improvement compared to D80B20. D80B20N150 reaches approximately $4.90\times10^{-4}$, marking a ~9.6% increase over D80B20 and confirming its superior combustion behavior.

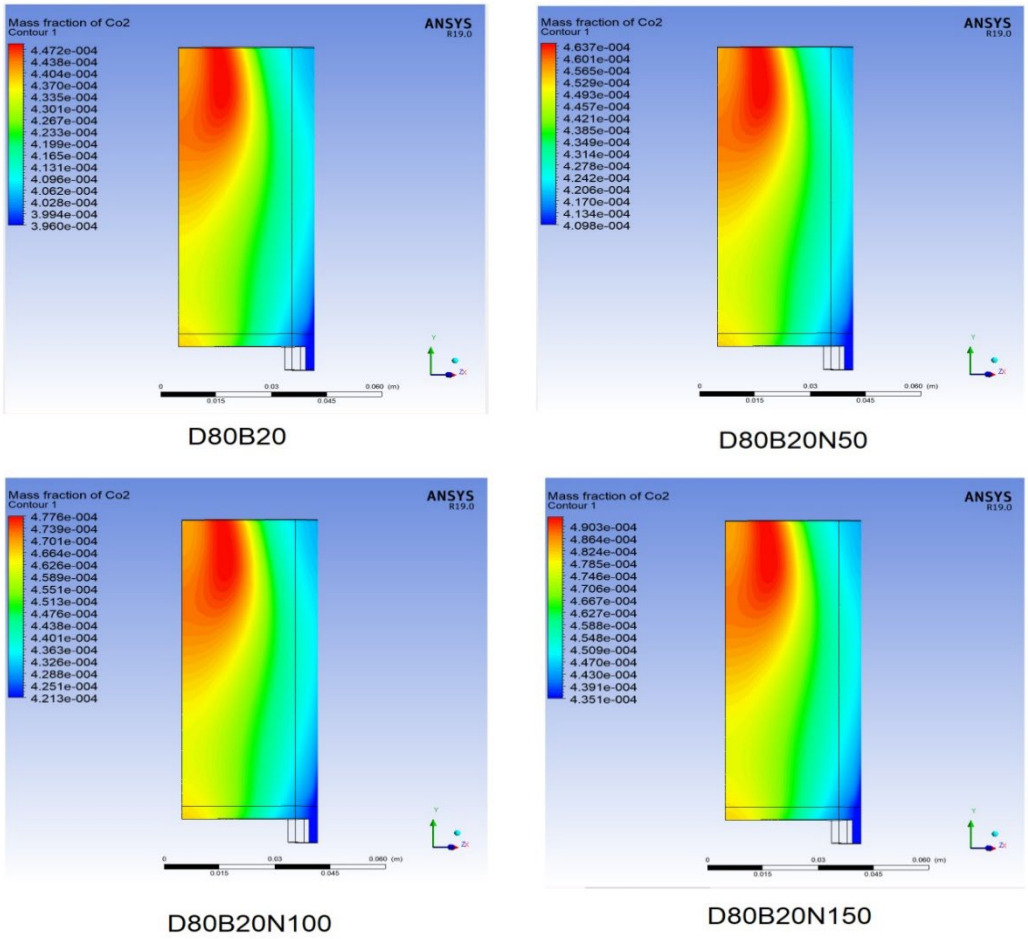


Figure 5.38. Influence of nanoparticle-enriched biodiesel on $CO_2$ mass fraction at 1600 rpm and 200 N·m load.

Figure 5.39 presents the $CO_2$ mass fraction contours for four biodiesel fuel blends, D80B20, D80B20N50, D80B20N100, and D80B20N150, under an engine load of 200 Nm and 1800 rpm engine speed. The figure is the final part of the series showing combustion behavior across increasing rpm levels. Even at the highest tested engine speed of 1800 rpm, nanoparticle-enriched biodiesel blends (especially D80B20N150) outperform plain biodiesel (D80B20) regarding $CO_2$ production, an indicator of complete combustion. While the percentage improvements decrease with higher rpm, the consistent trend of better oxidation efficiency underscores the value of $Al_2O_3$ additives in biodiesel combustion enhancement. Higher nanoparticle content continues to improve combustion efficiency and reduce incomplete oxidation. The fuel-air mixing is visibly more uniform, and the reaction zone is more defined with higher additive concentrations. The lower $CO_2$ output at very high speeds may reflect the need

to optimize ignition timing and injection strategies when using nanoparticle-enhanced fuels. D80B20 shows a peak $CO_2$ mass fraction of approximately $4.05\times10^{-4}$, which is lower than previous engine speeds (especially 1600 rpm), possibly due to shortened combustion duration at higher rpm. D80B20N50 rises slightly to $4.15\times10^{-4}$, marking a 2.5% increase over D80B20. D80B20N100 records a value of ~$4.17\times10^{-4}$, showing a ~3% increase. D80B20N150, with the highest nanoparticle concentration, peaks at ~$4.21\times10^{-4}$, reflecting a ~4% enhancement over the base D80B20 blend.

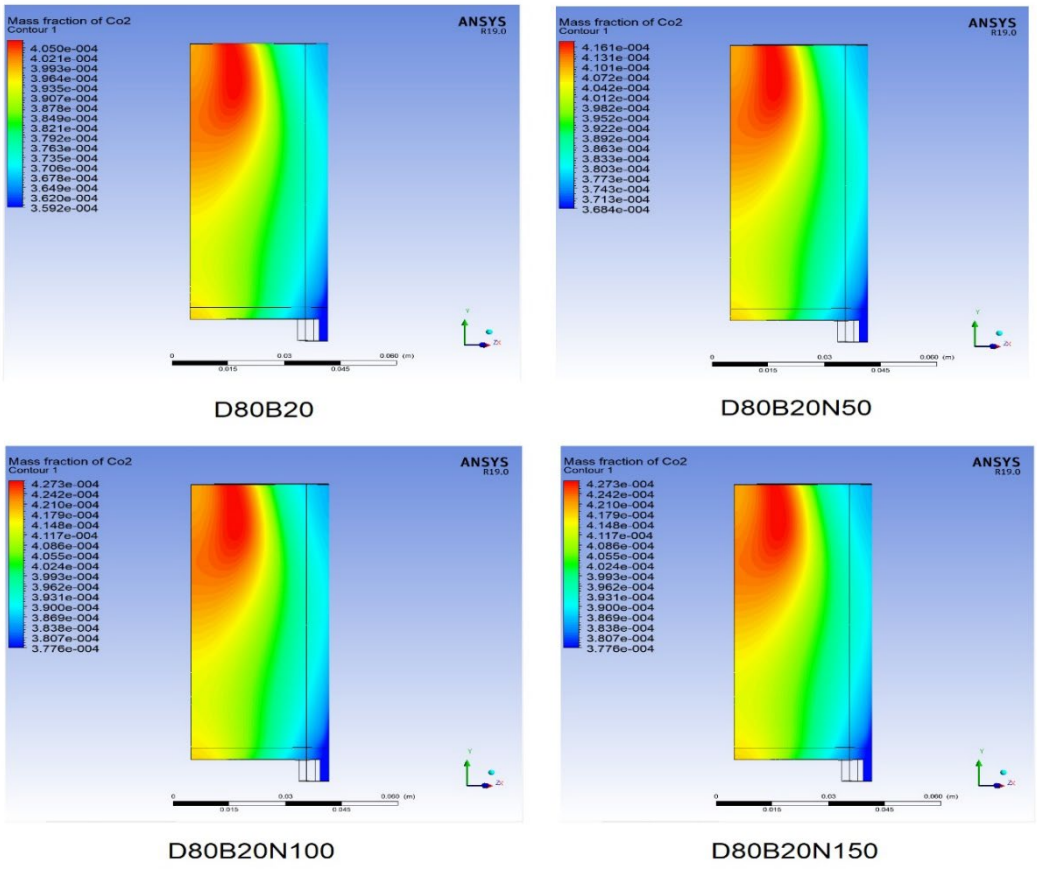


Figure 5.39. Effect of nanoparticle-enhanced biodiesel on $CO_2$ mass fraction at high engine speed (1800 rpm)

Figure 5.40 illustrates the variation in $CO_2$ emissions (Vol.%) across different engine speeds (1150 to 1800 rpm) for several fuel blends. The findings reinforce the effectiveness of biodiesel-nano blends in reducing carbon dioxide emissions. While biodiesel alone offers noticeable environmental benefits over diesel, the addition of $Al_2O_3$ nanoparticles drastically improves emission profiles, especially at high engine

speeds. The D80B20N150 blend is the most efficient in reducing $CO_2$ emissions, making it a promising candidate for cleaner combustion strategies. $CO_2$ emissions decline steadily as engine speed increases for all fuel types. This is likely due to shorter combustion durations at higher speeds, reducing complete oxidation. The nano-additives further reduce $CO_2$ emissions beyond what's observed in D100 and D80B20, with the most significant reduction seen in D80B20N150. At 1800 rpm, D80B20N150 yields a ~47% reduction compared to D100 (from ~7.2% to ~3.8%). As the nanoparticle concentration increases (from 50 → 100 → 150 ppm), $CO_2$ emissions continue to drop at each engine speed.

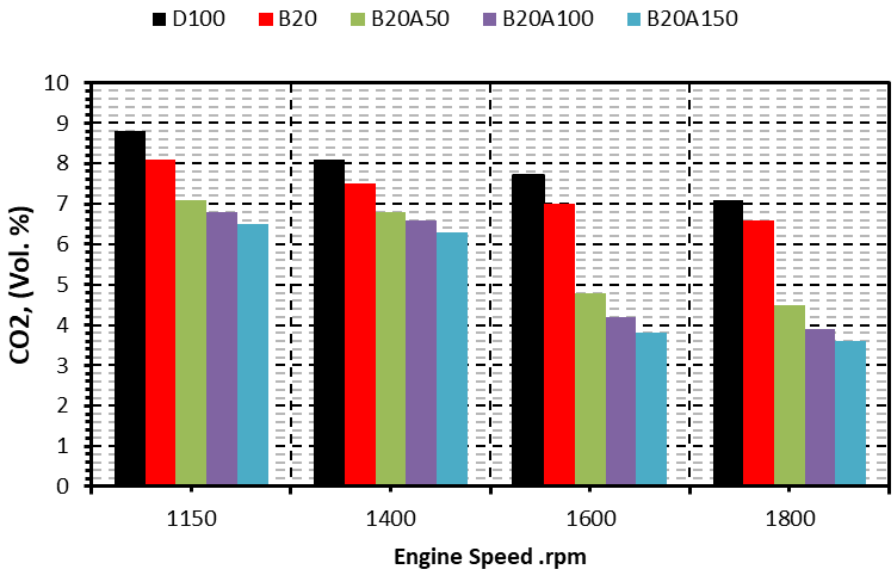


Figure 5.40. Influence of engine speed on $CO_2$ emissions for diesel and biodiesel-nanoparticle blends at 200 Nm load.

Figure 5.41 illustrates the mass fraction distribution of $NO_x$ emissions for different fuel blends under consistent engine operating conditions, specifically a load of 200 Nm and an engine speed of 1150 rpm for four fuel types. Each subplot within the figure presents the spatial distribution of $NO_x$ concentration inside the engine cylinder, derived from ANSYS simulation results. The fuel types analyzed include D80B20 (a baseline biodiesel blend) and its nanoparticle-enhanced variants: D80B20N50, D80B20N100, and D80B20N150, which are blended with 50 ppm, 100 ppm, and 150

ppm of $Al_2O_3$ nanoparticles, respectively. The findings illustrate that while the addition of $Al_2O_3$ nanoparticles enhances combustion efficiency, it also leads to a modest increase in $NO_x$ emissions, especially at 100 ppm concentration. However, the trade-off might be acceptable considering the parallel reduction in CO and HC emissions, and the enhancement of thermal and combustion performance. The highest $NO_x$ mass fraction was recorded for D80B20N100, peaking at approximately $3.71e^{19}$. D80B20N50 and D80B20N150 showed similar but slightly lower $NO_x$ intensities. The baseline blend D80B20 exhibited the lowest $NO_x$ emission zone near the combustion core. $NO_x$ is formed primarily via the thermal NO mechanism, where nitrogen reacts with oxygen at high combustion temperatures (>1800 K). The Zeldovich mechanism explains this, and it's heavily influenced by flame temperature, residence time, and local oxygen availability. $Al_2O_3$ nanoparticles enhance combustion by promoting oxygen diffusion, improving atomization, and shortening ignition delay. This results in higher in-cylinder temperatures, accelerating $NO_x$ formation. Therefore, $NO_x$ mass fraction increases with nanoparticle concentration, especially in D80B20N100, where optimal combustion conditions cause peak $NO_x$ emissions. Though biodiesel contains oxygen, its lower calorific value and longer ignition delay lead to lower peak temperatures and less thermal $NO_x$ production at low speeds.

Table 5.2 reinforces that $Al_2O_3$ nanoparticles provide a strategic advantage in reducing $NO_x$ emissions while maintaining combustion quality. This supports their viability for greener biodiesel applications, especially when operated at mid-range speeds (1400–1600 rpm), where the best emission-performance balance is achieved.

Table 5.2. Comparative variability in $NO_x$ mass fraction percentages for biodiesel-nanoparticle blends versus pure diesel across engine speeds.

| | **Engine speed** | | | |
|---|---|---|---|---|
| Fuel samples | 1150 rpm | 1400 rpm | 1600 rpm | 1800 rpm |
| D80B20 | 5.7% | 3.85% | 2.96% | 5.24% |
| D80B20N50 | 4.13% | 2.4% | 2.84% | 3.4% |
| D80B20N100 | 3.3% | 1.8% | 1.75% | 2.7% |
| D80B20N150 | 2.86% | 1.06% | 1.1% | 1.6% |

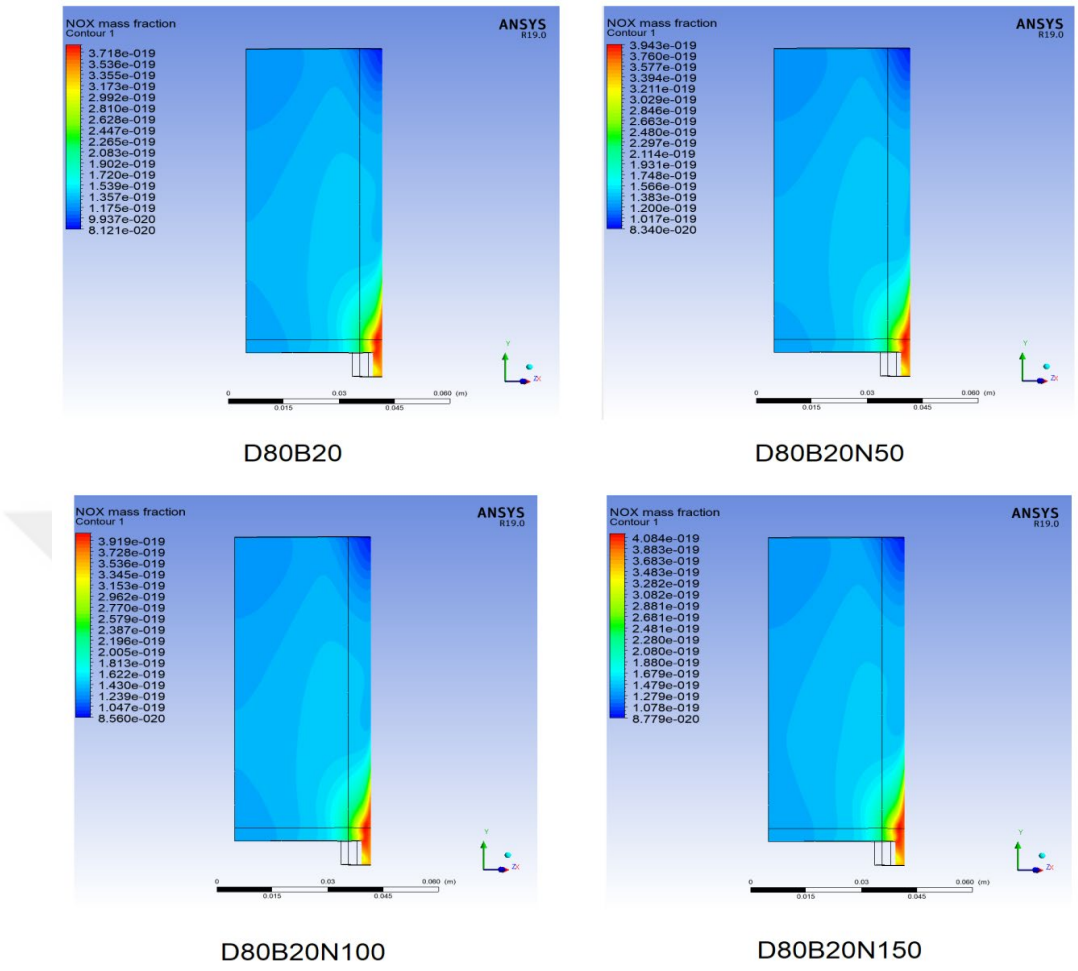


Figure 5.41. Numerical contours of $NO_x$ mass fraction for various nano-biodiesel blends at 200 Nm load and 1150 rpm.

Figure 5.42 illustrates the variation in nitrogen oxide ($NO_x$) mass fraction within the combustion chamber for four fuel samples: D80B20, D80B20N50, D80B20N100, and D80B20N150, under a constant engine load of 200 N·m and engine speed of 1400 rpm. Using nano-enhanced biodiesel fuels, particularly with 150 ppm $Al_2O_3$ (D80B20N150), is highly effective in reducing $NO_x$ emissions at medium engine speeds. Across all fuel blends, it is evident that the $NO_x$ emissions are concentrated in the regions closest to the injector nozzle and combustion core, where the temperature and oxygen availability are typically highest. The D80B20 sample exhibits the highest $NO_x$ mass fraction intensity, confirming that biodiesel without nanoparticle enhancement leads to elevated $NO_x$ formation due to prolonged ignition delay and

incomplete charge cooling. D80B20N50 demonstrates a notable decline in high $NO_x$ regions, likely due to enhanced combustion efficiency and reduced ignition delay. D80B20N100 further suppresses $NO_x$ formation, showing a more uniform and cooler temperature profile in the contour plot. D80B20N150 exhibits the lowest $NO_x$ mass fraction values among all blends, confirming the superior effect of higher nanoparticle concentrations on reducing thermal $NO_x$. The contour appears significantly more homogeneous and freer of red-hot zones, indicating efficient, clean combustion.

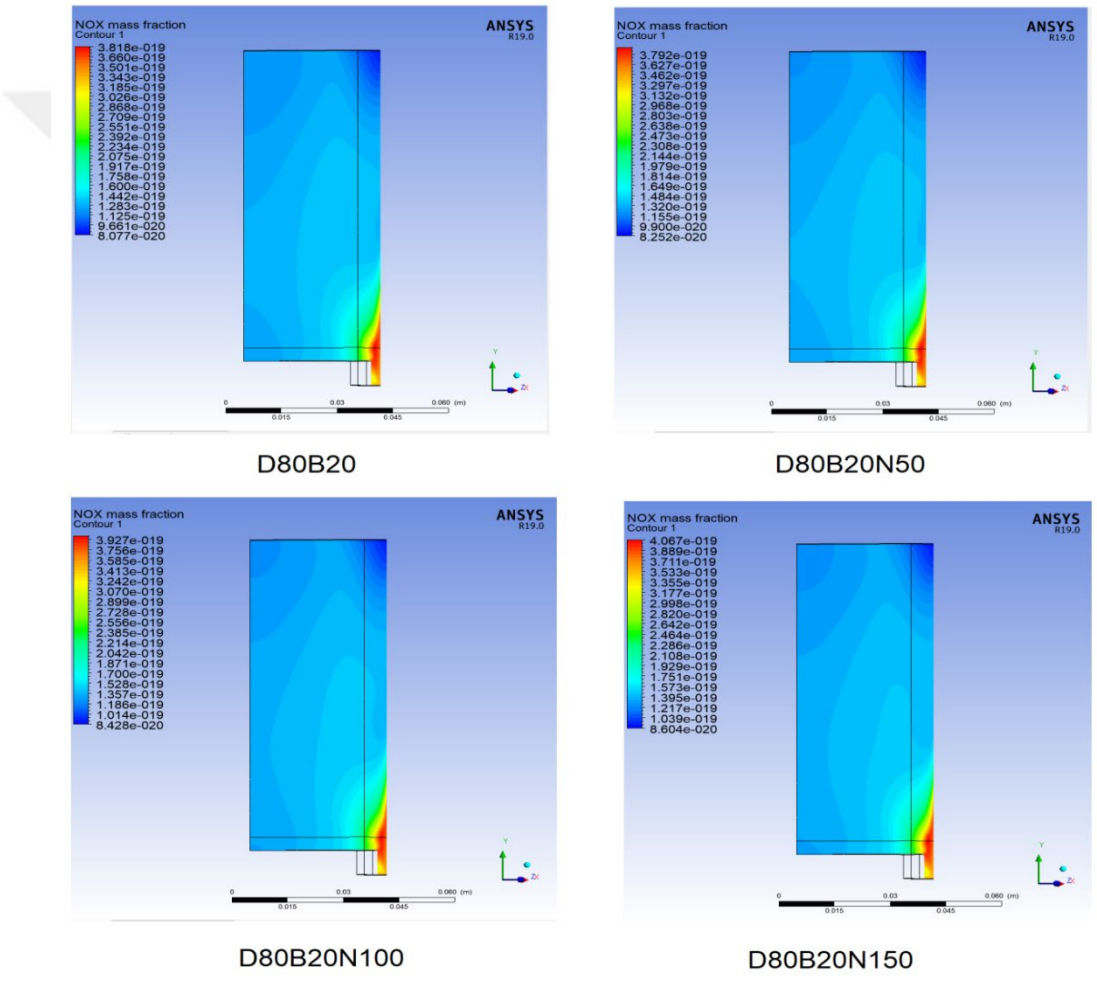


Figure 5.42. Contours of $NO_x$ mass fraction for various biodiesel-nano fuel blends at 1400 rpm and 200 Nm load.

Figure 5.43 presents the simulated $NO_x$ (nitrogen oxide) mass fraction contours for four fuel types—D80B20, D80B20N50, D80B20N100, and D80B20N150, under engine conditions of 1600 rpm and 200 N·m load. At medium-high engine speed (1600

rpm), the use of nanoparticle-enriched biodiesel blends, especially D80B20N150, significantly mitigates $NO_x$ emissions while supporting efficient combustion. The findings observed that D80B20 exhibits the most intense $NO_x$ emission zones, with values reaching approximately 3.47e-19, concentrated near the injector and cylinder wall. This is due to higher combustion temperatures and longer ignition delay periods typical of biodiesel combustion without enhancements. As the concentration of $Al_2O_3$ nanoparticles increases, there is a clear decrease in $NO_x$ mass fraction intensity. D80B20N50 presents a significant drop in $NO_x$ formation, indicating improved combustion efficiency and reduction in peak flame temperature. For D80B20N100, the $NO_x$ emission zone is reduced further, and uniformity of the emission profile improves. In contrast, for D80B20N150, the lowest $NO_x$ levels are observed (~2.15e-19), and the contour map shows a substantial reduction in the high-temperature $NO_x$ production zones.

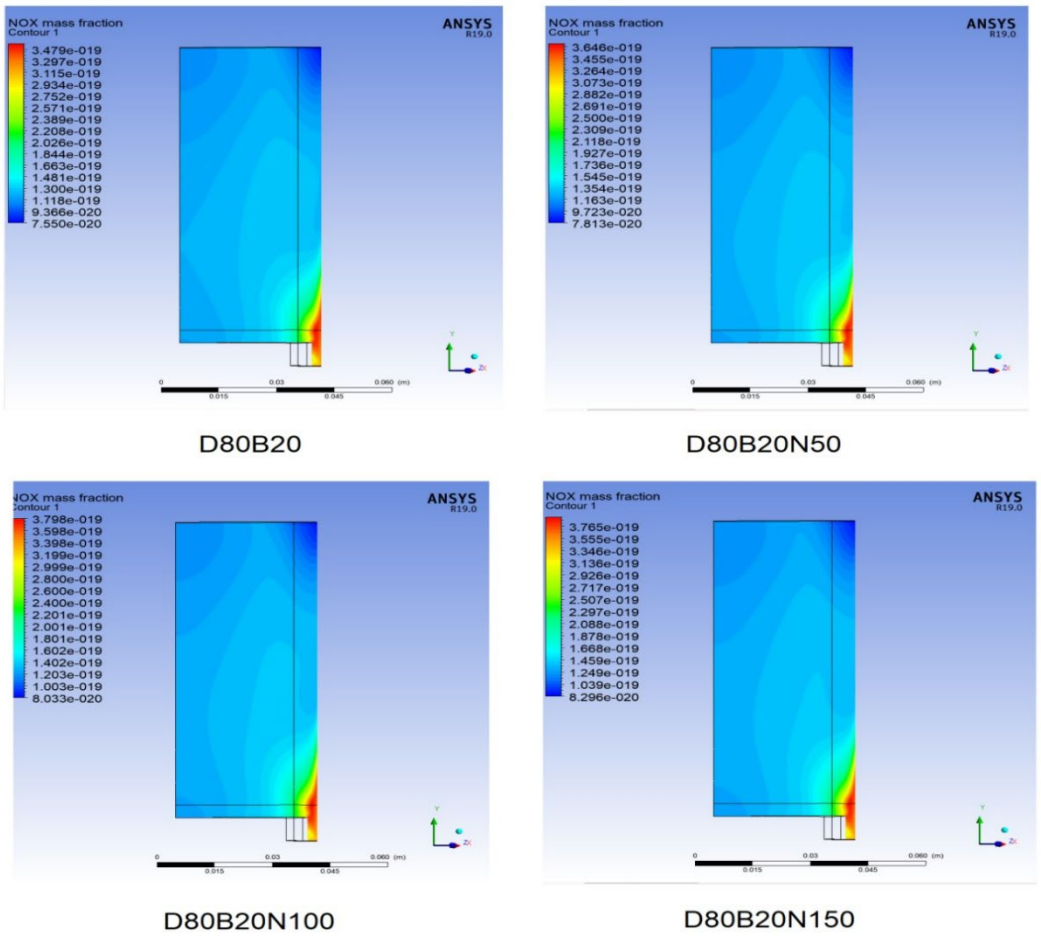


Figure 5.43. Contours of $NO_x$ mass fraction for biodiesel-nanoparticle blends at 1600 rpm and 200 N·m load.

Figure 5.44 illustrates the contours of $NO_x$ mass fraction for four biodiesel-nanoparticle fuel samples (D80B20, D80B20N50, D80B20N100, and D80B20N150) at a high engine speed of 1800 rpm and a load of 200 N·m. At a speed of 1800 rpm, which mimics near full-load engine conditions, the use of $Al_2O_3$ nanoparticle-enhanced biodiesel blends, especially D80B20N150, significantly curbs $NO_x$ emissions while supporting combustion efficiency. At higher speeds, $NO_x$ emissions tend to rise due to increased combustion pressure and temperature, promoting thermal NO formation. The presence of nanoparticles such as $Al_2O_3$ enhances combustion uniformity and speeds up the evaporation and ignition phases; lowers flame temperature by improving heat transfer, hence reducing $NO_x$ formation; and functions as a catalyst, aiding complete combustion and reducing free radicals that contribute to $NO_x$. The results referenced increased in $NO_x$ emissions for various fuel blends relative

to the standard diesel (D100) at 1800 rpm. The baseline biodiesel blend, D80B20, exhibits a 5.24% increase in $NO_x$ emissions compared to D100. However, the inclusion of $Al_2O_3$ nanoparticles in the fuel blends results in a noticeable reduction in $NO_x$ emissions. Specifically, D80B20N50 shows a 3.4% increase, D80B20N100 a 2.7% increase, and D80B20N150 the lowest increase at just 1.6%.

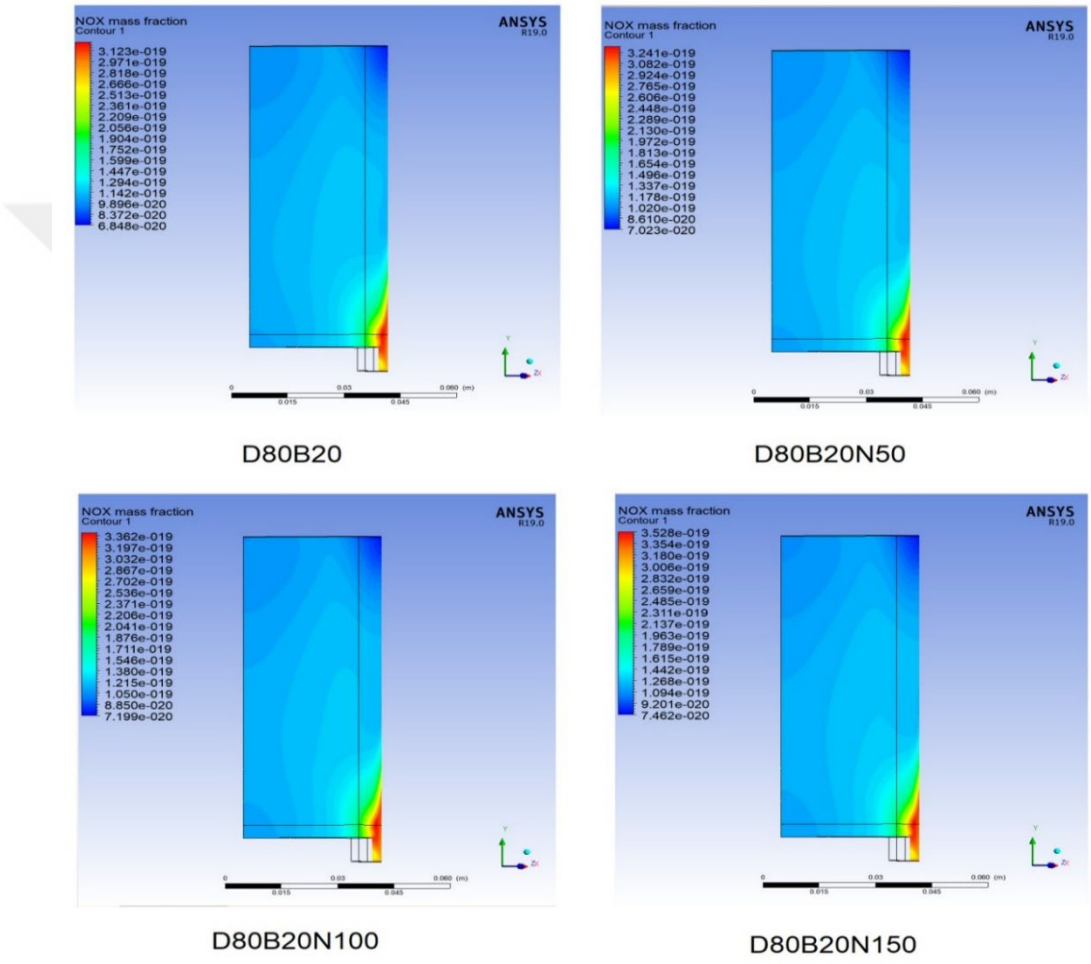


Figure 5.44. $NO_x$ mass fraction contours at 1800 rpm and 200 N·m load for biodiesel–nanoparticle blends.

Figure 5.45 presents the measured $NO_x$ emissions (in ppm) across four engine speeds (1150, 1400, 1600, and 1800 rpm) for six fuel blend samples. The results in the figure reinforce the beneficial role of $Al_2O_3$ nanoparticles in mitigating $NO_x$ emissions across increasing engine speeds. While $NO_x$ emissions naturally rise with speed due to elevated in-cylinder temperatures, nanoparticle addition suppresses $NO_x$ formation at

150 ppm (D80B20N150).$NO_x$ emissions increase with engine speed for all fuel samples. This trend is expected due to higher combustion temperatures and shorter ignition delays at higher speeds. At 1150 rpm, $NO_x$ emissions are nearly equivalent across all blends (~600 ppm), with slight reductions observed in the nanoparticle-enhanced fuels. At an engine speed of 1800 rpm, a significant distinction in $NO_x$ emission levels is evident among the tested fuel samples. The conventional diesel fuel (D100) produces the highest $NO_x$ emissions, measuring just under 980 ppm. The biodiesel blend D80B20 achieves a slight reduction in $NO_x$ emissions, though the values remain close to those of pure diesel. In contrast, the nanoparticle-enhanced blends, ranging from D80B20N50 to D80B20N150, demonstrate a gradual and consistent decrease in $NO_x$ emissions. Among these, D80B20N150 yields the most significant improvement, recording the lowest emission level at approximately 920 ppm.

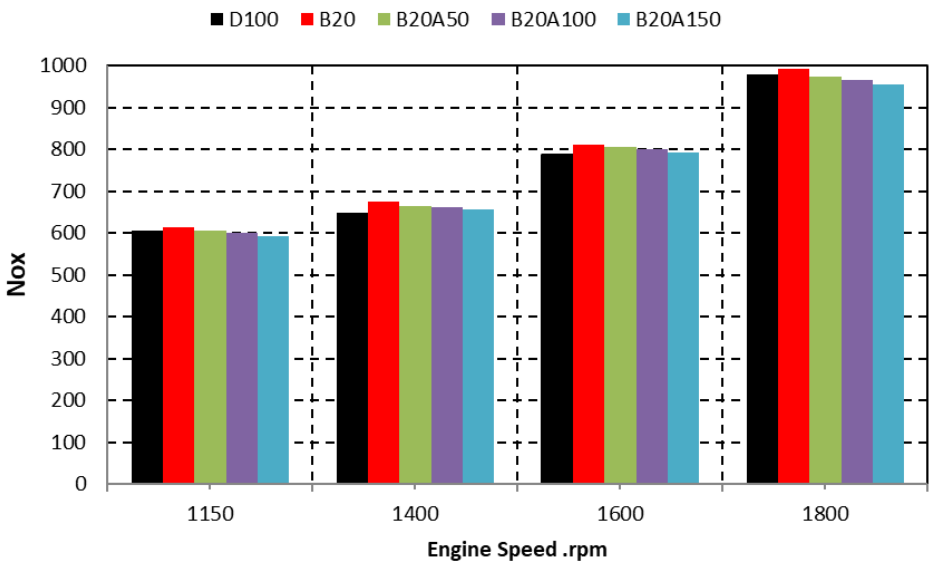


Figure 5.45. Variation of $NO_x$ emissions with engine speed for diesel and biodiesel–nanoparticle blends.

## 5.4. VALIDATION OF NUMERICAL MODELING

### 5.4.1. Break Thermal Efficiency

Figure 5.46 compares experimental and numerical Brake Thermal Efficiency (BTE) values for two fuel samples: D80B20 and D80B20N150. The analysis spans a range of engine loads from 0% to 100%. The results observed that BTE increases steadily with increasing engine load for both fuel blends, which is typical behavior due to improved combustion and lower relative heat losses at higher loads. D80B20N150 consistently outperforms D80B20 in both experimental and numerical results, indicating the efficiency-enhancing role of nanoparticles. Numerical results slightly overestimate BTE compared to the experimental values. This discrepancy is expected due to idealized assumptions in the simulation (e.g., perfect mixing, neglect of heat losses, etc.). The consistent agreement in trends between computational and experimental results confirms the reliability of the simulation model.

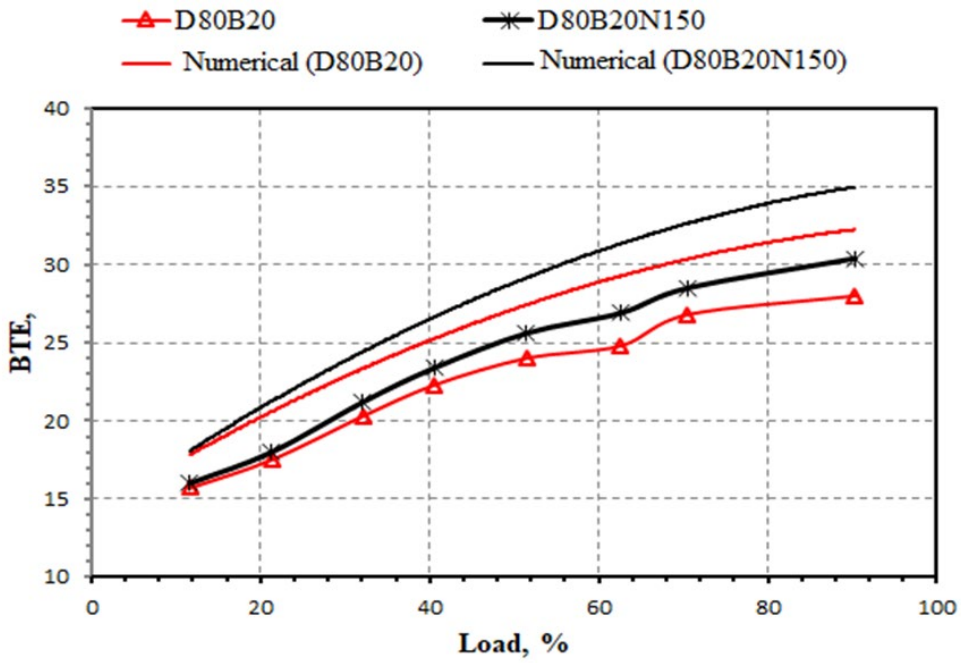


Figure 5.46. Comparison of experimental and numerical results of BTE for D80B20 and D80B20N150.

Figure 5.47 and Table 5.3 confirm the validity of the numerical simulation results through comparison with published data. The results support the hypothesis that

adding nanoparticles to biodiesel blends significantly enhances combustion, reflected in the higher peak pressures observed across all loading conditions. The current numerical simulation results demonstrate significantly higher peak pressure values than previously published experimental data, particularly under 50% load conditions. For instance, the D80B20 blend achieved a peak pressure of 76.1 kPa in the current study, notably higher than the 57 kPa reported in earlier studies. Similarly, the D80B20N150 blend recorded a peak pressure of 79.8 kPa, exceeding the previously published value of 64 kPa. Numerical simulations slightly overestimate the peak cylinder pressure. However, the trend consistency between both methods confirms the model's validity and reliability.

Table 5.3. Validate the current results for the cylinder's peak pressure against published data.

| Fuel Type | Current work | | | |
|---|---|---|---|---|
| | No load (Kpa) | 50% load (Kpa) | No load (Kpa) | 50% load (Kpa) |
| D80B20 | 58.2 | 76.1 | 45 | 57 |
| D80B20N50 | 59.8 | 77.2 | 46 | 59 |
| D80B20N100 | 61.3 | 78.1 | 47 | 62 |
| D80B20N150 | 62.4 | 79.8 | 48 | 64 |

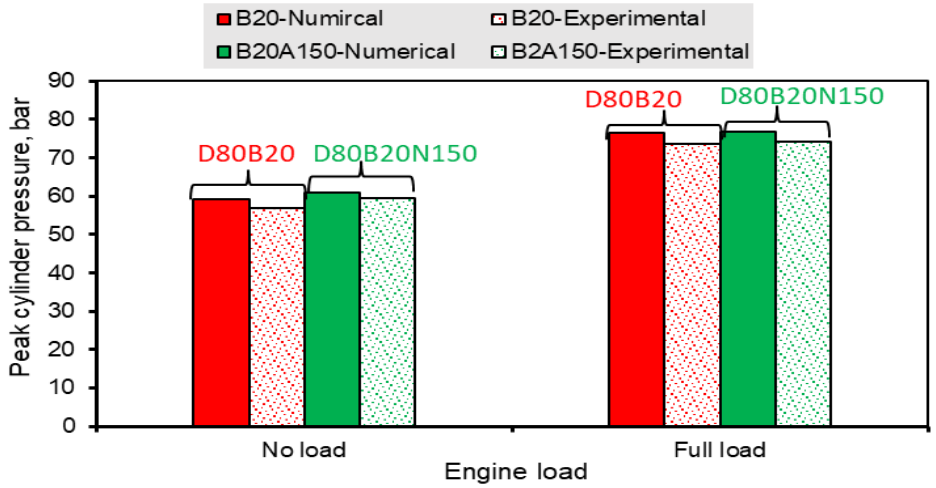


Figure 5.47. Analyzing the relationship between engine load and peak pressure for D80B20 and D80B20N150 blends using numerical and experimental methods.

### 5.4.2. Emissions

Figure 5.48 illustrates the variation of carbon dioxide ($CO_2$) emissions in volume percentage (% Vol.) concerning engine speed (rpm) for two fuel types—B20 and B20 blended with 150 ppm of $Al_2O_3$ nanoparticles (B20N150). Both numerical (simulated) and experimental results are presented at a constant engine load of 200 N·m. The numerical simulation results show that adding $Al_2O_3$ nanoparticles leads to a marked reduction in $CO_2$ emissions at all engine speeds. The most significant drop occurs at higher engine speeds (1600–1800 rpm), where the $CO_2$ emissions from B20N150 are nearly half those from B20 alone. Also, the experimental values closely follow the numerical trend, reinforcing the accuracy of the simulations. Similar to numerical data, $CO_2$ emissions from B20N150 were significantly lower than B20, particularly at higher engine speeds, indicating better fuel oxidation and combustion with nanoparticle presence.

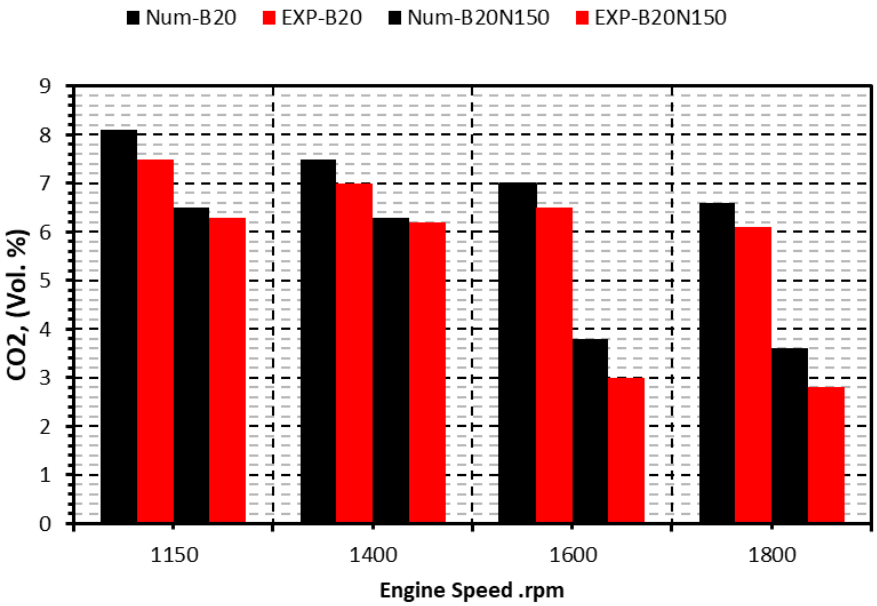


Figure 5.48. Comparison of numerical and experimental $CO_2$ emissions for B20 and B20N150 fuel blends at varying engine speeds under 200 N·m load.

Figure 5.49 presents the variation in $NO_x$ emissions (ppm) against engine speed (rpm) for two biodiesel fuel blends: B20: 80% diesel + 20% biodiesel and B20N150: B20

blended with 150 ppm of $Al_2O_3$ nanoparticles. The data includes numerical simulation results (Num) and experimental results (EXP), measured at a constant engine load of 200 N·m. At low engine speed (1150 rpm), B20N150 achieves up to ~6.7% $NO_x$ reduction experimentally, the highest among all speed levels, indicating optimal nanoparticle performance under this condition. The gap in $NO_x$ reduction narrows slightly at higher engine speeds, likely due to temperature increase overcoming the moderating effect of nanoparticles. Experimental and numerical values track closely, supporting the reliability of the computational fluid dynamics (CFD) approach used in simulation. The experimental reductions (3.8%–6.7%) align well with numerical trends, reinforcing the potential of B20N150 as a low-emission alternative fuel.

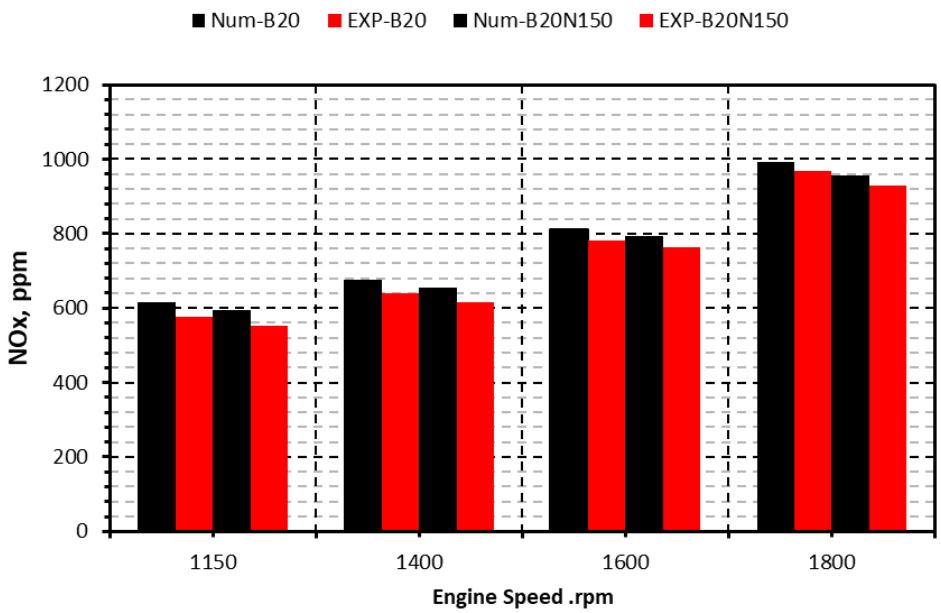


Figure 5.49. Comparative assessment of numerical and experimental $NO_x$ emissions for B20 and B20N150 biodiesel blends at varying engine speeds under constant load.

# PART 6

# CONCLUSIONS AND RECOMMENDATIONS

## 6.1. CONCLUSIONS

In this chapter, the theoretical and experimental results of the work are discussed and summarized to study the effect of nanoparticles ($Al_2O_3$) with biodiesel on combustion characteristics and engine performance, as well as the future of internal combustion engine emissions. In the present experimental investigation for a four-stroke, four-cylinder diesel engine, to study experimentally and theoretically the effect of nanoparticle concentrations of nano-aluminum trioxide with biodiesel derived from water hyacinth on engine performance, emissions, and combustion characteristics, and to determine the current main objectives, the following conclusions were reached. The following conclusions were reached.

**Performance of the Engine**

- At both full and half load, the brakes' thermal efficiency improved, and the best increase was when adding the nanomaterial with all blends and, respectively, D80B20N150 ppm, and the percentages were 34%, 45%, 47%, and 48% compared to pure diesel fuel. However, the calorific value decreased with diesel fuel and biodiesel (D80B20) compared to other blends and conventional fuel, but was optimal at half loads. At a speed of 1800 rpm.
- Reduction in fuel consumption mixed with nanoparticles and biodiesel (BSFC) at medium and high loads, with percentages of 52%, 55%, and 58%, respectively, compared to conventional fuel (D100). The best reduction was achieved when adding nanoparticles to biodiesel (D80B20N150) ppm. Compared to pure diesel fuel, fuel consumption (D80B20) decreased by 3% at 1800 rpm and a load of 200 Nm.

- The exhaust gas temperature decreased by increasing doses of biofuel with nanoparticles ($Al_2O_3$) and for all mixtures under all half and high load conditions. At a speed of 1800 rpm, the exhaust temperature decreased for biodiesel and pure diesel (D80B20) compared to pure diesel (D100) by 3.4%. When nanoparticles are added to different samples (D80B20N50, D80B20N150, and D80B20N100) at varying concentrations (ppm) compared to pure diesel fuel, the percentage decrease is 4%, 4.4%, and 6%, respectively. During the experiment using the ANSYS Fluent program, it was observed that adding biodiesel (D80B20) to pure diesel (D100) decreased temperature. Additionally, adding nanoparticles at different rates of 9%, 9.1%, 8.90%, and 11.1% compared to pure diesel fuel reduces temperature. This decrease is considered a good factor.

**The engine emission parameters.**

- Carbon monoxide emissions decreased by adding biodiesel from (D80B20) with biodiesel fuel compared to pure diesel fuel D100 at medium and high loads and at a speed of 1800, where the decrease was 2.5%, and when adding nanoparticles ($AL_2O_3$) for pure diesel fuel with biodiesel, a reduction in CO emissions was observed, respectively (4%, 11%, 2%), where the best blender was (D80B20N100) compared to pure diesel fuel.
- $CO_2$ emissions increased at medium loads and low speeds when biodiesel was added to pure fuel, although they were less efficient than pure diesel fuel at 1800 rpm and under heavy loads. The best combination was D80B20N150 compared to pure diesel fuel D100, with percentages of 8%, 10%, and 11%, respectively. $CO_2$ is also important in preserving the environment. When adding the nanomaterial (D80B20N50), we noticed an increase in the friction mass, which increased to 11.5%. Regarding the increase in the nanomaterial (D80B20N100), the friction mass increases regularly from pure diesel and biodiesel to 11.6%. It appears that as the speed increases, the friction mass is larger at (D80B20N150) compared to diesel fuel with biodiesel (D80B20), and this increase is seen as a positive factor, as the friction mass increases by 11.7% when the nanomaterial (D80B20N150) is increased. Biodiesel and various

blends (D80B20, D80B20N50, D80B20N100, and D80B20N150) were modeled using ANSYS Fluent software to simulate the combustion of diesel fuel. The experimental results were strongly in accord with the expected ones.

## 6.2. RECOMMENDATIONS

- Conduct further engine testing under real-world conditions, particularly during heavy machinery and field equipment operation.
- Investigate the feasibility of blending animal-based biodiesel with $Al_2O_3$ nanoparticles and conventional diesel fuel.
- Explore the combined effects of biofuel, magnetic field intensity, and nanoparticles on the combustion characteristics, performance, and emissions of single- and four-cylinder diesel engines.
- Undertake an exergy analysis of a compression ignition (CI) engine operating on biofuel enhanced with nanomaterials to evaluate energy efficiency and sustainability.
- Perform an economic feasibility analysis of diesel engine operation under various biofuel and nanoparticle blending scenarios.

## REFERENCES


1. Atabani, A. E., Silitonga, A. S., Badruddin, I. A., Mahlia, T. M. I., Masjuki, H. H., and Mekhilef, S., "A comprehensive review on biodiesel as an alternative energy resource and its characteristics", ***Renewable And Sustainable Energy Reviews***, 16 (4): 2070–2093 (2012).

2. Ghazal, R. M., Akroot, A., Wahhab, H. A. A., Alhamd, A. E. J., Hamzah, A. H., and Bdaiwi, M., "Influence of Gas Fuel Enrichment with Hydrogen on the Combustion The Influence of Gas Fuel Enrichment with Hydrogen on the Combustion Characteristics of Combustors: A Review", (2024).

3. Nanaki, E. A., Koroneos, C. J., Xydis, G. A., & Rovas, D., "Comparative environmental assessment of Athens urban buses—Diesel, CNG and biofuel powered", ***Transport Policy***, (2014).

4. Beigzadeh, M., Pourfayaz, F., Ghazvini, M., and Ahmadi, M. H., "Energy and exergy analyses of solid oxide fuel cell-gas turbine hybrid systems fed by different renewable biofuels: A comparative study", ***Journal Of Cleaner Production***, 280: 124383 (2021).

5. Ghazal, R. M., Akroot, A., and Abdul Wahhab, H. A., "Flame Evolution Characteristics for Hydrogen/LPG Co-Combustion in a Counter-Burner", ***Applied Sciences (Switzerland)***, 15 (5): (2025).

6. Akroot, A., Kareem, S., Alfaris, A., and Bdaiwi, M., "Enhancing Diesel Engine Performance with Different Concentrations of Copper Oxide Nanoparticles in Biodiesel Blends", ***International Journal Of Design And Nature And Ecodynamics***, 19 (3): 907–916 (2024).

7. Hamzah, A. H., Al-Khafaji, H. M. H., and Hussein, T. S., "Optimizing Aging Time to Maximize Hardness and Fatigue Strength of Al-4wt% Cu Alloy.", ***International Journal Of Heat & Technology***, 42 (1): (2024).

8. Akroot, Abdulrazzak. and Namli, Lutfu., "Performance assessment of an electrolyte-supported and anode-supported planar solid oxide fuel cells hybrid system", ***J Ther Eng***, 7 (7): 1921–1935 (2021).

9. Akroot, A., "Effect of Operating Temperatures on the Performance of a SOFCGT Hybrid System", ***International Journal Of Trend In Scientific Research And Development***, Volume-3 (Issue-3): 1512–1515 (2019).

10. Hassan, M. H. and Kalam, M. A., "An Overview of Biofuel as a Renewable Energy Source: Development and Challenges", ***Procedia Engineering***, 56: 39–53 (2013).

11. Bilgen, S., "Structure and environmental impact of global energy consumption", ***Renewable And Sustainable Energy Reviews***, 38: 890–902 (2014).

12. Akroot, A. and Al Shammre, A. S., "Economic and Technical Assessing the Hybridization of Solar Combined Cycle System with Fossil Fuel and Rock Bed Thermal Energy Storage in Neom City", ***Processes***, 12 (7): 1433 (2024).

13. Akroot, A. and Al Shammre, A. S., "Techno-Economic and Environmental Impact Analysis of a 50 MW Solar-Powered Rankine Cycle System", ***Processes***, 12 (6): 1059 (2024).

14. Agarwal, A. K., "Biofuels (alcohols and biodiesel) applications as fuels for internal combustion engines", ***Progress In Energy And Combustion Science***, 33 (3): 233–271 (2007).

15. OECD, I. E. A., "Technology roadmap: biofuels for transport", ***Paris, France: Organisation Of Economic Cooperation And Development (OECD). Int Energy Agency***, (2011).

16. Talal, W. and Akroot, A., "An Exergoeconomic Evaluation of an Innovative Polygeneration System Using a Solar-Driven Rankine Cycle Integrated with the Al-Qayyara Gas Turbine Power Plant and the Absorption Refrigeration Cycle", ***Machines***, 12 (2): 133 (2024).

17. Akroot, A., Hasan, H. A., and Bdaiwi, M., "Impact of Eucalyptus Biodiesel and Nanoparticle Additives on Diesel Engine Performance", ***International Journal Of Heat And Technology***, 42 (3): 755–764 (2024).

18. Thipse, S. S., "Alternative Fuels : Concepts, Technologies And Developments", ***Jaico Book Distributors***, (2010).

19. "Bioenergy Technologies Office | Department of Energy", **https://www.energy.gov/eere/bioenergy/bioenergy-technologies-office** (2025).

20. Hoekman, S. K., "Biofuels in the U.S. – Challenges and Opportunities", ***Renewable Energy***, 34 (1): 14–22 (2009).

21. Granda, C. B., Zhu, L., and Holtzapple, M. T., "Sustainable liquid biofuels and their environmental impact", ***Environmental Progress***, 26 (3): 233–250 (2007).

22. Bhattacharya, A. and Kumar, P., "Water hyacinth as a potential biofuel crop.", ***Electronic Journal Of Environmental, Agricultural And Food Chemistry***, 9: 112–122 (2010).

23. GhazaL, R. M., Akroot, A., and Wahhab, H. A. A., "Prediction of Premixed Flames Characteristics of Liquefied Petroleum Gas ( LPG ) / Hydrogen Gas Mixtures", ***Journal Of Engineering Science And Technology***, (Special Issue on ICCSD2023): 95–104 (2023).

24. Bjerg, J., "Energy Technology Perspectives 2008 Translating the ETP 2006 scenarios into technology R&D recommendations", .

25. Erdman, E., Vanderlinden, C., Gorbunova, K., and Guebert, J., "2007 Heiligendamm G8 Summit final compliance report", ***Toronto: G8 Research Group. Available At Http://Www. G8. Utoronto. Ca/Evaluations/2007compliance_final/07-Final. Pdf***, (2008).

26. Abanades, S., Abbaspour, H., Ahmadi, A., Das, B., Ehyaei, M. A., Esmaeilion, F., El Haj Assad, M., Hajilounezhad, T., Jamali, D. H., and Hmida, A., "A critical review of biogas production and usage with legislations framework across the globe", ***International Journal Of Environmental Science And Technology***, 1–24 (2022).

27. Walker, D. A., "Biofuels, facts, fantasy, and feasibility", ***Journal Of Applied Phycology***, 21 (5): 509–517 (2009).

28. Rao, G. L. N., Ramadhas, A. S., Nallusamy, N., and Sakthivel, P., "Relationships among the physical properties of biodiesel and engine fuel system design requirement", ***International Journal Of Energy And Environment***, 1 (5): 919–926 (2010).

29. Romero, C. A., Correa, P., Ariza Echeverri, E. A., and Vergara, D., "Strategies for reducing automobile fuel consumption", ***Applied Sciences***, 14 (2): 910 (2024).

30. Hamzah, A. H., Akroot, A., and Jaber, J. A., "Analytical Investigation of Biodiesel Mixed Levels and Operation Factors' Effects on Engine Performance by RCM", ***International Journal Of Design And Nature And Ecodynamics***, 17 (6): 863–873 (2022).

31. Lalitha, P., Sripathi, S. K., and Jayanthi, P., "Secondary metabolites of Eichhornia crassipes (waterhyacinth): a review (1949 to 2011)", ***Natural Product Communications***, 7 (9): 1934578X1200700939 (2012).

32. Demirbas, A. and Karslioglu, S., "Biodiesel production facilities from vegetable oils and animal fats", ***Energy Sources, Part A***, 29 (2): 133–141 (2007).

33. Fadil, A., Mashkour, M. A., and Abdul Wahhab, H. A., "Investment of blending biofuels and nanoparticles with conventional diesel fuel to improve combustion process—a review", ***Advances In Material Science And Engineering: Selected Articles From ICMMPE 2021***, 95–107 (2022).

34. Wang, M., "Energy and greenhouse gas emissions impacts of fuel ethanol", (2005).

35. Sayago, U. F. C., "Design of a sustainable development process between phytoremediation and production of bioethanol with Eichhornia crassipes", ***Environmental Monitoring And Assessment***, 191 (4): 221 (2019).

36. Saratale, R. G., Cho, S.-K., Ghodake, G. S., Shin, H.-S., Saratale, G. D., Park, Y., Lee, H.-S., Bharagava, R. N., and Kim, D.-S., "Utilization of noxious weed water hyacinth biomass as a potential feedstock for biopolymers production: A novel approach", ***Polymers***, 12 (8): 1704 (2020).

37. Sims, R. E. H., Mabee, W., Saddler, J. N., and Taylor, M., "An overview of second generation biofuel technologies", ***Bioresource Technology***, 101 (6): 1570–1580 (2010).

38. Wang, M. Q., "GREET 1.5: Transportation Fuel-Cycle Model. Vol. 1: Methodology, Development, Use, and Results", ***Argonne National Laboratory***, (1999).

39. Rajora, K., Tyagi, S., Sarma, K., Sarma, A. K., and Jena, R., "Evaluation of water hyacinth utility through geospatial mapping and in situ biomass estimation approach: a case study of Deepor beel (wetland), Assam, India", ***Environmental Monitoring And Assessment***, 195 (11): 1277 (2023).

40. El-Araby, R., "Biofuel production: exploring renewable energy solutions for a greener future", ***Biotechnology For Biofuels And Bioproducts***, 17 (1): 129 (2024).

41. Gil, A. F., "Biofuels Under Scrutiny from Regulators: Europe's Short-term Decarbonization", (2021).

42. Wauton, I. and William-Ebi, D., "Characterization of water hyacinth (Eichhornia crassipes) for the production of thermochemical fuels", ***J Multidiscip Eng Sci Stud***, 5 (7): 2661–2665 (2019).

43. Lovarelli, D. and Bacenetti, J., "Exhaust gases emissions from agricultural tractors: State of the art and future perspectives for machinery operators", ***Biosystems Engineering***, 186: 204–213 (2019).

44. Malik, M. A. I., Kalam, M. A., Abbas, M. M., Silitonga, A. S., and Ikram, A., "Recent advancements, applications, and technical challenges in fuel additives-assisted engine operations", ***Energy Conversion And Management***, 313: 118643 (2024).

45. Saxena, V., Kumar, N., and Saxena, V. K., "A comprehensive review on combustion and stability aspects of metal nanoparticles and its additive effect on diesel and biodiesel fuelled CI engine", ***Renewable And Sustainable Energy Reviews***, 70: 563–588 (2017).

46. Hamzah, A. H., Akroot, A., Abdul Wahhab, H. A., Ghazal, R. M., Alhamd, A. E. J., and Bdaiwi, M., "Effects of nano-additives in developing alternative fuel strategy for CI engines: A critical review with a focus on the performance and emission characteristics", ***Results In Engineering***, 22: 102248 (2024).

47. Zhao, H., Holladay, J. E., Brown, H., and Zhang, Z. C., "Metal chlorides in ionic liquid solvents convert sugars to 5-hydroxymethylfurfural", ***Science***, 316 (5831): 1597–1600 (2007).

48. Heuer, A. H., "Oxygen and aluminum diffusion in α-Al2O3: How much do we really understand?", ***Journal Of The European Ceramic Society***, 28 (7): 1495–1507 (2008).

49. Xia, M., Ji, S., Fu, Y., Dai, J., Zhang, J., Ma, X., and Liu, R., "Alumina ceramic nanofibers: an overview of the spinning gel preparation, manufacturing process, and application", ***Gels***, 9 (8): 599 (2023).

50. Ivanova, A. S., "Aluminum oxide and systems based on it: Properties and applications", ***Kinetics And Catalysis***, 53: 425–439 (2012).

51. Ivanova, A. S., "Aluminum oxide and systems based on it: Properties and applications", ***Kinetics And Catalysis***, 53: 425–439 (2012).

52. Cruickshank, Brandon. and Chang, Raymond., "Problem-Solving Workbook to Accompany General Chemistry, the Essential Concepts, Fifth Edition, Raymond Chang", ***McGraw-Hill Higher Education***, 546 (2008).

53. Aljuboury, M. M., "Review Influence Normal Diesel Emissions on Agricultural Environment", ***J Appl Mech Eng***, 10: 396 (2021).

54. Wang, X., Zhang, J., Wang, G., Han, J., Dai, M., and Sun, Z. Y., "A comprehensive review on the properties of nanofluid fuel and its additive effects to compression ignition engines", ***Applied Surface Science***, 504: 144581 (2020).

55. Al-Kayiem, H. H., Wahhab, H. A. A., Magaril, E., and Aziz, A. R. A., "Performance and emissions investigation of a single cylinder diesel engine using enhanced blend biodiesel by nanoparticles", (2018).

56. Fadil, A., Mashkour, M. A., and Abdul Wahhab, H. A., "Investment of blending biofuels and nanoparticles with conventional diesel fuel to improve combustion process—a review", ***Advances In Material Science And Engineering: Selected Articles From ICMMPE 2021***, 95–107 (2022).

57. Hamzah, A. H., Wahhab, H. A. A., Akroot, A., Alawee, W. H., and Mahdi, L. A. A.-A., "Analytical Study of Intake Air Temperature Effect on SI Engine Performance and Emissions", (2024).

58. Vohra, G., Kumar, V., Singh, H., and Sham, R., "Effect of Biodiesel on the Performance and Emission Characteristics of Diesel Engines", ***International Journal Of Engineering Research And Technology***, 13 (6): (2020).

59. Jumaa, H. and Mashkour, M. A., "Humidification Effect on the Performance and Emissions of (DI) Diesel Engine Running on Diesel Fuel with Biodiesel Blended Nano Additives", ***Engineering And Technology Journal***, 39 (05 Part A): 790–803 (2021).

60. Yaser, H. S., Abdul Wahhab, H. A., and Dhahad, H. A., "Survey to water-in-diesel emulsion characteristics as an alternative fuel for CI engine", Advances in Material Science and Engineering: Selected Articles from ICMMPE 2021, ***Springer***, 81–94 (2022).

61. Abdul Wahhab, H. A. and Al-Kayiem, H. H., "Environmental risk mitigation by biodiesel blending from Eichhornia crassipes: performance and emission assessment", ***Sustainability***, 13 (15): 8274 (2021).

62. Devarajan, Y., Nagappan, B., and Subbiah, G., "A comprehensive study on emission and performance characteristics of a diesel engine fueled with nanoparticle-blended biodiesel", ***Environmental Science And Pollution Research***, 26: 10662–10672 (2019).

63. Fadil, A., Mashkour, M. A., and Wahhab, H. A. A., "Influence of alumina nanoparticles additives into biofuel (water hyacinth)-diesel mixture on diesel engine performance and emissions: Einfluss von Aluminiumoxid-Nanopartikeln als Zusatz zu einem Biokraftstoff (Wasserhyazinthe)-Diesel-Gemisch auf die Leistung und die Emissionen von Dieselmotoren", ***Materialwissenschaft Und Werkstofftechnik***, 54 (9): 1107–1113 (2023).

64. Devarajan, Y., Munuswamy, D., Nagappan, B., and Subbiah, G., "Experimental assessment of performance and exhaust emission characteristics of a diesel engine fuelled with Punnai biodiesel/butanol fuel blends", ***Petroleum Science***, 16: 1471–1478 (2019).

65. Borthakur, P. P., "Nanoparticle Enhanced Biodiesel Blends: Recent Insights and Developments", ***Hybrid Advances***, 100442 (2025).

66. Modi, V., Rampure, P. B., Babbar, A., Kumar, R., Nagaral, M., Bhowmik, A., Pandey, S., Hasnain, S. M. M., Ali, M. M., and Bashir, M. N., "Nanoparticle-enhanced biodiesel blends: A comprehensive review on improving engine performance and emissions", ***Materials Science For Energy Technologies***, (2024).

67. Soudagar, M. E. M., Nik-Ghazali, N.-N., Kalam, M. A., Badruddin, I. A., Banapurmath, N. R., Ali, M. A. Bin, Kamangar, S., Cho, H. M., and Akram, N., "An investigation on the influence of aluminium oxide nano-additive and honge oil methyl ester on engine performance, combustion and emission characteristics", ***Renewable Energy***, 146: 2291–2307 (2020).

68. Sajeevan, A. C. and Sajith, V., "Diesel engine emission reduction using catalytic nanoparticles: an experimental investigation", ***Journal Of Engineering***, 2013 (1): 589382 (2013).

69. Pawar, C., Shreeprakash, B., Mokshanatha, B., Nikam, K. C., Motgi, N., Jathar, L. D., Shelare, S. D., Sharma, S., Dwivedi, S. P., and Bains, P. S., "Machine learning-based assessment of the influence of nanoparticles on biodiesel engine performance and emissions: a critical review", ***Archives Of Computational Methods In Engineering***, 32 (1): 499–533 (2025).

70. Elkelawy, M., Alm ElDin Mohamad, H., Abo-Samra, S., and Abd-Elhay Elshennawy, I., "Nanoparticles additives for diesel/biodiesel fuel blends as a performance and emissions enhancer in the applications of direct injection diesel engines: A comparative review", ***Journal Of Engineering Research***, 7 (1): 112–121 (2023).

71. Gunti, S., McCrory, M., Kumar, A., and Ram, M. K., "Enhanced photocatalytic remediation using graphene (G)-titanium oxide (TiO2) nanocomposite material in visible light radiation", ***American Journal Of Analytical Chemistry***, 7 (7): 576–587 (2016).

72. Sandra, V., Stojanovic, B., Ivanović, L., Miladinovic, S., and Milojević, S., "Application of nanocomposites in the automotive industry", (2019).

73. Rangabashiam, D., V, J., S, G., and Rameshbabu, A., "Emission, performance, and combustion study on nanoparticle-biodiesel fueled diesel engine", ***Energy Sources, Part A: Recovery, Utilization, And Environmental Effects***, 45 (3): 8396–8407 (2023).

74. Hosseinzadeh-Bandbafha, H., Tabatabaei, M., Aghbashlo, M., Khanali, M., Khalife, E., Roodbar Shojaei, T., and Mohammadi, P., "Consolidating emission indices of a diesel engine powered by carbon nanoparticle-doped diesel/biodiesel emulsion fuels using life cycle assessment framework", ***Fuel***, 267: 117296 (2020).

75. Sunil, S., Prasad, B. S. C., and Kakkeri, S., "Studies on titanium oxide nanoparticles as fuel additive for improving performance and combustion parameters of CI engine fueled with biodiesel blends", ***Materials Today: Proceedings***, 44: 489–499 (2021).

76. Rangabashiam, D., Jayaprakash, V., Ganesan, S., Nagaraj, M., and Rameshbabu, A., "Emission, performance, and combustion study on nanoparticle-biodiesel fueled diesel engine", ***Energy Sources, Part A: Recovery, Utilization And Environmental Effects***, 45 (3): 8396–8407 (2023).

77. Gad, M. S., Hashish, H. M. A., Hussein, A. K., Ben Hamida, M. B., Abdulkader, R., and Nasef, M. H., "Effect of different configurations of hybrid nano additives blended with biodiesel on CI engine performance and emissions", ***Scientific Reports***, 14 (1): 19528 (2024).

78. Jin, C., Wei, J., Chen, B., Li, X., Ying, D., Gong, L., and Fang, W., "Effect of nanoparticles on diesel engines driven by biodiesel and its blends: A review of 10 years of research", ***Energy Conversion And Management***, 291: 117276 (2023).

79. Perumal, V. and Ilangkumaran, M., "The influence of copper oxide nano particle added pongamia methyl ester biodiesel on the performance, combustion and emission of a diesel engine", ***Fuel***, 232: 791–802 (2018).

80. El-Seesy, A. I., Attia, A. M. A., and El-Batsh, H. M., "The effect of Aluminum oxide nanoparticles addition with Jojoba methyl ester-diesel fuel blend on a diesel engine performance, combustion and emission characteristics", ***Fuel***, 224: 147–166 (2018).

81. Chandrasekaran, V., Arthanarisamy, M., Nachiappan, P., Dhanakotti, S., and Moorthy, B., "The role of nano additives for biodiesel and diesel blended transportation fuels", ***Transportation Research Part D: Transport And Environment***, 46: 145–156 (2016).

82. El-Seesy, A. I., Attia, A. M. A., and El-Batsh, H. M., "The effect of Aluminum oxide nanoparticles addition with Jojoba methyl ester-diesel fuel blend on a diesel engine performance, combustion and emission characteristics", ***Fuel***, 224: 147–166 (2018).

83. Surendrababu, K., Muthurajan, K. G., Prabhahar, M., Prakash, S., Saravana Kumar, M., and Jayakumar, M., "Performance, emission, and study of DI diesel engine running on pumpkin seed oil methyl ester with the effect of copper oxide nanoparticles as an additive", ***Journal Of Nanomaterials***, 2022 (1): 3800528 (2022).

84. Elsharkawy, E. A., Al-Sood, M. M. A., El-Fakharany, M. K., and Ahmed, M., "Comparative study of combustion, performance, and emissions of a diesel engine fuelled with biodiesel blend with metallic and organic nano-particles", ***International Journal Of Global Warming***, 22 (2): 133–159 (2020).

85. Khan, T. M. Y., "Direct transesterification for biodiesel production and testing the engine for performance and emissions run on biodiesel-diesel-nano blends", ***Nanomaterials***, 11 (2): 417 (2021).

86. Dharsini, P. S. P., Ahalya, N., Kaliappan, S., Sekar, S., Patil, P. P., Pragna, V., Pathinettampadian, G., Isaac JoshuaRamesh Lalvani, J., and Menasbo, K., "Performance and environmental effects of CeO2/ZrO2 nanocomposite in triple blend methyl ester of pumpkin and neem seed oil dosed with diesel on IC engine", ***Journal Of Nanomaterials***, 2022 (1): 5736453 (2022).

87. Bunyan, S. T. and Abed, A.-K. M., "Experimental Investigation of the Influence of Adding Alumina to Diesel Fuel on the Engine Performance and Emission Characteristics", ***Engineering And Technology Journal***, 38 (4A): 523–529 (2020).

88. Gumus, S., Ozcan, H., Ozbey, M., and Topaloglu, B., "Aluminum oxide and copper oxide nanodiesel fuel properties and usage in a compression ignition engine", ***Fuel***, 163: 80–87 (2016).

89. Matus, K., Łamacz, A., and Liszka, B., "Characterization of $CeO_2$, $ZrO_2$, and $CeZrO_2$ crystals on CNT", ***Acta Physica Polonica A***, 130 (4): 966–968 (2016).

90. Ali, O. M., Mamat, R., Masjuki, H. H., and Abdullah, A. A., "Analysis of blended fuel properties and cycle-to-cycle variation in a diesel engine with a diethyl ether additive", ***Energy Conversion And Management***, 108: 511–519 (2016).

91. Örs, I., Sarıkoç, S., Atabani, A. E., Ünalan, S., and Akansu, S. O., "The effects on performance, combustion and emission characteristics of DICI engine fuelled with TiO2 nanoparticles addition in diesel/biodiesel/n-butanol blends", ***Fuel***, 234: 177–188 (2018).

92. Kumar, S., Dinesha, P., and Bran, I., "Influence of nanoparticles on the performance and emission characteristics of a biodiesel fuelled engine: an experimental analysis", ***Energy***, 140: 98–105 (2017).

93. Nithya, S., Manigandan, S., Gunasekar, P., Devipriya, J., and Saravanan, W. S. R., "The effect of engine emission on canola biodiesel blends with TiO2", ***International Journal Of Ambient Energy***, 40 (8): 838–841 (2019).

94. Ramesh, D. K., Kumar, J. L. D., Kumar, S. G. H., Namith, V., Jambagi, P. B., and Sharath, S., "Study on effects of alumina nanoparticles as additive with poultry litter biodiesel on performance, combustion and emission characteristic of diesel engine", ***Materials Today: Proceedings***, 5 (1): 1114–1120 (2018).

95. Wu, Q., Xie, X., Wang, Y., and Roskilly, T., "Effect of carbon coated aluminum nanoparticles as additive to biodiesel-diesel blends on performance and emission characteristics of diesel engine", ***Applied Energy***, 221: 597–604 (2018).

96. Hosseini, S. H., Taghizadeh-Alisaraei, A., Ghobadian, B., and Abbaszadeh-Mayvan, A., "Effect of added alumina as nano-catalyst to diesel-biodiesel blends on performance and emission characteristics of CI engine", ***Energy***, 124: 543–552 (2017).

97. Ong, H. C., Milano, J., Silitonga, A. S., Hassan, M. H., Shamsuddin, A. H., Wang, C.-T., Mahlia, T. M. I., Siswantoro, J., Kusumo, F., and Sutrisno, J., "Biodiesel production from Calophyllum inophyllum-Ceiba pentandra oil mixture: Optimization and characterization", ***Journal Of Cleaner Production***, 219: 183–198 (2019).

98. Bitire, S. O., Jen, T.-C., and Belaid, M., "Yield response from the catalytic conversion of parsley seed oil into biodiesel using a heterogeneous and homogeneous catalyst", ***ACS Omega***, 6 (39): 25124–25137 (2021).

99. Bitire, S. O., Jen, T.-C., and Belaid, M., "Production and optimization of biodiesel from parsley seed oil using KOH as catalyst for automobiles technology", ***The International Journal Of Advanced Manufacturing Technology***, 116 (1): 315–329 (2021).

100. Parida, M. K., Mohapatra, P., Patro, S. S., and Dash, S., "Effect of TiO2 nano-additive on performance and emission characteristics of direct injection compression ignition engine fueled with Karanja biodiesel blend", ***Energy Sources, Part A: Recovery, Utilization, And Environmental Effects***, 46 (1): 7521–7530 (2024).

101. Keera, S. T., El Sabagh, S. M., and Taman, A. R., "Castor oil biodiesel production and optimization", ***Egyptian Journal Of Petroleum***, 27 (4): 979–984 (2018).

102. Ala'a, H., Jamil, F., Al-Haj, L., Al-Hinai, M. A., Baawain, M., Myint, M. T. Z., and Rooney, D., "Efficient utilization of waste date pits for the synthesis of green diesel and jet fuel fractions", ***Energy Conversion And Management***, 127: 226–232 (2016).

103. Fattah, I. M. R., Masjuki, H. H., Kalam, M. A., Hazrat, M. A., Masum, B. M., Imtenan, S., and Ashraful, A. M., "Effect of antioxidants on oxidation stability of biodiesel derived from vegetable and animal based feedstocks", ***Renewable And Sustainable Energy Reviews***, 30: 356–370 (2014).

104. Parmar, C. A., Patel, T. M., Patel, P. R., and Rathod, G. P., "Parametric Optimization of Variable Compression Ratio Diesel Engine Fueled with PalmSeedBiodiesel and its Blend using the Taguchi Method for SFC", .

105. Agrawal, T., Gautam, R., Agrawal, S., Singh, V., Kumar, M., and Kumar, S., "Optimization of engine performance parameters and exhaust emissions in compression ignition engine fueled with biodiesel-alcohol blends using taguchi method, multiple regression and artificial neural network", ***Sustainable Futures***, 2: 100039 (2020).

106. Raja, S., Natarajan, S., Eshwar, D., and Alphin, M. S., "Energy and exergy analysis and multi-objective optimization of a biodiesel fueled direct ignition engine", ***Results In Chemistry***, 4: 100284 (2022).

107. Asokan, M. A., Vijayan, R., Prabu, S. S., and Venkatesan, N., "Experimental studies on the combustion characteristics and performance of a DI diesel engine using kapok oil methyl ester/diesel blends", ***International Journal Of Oil, Gas And Coal Technology***, 12 (1): 105–119 (2016).

108. Datta, A. and Mandal, B. K., "Engine performance, combustion and emission characteristics of a compression ignition engine operating on different biodiesel-alcohol blends", ***Energy***, 125: 470–483 (2017).

109. Aliyu, B., Shitanda, D., Walker, S., Agnew, B., Masheiti, S., and Atan, R., "Performance and exhaust emissions of a diesel engine fuelled with Croton megalocarpus (musine) methyl ester", ***Applied Thermal Engineering***, 31 (1): 36–41 (2011).

110. Jado, A. and Pan, J., "A study on the performance and emission of diesel engine with Jatropha biodiesel and its blends at different engine load", ***Authorea Preprints***, (2020).

111. Masera, K., "BIODIESEL-BIODIESEL MIXTURES TO UPGRADE FUEL PROPERTIES AND LOWER EXHAUST GAS EMISSIONS KEMAL MASERA BIODIESEL-BIODIESEL MIXTURES TO UPGRADE FUEL PROPERTIES AND LOWER EXHAUST GAS EMISSIONS", (2019).

112. Gao, J., Wang, X., Song, P., Tian, G., and Ma, C., "Review of the backfire occurrences and control strategies for port hydrogen injection internal combustion engines", ***Fuel***, 307: 121553 (2022).

113. Udayakumar, P. and Kasiraman, G., "Performance and emission of ci engine fueled by turpentine and cottonseed oil blends at various injection pressures", (2020).

114. Özgür, C., "Optimization of biodiesel yield and diesel engine performance from waste cooking oil by response surface method (RSM)", ***Petroleum Science And Technology***, 39 (17–18): 683–703 (2021).

115. Feng, S., Xu, S., Yuan, P., Xing, Y., Shen, B., Li, Z., Zhang, C., Wang, X., Wang, Z., and Ma, J., "The impact of alternative fuels on ship engine emissions and aftertreatment systems: A review", ***Catalysts***, 12 (2): 138 (2022).

116. Xiao, H., Guo, F., Wang, R., Yang, X., Li, S., and Ruan, J., "Combustion performance and emission characteristics of diesel engine fueled with iso-butanol/biodiesel blends", ***Fuel***, 268: 117387 (2020).

117. Milošević, M. S., Stamenković, D. S., Milojević, A. P., and Tomić, M. M., "MODELING THERMAL EFFECTS IN BRAKING SYSTEMS OF RAILWAY VEHICLES.", ***Thermal Science***, 16: (2012).

118. Akroot, A., Ekici, Ö., and Köksal, M., "Process modeling of an automotive pem fuel cell system", ***International Journal Of Green Energy***, (2019).

119. Kadhim, N. S., "Experimental investigation of three various sources of diesel fuel on the engine performance", ***Journal Of Babylon University/Pure And Applied Sciences***, 21 (8): 2955 (2013).

120. Srinivasan, S. K., Kuppusamy, R., and Krishnan, P., "Effect of nanoparticle-blended biodiesel mixtures on diesel engine performance, emission, and combustion characteristics", ***Environmental Science And Pollution Research***, 28 (29): 39210–39226 (2021).

121. Premalatha, R. P., Parameswari, E., Davamani, V., Malarvizhi, P., and Avudainayagam, S., "Biosorption of Chromium (III) from Aqueous Solution by Water Hyacinth Biomass.", ***Madras Agricultural Journal***, 106: (2019).

122. Thamarai Kannan, B., Sathish, T., Sathyamurthy, R., and Erko, K. G., "Use of waste fish oil biodiesel blended with aluminium oxide nanoparticle in IC engines: an experimental on performance, combustion and emission study", ***Scientific Reports***, 12 (1): 12930 (2022).

123. Altarazi, Y. S. M., Yu, J., Gires, E., Ghafir, M. F. A., Lucas, J., and Yusaf, T., "Effects of biofuel on engines performance and emission characteristics: A review", ***Energy***, 238: 121910 (2022).

124. Dehhaghi, M., Panahi, H. K. S., Aghbashlo, M., Lam, S. S., and Tabatabaei, M., "The effects of nanoadditives on the performance and emission characteristics of spark-ignition gasoline engines: A critical review with a focus on health impacts", ***Energy***, 225: 120259 (2021).

125. Devarajan, Y., Munuswamy, D., Nagappan, B., and Subbiah, G., "Experimental assessment of performance and exhaust emission characteristics of a diesel engine fuelled with Punnai biodiesel/butanol fuel blends", ***Petroleum Science***, 16: 1471–1478 (2019).

126. Kalam, A., Rahman, L., and Ahmed, N., "Removal of toxic Congo red dye using water hyacinth petiole, an efficient and selective adsorbent", ***Journal Of The Chemical Society Of Pakistan***, 41 (5): 825–833 (2019).

127. ARAUJO CANAZART, D., RODRIGUES DA COSTA NUNES, A., SANCHES, M., and CONTE, H., "PHYTOREMEDIATION AGRO INDUSTRIAL WASTEWATER OF USING MACROPHYTE: Eichhornia crassipes.", ***Brazilian Journal Of Surgery & Clinical Research***, 17 (3): (2016).

128. Singh, M. and Sandhu, S. S., "Performance and emission characteristics of an indirect injection (IDI) multi-cylinder compression ignition (CI) engine using diesel/Argemone maxicana biodiesel blends", ***RSC Advances***, 5 (110): 91069–91081 (2015).

129. Abdullah, I. S., Khalid, A., Jaat, N., Nursal, R. S., Koten, H., and Karagoz, Y., "A study of ignition delay, combustion process and emissions in a high ambient temperature of diesel combustion", ***Fuel***, 297: 120706 (2021).

130. Varatharajan, K., Cheralathan, M., and Velraj, R., "Mitigation of NOx emissions from a jatropha biodiesel fuelled DI diesel engine using antioxidant additives", ***Fuel***, 90 (8): 2721–2725 (2011).

131. Wei, J., He, C., Fan, C., Pan, S., Wei, M., and Wang, C., "Comparison in the effects of alumina, ceria and silica nanoparticle additives on the combustion and

emission characteristics of a modern methanol-diesel dual-fuel CI engine", ***Energy Conversion And Management***, 238: 114121 (2021).

132. Ashok, B., Nanthagopal, K., Jeevanantham, A. K., Bhowmick, P., Malhotra, D., and Agarwal, P., "An assessment of calophyllum inophyllum biodiesel fuelled diesel engine characteristics using novel antioxidant additives", ***Energy Conversion And Management***, 148: 935–943 (2017).

133. Lapuerta, M., Armas, O., and Rodriguez-Fernandez, J., "Effect of biodiesel fuels on diesel engine emissions", ***Progress In Energy And Combustion Science***, 34 (2): 198–223 (2008).

134. Gautam, R., Chauhan, B. S., and Lim, H. C., "Influence of variation of injection angle on the combustion, performance and emissions characteristics of jatropha ethyl ester", ***Energy***, 254: 124436 (2022).

135. Gad, M. S. and Jayaraj, S., "A comparative study on the effect of nano-additives on the performance and emissions of a diesel engine run on Jatropha biodiesel", ***Fuel***, 267: 117168 (2020).

136. ČEDík, J., PExA, M., PETERkA, B., Holubek, M., Mader, D., and PRAžAN, R., "Effect of biobutanol-sunflower oil-diesel fuel blends on combustion characteristics of compression ignition engine", ***Acta Technol. Agric***, 21 (4): 130–135 (2018).

137. Agarwal, A. K., Singh, A. P., and Maurya, R. K., "Evolution, challenges and path forward for low temperature combustion engines", ***Progress In Energy And Combustion Science***, 61: 1–56 (2017).

138. Khalaf, M., Abdel-FadEel, W., Abdelhady, S., and Esmail, M., "Performance and emissions of a diesel engine fueled with a biofuel extracted from Jatropha seeds", ***International Journal Of Applied Energy Systems***, 4 (2): 40–51 (2022).

139. Krishana, K., Kanth, M. S., Maneiah, D., Kumar, B. S. P., Reddy, K. V. K., and Reddy, A. R., "CFD analysis of karanja oil methyl ester (KOME) blend B20 and hydrogen using ANSYS-Fluent", ***Materials Today: Proceedings***, 76: 495–517 (2023).

140. D'Silva, R., D'Souza, F., Pinto, D., Tauro, C., Saldanha, P., and Bhat, T., "Taguchi method to study the performance and emission characteristics of CI engine fuelled with blends of Jatropha biodiesel & Titanium dioxide nanoadditive", ***Materials Today: Proceedings***, 92: 202–208 (2023).

141. Dixit, S., Kumar, A., Kumar, S., Waghmare, N., Thaku, H. C., and Khan, S., "CFD analysis of biodiesel blends and combustion using Ansys Fluent", ***Materials Today: Proceedings***, 26: 665–670 (2020).

## RESUME

Ameer Hasan Hamza AL-MAAMOURI holds a bachelor's degree in mechanical engineering from Al-Musayyab Technical College, which was awarded in 2010. He earned his master's degree in mechanical engineering from the Turkish Aeronautical Association University in Turkey in 2017. In 2025, he completed his Ph.D. in the Department of Mechanics at Karabük University, also in Turkey.